Contents

Technical Articles

New Products

Visualization of Lubricating Grease in Ball Bearing Using X-ray CT and Validation of Digital Simulation

Takashi Noda, Shinji Miyata and Masato Taniguchi
NSK Ltd.

1. Introduction

Information about grease condition, such as flow movement, shape, and distribution, is useful in developing grease lubrication to extend bearing service life. However, visually observing grease in bearings has been difficult due to the obstruction of seals used to prevent grease from splashing or leaking. While removing the seals enables a certain level of direct observation, accurately determining the condition of grease can still be problematic, since a quantity of grease adhering to the surface of the seals could be scraped off when the seals are removed. Conventional methods for assessing grease condition have included the use of colored grease or radioactive grease[1] to observe primary and branch flows in rolling bearings as well as the use of a high-speed camera to view the grease without seals installed[2]. But observation with these methods is limited. The first only provides qualitative and quantitative information about grease movement, while the latter is limited to the external surface shape of grease with no useful information on internal condition. We refer to the surface of grease mentioned here as the boundary between grease and other substances, while the internal condition is the inner space enclosed by grease. In this research, to overcome the various problems and other issues associated with the aforementioned methods, we have captured X-ray CT images of bearings with sealed grease by using a non-destructive inspection technology and have gained knowledge of the internal condition of grease.

2. Measurement Conditions

Aqua-Bearing 6001QT-3 high corrosion-resistance resin bearings were used in this test. These consist of inner and outer rings made of fiber-reinforced special fluorine resin, a composite of fluorine resin and carbon fiber; a cage made of fluorine resin with superior corrosion resistance and self-lubrication; and special glass rolling elements. Urea grease was used as a lubricant to fill 53% of the space volume.

3. Measurement Results

The location of the cross section is expressed with the Z-axis coordinate, of which the "0" and "1" values correspond to the left and right ends of a bearing, as shown on the left side of Figure 1. The right side of Figure 1 shows a CT image of a bearing at $Z = 0.36$. The CT image is displayed in grayscale corresponding to X-ray permeability. Substances with low permeability appear in a lighter shade, while those with high permeability, such as air, are displayed in a darker shade. For this test, air is shown with the darkest contrasting shade. Substances with similar X-ray permeability appear at the same level of gray. Comparing levels of gray in the CT image in Figure 1 allows for clear differentiation between the inner and outer rings, cage, rolling elements, and grease. It can also reveal the presence of air bubbles and foreign matter in addition to the condition of grease.
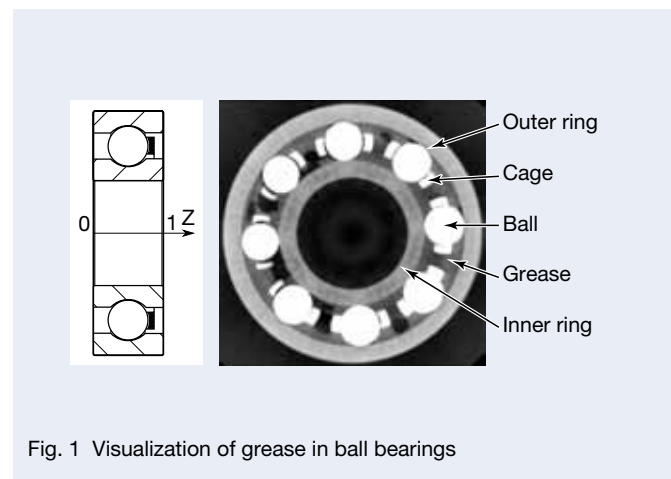

Fig. 1 Visualization of grease in ball bearings

4. Discussion

We discussed the transition of the grease condition resulting from bearing rotation as follows and used the inner ring of the Aqua-Bearing from the previously mentioned test and rotated it at 600 rpm with an axial load of 10 N.

4.1. Grease distribution

The CT images of the initial state and at one minute after rotation are respectively shown in Figure 2 (a) and (b). The cross section locations are at Z = 0.29, 0.36, 0.44, and 0.63, from left to right.

Figure 2 shows that the transition of grease condition before and after rotation was clearly captured. The CT image captured after rotation indicates that grease was removed from near the inner and outer rings and rolling elements, which tend to be subject to the impact of shear force. Other observed characteristics include the even distribution of grease between the rolling elements and a homothetic shape formation. This indicates that after the grease has been removed from the race surfaces, it spreads out evenly between the rolling elements due to

bearing rotation or through the processes of trapping and movement, in spite of its uneven distribution when the bearing is filled.

4.2. Churning and channeling

One of the most interesting phenomena in grease lubrication is the transition of lubrication state from churning to channeling. Bearing rotation is generally assumed to remove grease from a raceway (churning phase), and the grease collects in places that do not contribute to lubrication, such as at the seal or groove shoulder. In this section, the observation point is fixed as the basis for discussing the aforementioned phenomenon based on reviewing the CT images before and after bearing rotation. Figure 3 (a) through (c) show the grease conditions at the initial point, and at one minute and five minutes after the start of rotation. The cross section locations are at Z = 0.29, 0.36, and 0.63, respectively, from left. In addition, since the difference of conditions between rolling elements is not as significant, as previously mentioned, this sampling is considered to adequately reflect the results of the experiment.

(a) Initial test conditions

(b) After approximately one minute of rotation
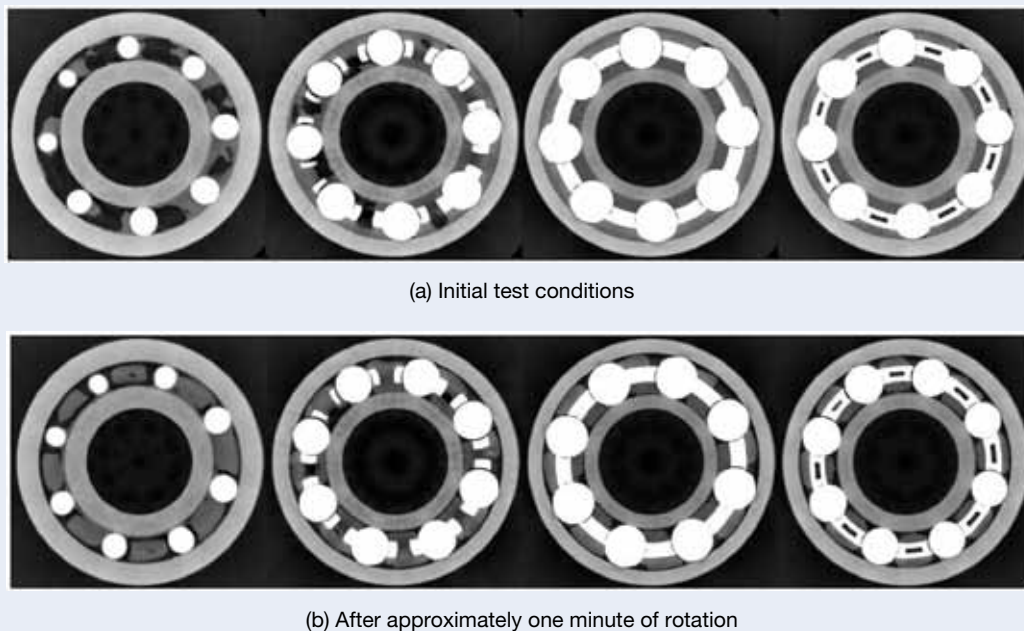
Fig. 2 Grease distribution

Figure 3 (a) and (b) show a significant movement of grease at the initial stage of rotation, which indicates a churning phase during which extensive agitation of grease occurs. On the other hand, Figure 3 (b) and (c) show almost no change in the shape of the grease. This means that at this stage of churning, grease has already been removed from the race surface. There was little change in this state even after 10 minutes of rotation.

Therefore, the experiment has indicated that the transition from churning to channeling took several minutes. While achieving a consistent bearing torque is believed to take several minutes, the grease settles into a stable state within a significantly shorter period and may reach an overall stationary state. Furthermore,

Figure 3 (b) and (c) show that once the grease is removed, it is unlikely to return to the race surface. Also, the results confirm that grease does not contribute to lubrication but accumulates near seals and cages, areas that are unlikely to be subject to shearing.

(a) Initial test conditions

(b) After approximately one minute of rotation

(c) After approximately five minutes of rotation
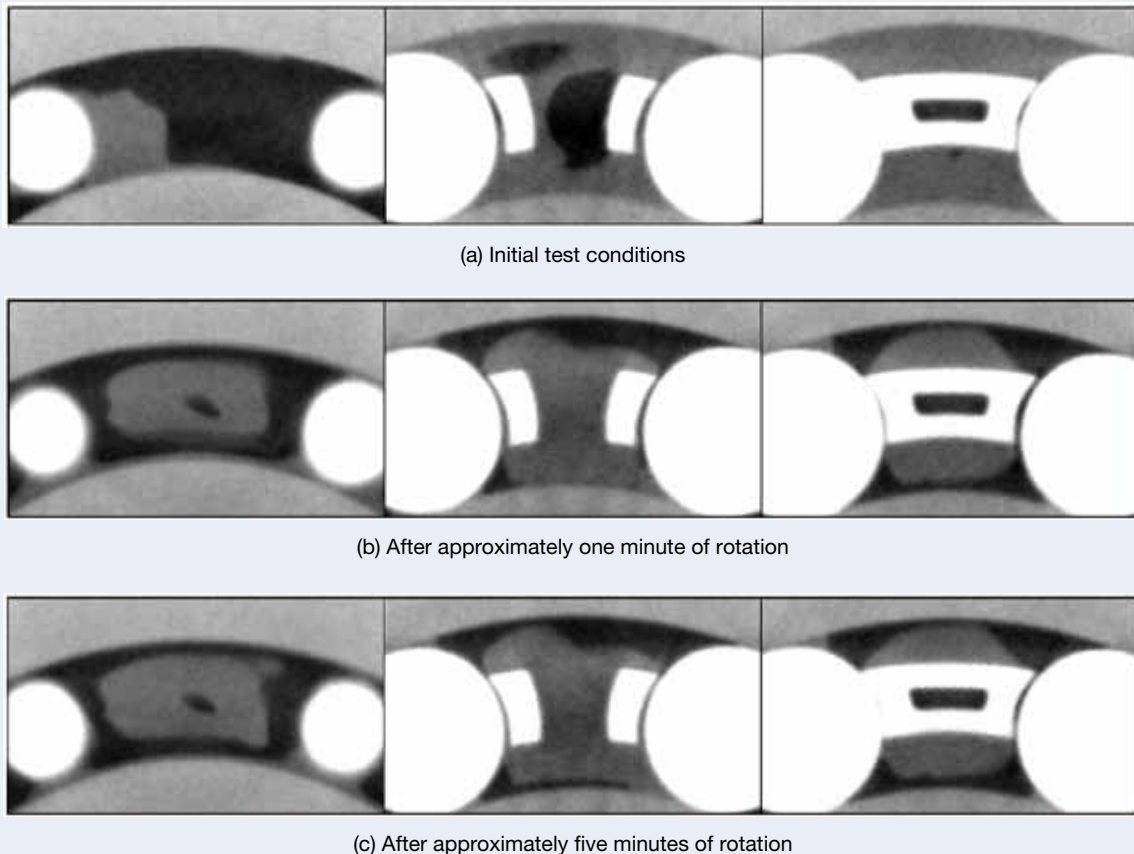
Fig. 3 Transition of grease state from churning to channeling

4.3. Validation of numerical analysis

We examined the validity of the gas-liquid two-phase flow analysis of lubrication grease that we implemented[2]. Figure 4 (a) and (b) show the results of analysis and experimentation. The site of the cross section is $Z = 0.31$. The results of the calculation are displayed using black for air, other regions for grease, and color codes to express viscosity. This indicates that distributions and adhesion conditions of both grease and air during channeling correspond qualitatively. Therefore, this experiment validates the numerical analysis reported in our previous article[2].

(a) Calculated   (b) Experimental
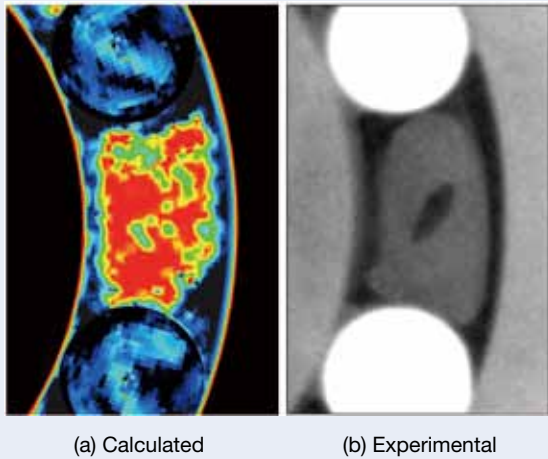
Fig. 4 Calculated grease behavior compared with experimental results

5. Conclusion

Grease conditions inside the bearings were visualized by tomography image using X-ray CT. Transition from churning to channeling was confirmed at multiple cross sections. Validity of the gas-liquid two-phase flow analysis of lubrication grease that we implemented[2] was demonstrated by this experiment.

References

1) Shonozaki, Shigematsu, and Urai, "A study on the behaviors of grease in the ball bearing," Journal of Japan Society of Lubrication Engineers 8, 4 (1963), pp. 237–242.
2) T. Noda, S. Miyata, and M. Taniguchi, "Analysis and experimental verification of the gas-liquid two-phase flow of lubrication grease in ball bearings," JAST Tribology conference proceedings (Tokyo 2010–5), pp. 243–244.

Takashi Noda

Shinji Miyata

Masato Taniguchi

Visualization of Grease Behavior in a Ball Bearing Using X-ray CT

Takashi Noda, Kenichi Shibasaki and Shinji Miyata
NSK Ltd.

1. Introduction

A thorough understanding of grease behavior is required for the development of grease lubrication to extend bearing service life. We visualized the behavior of grease inside bearings by using X-ray computed tomography (CT)[1]. The transition of lubrication state from churning to channeling is discussed here using CT images with a reduced level of artifacts due to the careful selection of bearing components that best allowed for the X-ray permeability of grease. While we have confirmed the channeling status by determining the state of the grease interface, which was relatively constant over time, the grayscale expression was not sufficient to identify the presence of fluid inside the grease. For this article, and in an effort to further study the channeling state, we examined the flow condition inside grease using the marble patterns of the fluid of two types of grease having different linear absorption coefficients.

2. Outline of CT Image and Measurement Conditions

We generated CT images at a grayscale resolution of 8 bits and 256 gradations for this journal. Grayscale resolution varies depending on X-ray controller settings as well as the size and configuration of the observed objects, even if they are made of the same materials. We therefore disregarded the absolute grayscale value and instead focused on the relative differences between the components.

We observed a 6001 series bearing consisting of inner and outer rings made of fiber-reinforced special fluorine resin, which is a composite of fluorine resin and carbon fiber; a fluorine resin cage; and a special glass rolling element. We used two types of grease as lubricant: a urea grease and a barium grease, of which the composition and properties are shown in Table 1. The X-ray controller was set at 55 kV tube voltage and 260 mA tube current. After capturing an image of the initial state, the inner ring was rotated at 600 rpm, with subsequent images captured at one minute and five minutes.

3. Measurement Results

The location of the cross section is expressed with the Z-axis coordinate, of which the "0" and "1" values correspond to the left and right ends of the bearing, as shown on the left side of Figure 1. The right side of Figure 1 shows a CT image of the bearing at $Z = 0.38$, immediately after it was filled with grease.
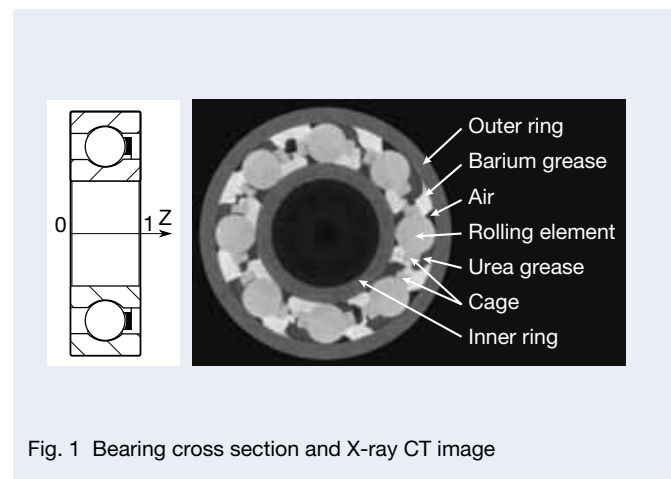

Fig. 1 Bearing cross section and X-ray CT image

Table 1 Physical properties and composition of two grease types

Lubricant	Thickener	Base Oil	Base Oil Kinetic Viscosity [mm²/s] (40°C)	Density [g/cm³]	Worked Penetration
Urea grease	Urea	POE	30.5	0.93	264
Barium grease	Barium complex soap	MO + Ester	23.0	0.99	280

4. Discussion Regarding Churning and Channeling

Figure 2 shows the grease conditions at the initial state and at one minute and five minutes after rotation. After one minute, layers of air appeared between the grease and the inner and outer rings and the rolling elements. We believe that this was caused by the movement of grease in contact with a friction surface to a location with less impact from shearing or to other slices. In addition, we observed that portions of grease deformed in the direction of shear force by the molecular viscosity of the grease. This was more evident on the inner ring side, which is subject to higher shear force. The grease (gray) that adhered to the upper right side and lower left side of the barium grease (white) is shown with an intermediate shade along with the mixture of urea and barium grease, which we consider as evidence of the agitation, or churning. The CT image captured at five minutes after the rotation shows little evidence of change from the one-minute mark and allows for observation of the shape and distribution equivalent to that at one minute after rotation. On the other hand, grease that had been trapped in the wedge-shaped regions between the inner ring and the rolling elements at one minute after rotation had been replaced by air at the five-minute mark, indicating there was still some flow movement. The following facts confirmed by this measurement generally align with the traditional understanding of channeling[2]: grease that adheres to a friction surface separates from the friction surface when air enters in between, after the process of trapping and dragging; and grease that has accumulated on the cages maintains its state. Furthermore, under these test conditions, the agitation of grease was not so severe as to completely change the original shape of the grease at the initial stage, and a relatively moderate flow was dominant, mainly at the surface layer.

Observation of the upper side of Figure 3, a 256-color spectrum of the CT image on the right side of Figure 1, clarified the relative positions of the respective components. The air and the urea and barium grease do not overlap, indicating that they can be identified separately on a CT image, whereas the cages and rolling elements at the same level are not as easily differentiated. Figure 3 shows the rate of change of pixel intensity of each grayscale value. The solid line δ_1 shows the change from initial state to one minute after rotation, and the dotted line δ_5 shows the change from one minute to five minutes through the difference of pixel intensity by grayscale value, data that indicates only the air and grease behavior, not the bearing itself. From the graph, we can observe a churning status involving significant change during the initial one-minute mark and also subtle channeling characteristics during the four minutes that followed. When we closely examined the behavior of the grease, we were able to confirm that both the urea and barium grease decreased at each slice and that the same amount increased, mainly at the grayscale values 100 through 150, in the mixed grease after agitation was identified. The larger increase of mixed grease at $Z = 0.25$ and 0.75 outside the bearing, compared to the center of the bearing, allows us to presume that the agitated grease was removed from the race surface on the outer side.

Figure 4 shows the numerical analysis results
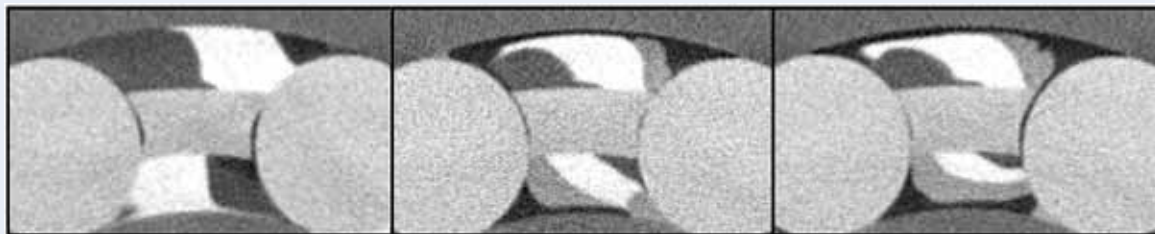
Fig. 2　From left, initial test condition, and approximately one minute and five minutes after rotation
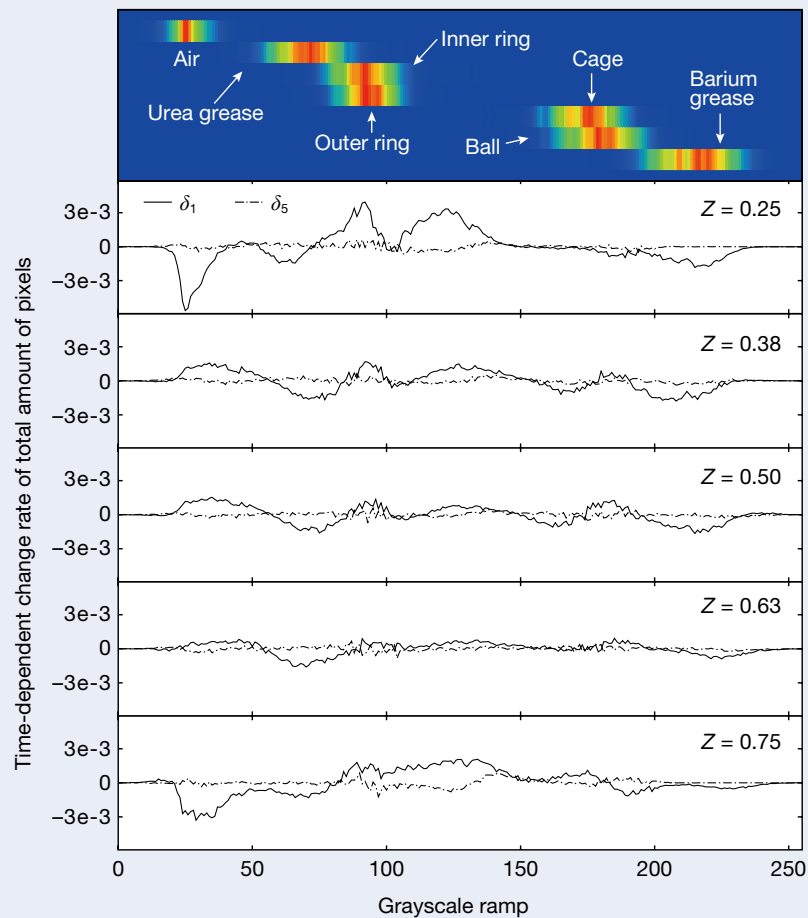
Fig. 3 2D Spectra of X-ray CT image and grease behavior showing changes in pixel intensity value

implemented under the same conditions used for this research. The method of analysis is the same as that used in the experiments reported in our previous article[1], in which non-Newtonian viscosity of the urea and barium grease was adapted to examine the conditions of each phase. From the figure, we can see that the shape and deformation of grease are qualitatively the same. Also, we have similarly confirmed through numerical analysis that grease behavior stabilizes when the grease accumulates on cages and reaches the channeling state with the intervention of air between the grease and friction surface.

5. Conclusion

We have gained a wider understanding of channeling by visualizing the fluidity of grease through the X-ray CT images of ball bearings using two types of grease with different linear absorption coefficients. Numeric analysis validates these phenomena.
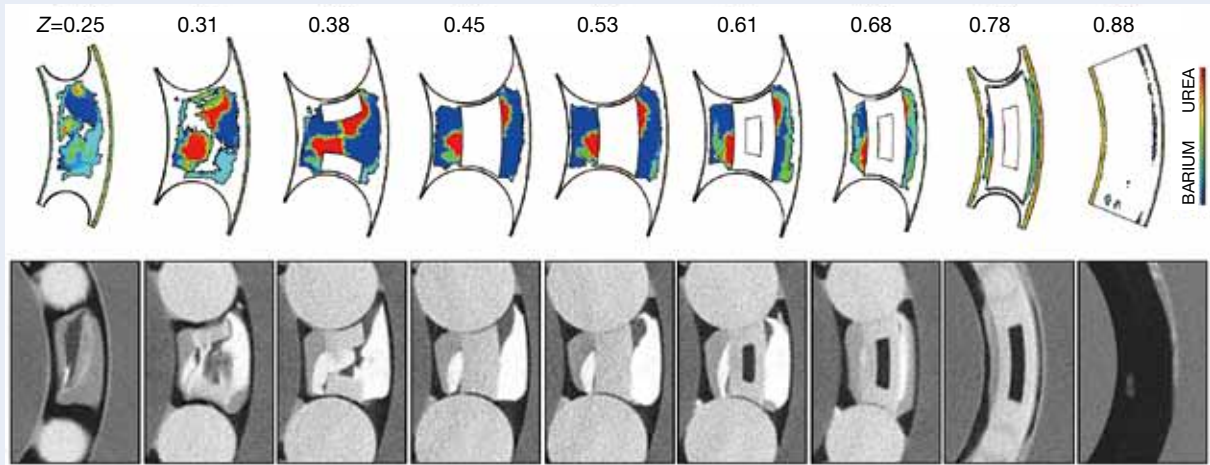
Fig. 4 Unstable grease behavior at the slice of each *Z* coordinate and an X-ray CT image after approximately five minutes of rotation in a ball bearing at the same slice of calculated results

References

1) T. Noda, S. Miyata, and M. Taniguchi, "Visualization of lubrication grease inside ball bearings using X-ray CT and verification of validity numerical analysis," JAST Tribology Conference Proceedings (Tokyo 2011–05) 273.
2) Example: Suzuki, "Lubrication behavior of grease in rolling bearings," Journal of Japanese Society of Lubrication Engineers 19, 4 (1974) 252.

Takashi Noda

Kenichi Shibasaki

Shinji Miyata

Low Torque Technology Using Grease and Application to Motor Bearings

Eri Watabe, Yujiro Toda and Atsushi Yokouchi
NSK Ltd.

1. Introduction

The need for lower torque bearing technology has increased in the wake of rising demand for energy-saving motors. Bearing torque in general consists of friction resistance at contact surfaces and agitation resistance of the lubricant inside the bearing. Methods for reducing grease torque include using a low viscosity base oil, reducing the thickener, and suppressing the volume of grease used to fill the bearing to mitigate agitation resistance. However, these methods have caused concern related to the reduced thickness of oil film, premature lubricant failure associated with increased oil separation, and insufficient durability. We therefore decided to examine low-torque technologies instead of these conventional methods.

Grease flow characteristics related to channeling and churning are known to have an influence on bearing torque of grease-sealed rolling bearings[1]. In particular, 60% to 80% of the total bearing torque of compact motor bearings is the result of grease agitation resistance. Therefore, we focused on grease channeling to test a technique for lowering torque by restraining agitation inside the bearing.

With regard to compact motor bearings, there is interest for quieter performance over extended periods during rotation in addition to low torque. In this study, we report a case in which a new Li soap that forms a strong oil film while maintaining a high channeling property is selected as a thickener and applied to lower motor bearing torque.

2. Method of Experiment

2.1 Applied grease

Table 1 shows the components and properties of the greases tested. Grease A, which is widely used for motor bearings, includes lithium 12-hydroxystearic (Li-12OH) as a thickener. Greases B through F use a new Li soap thickener made of Li-12OH and lithium decanoate and exhibit different channeling characteristics related to the concentration of thickener. The Li soap has a more rigid structure and a higher dropping point compared to Li-12OH. Only greases A and F contain the commonly used anti-oxidizing agent.

2.2 Test method

2.2.1 Yield stress measurement

We measured yield stress as a grease flow characteristic using a rheometer. Storage elastic modulus G' and loss elastic modulus G'', when shear stress is increased from 10 Pa to 5 000 Pa, were measured under oscillation conditions of a 10 Hz frequency and 30°C using a parallel plate. Yield stress was defined as a shearing stress when loss tangent, $\tan \delta \, (= G''/G')$, is equal to "1"[2].

2.2.2 Bearing torque test

We tested bearing torque using a deep groove ball bearing ($\phi 8 \times \phi 22 \times W7$) under the condition of 1 800 rpm rotation, 29.4 N axial load, and room temperature. Torque was measured at 60 minutes after starting rotation of the bearing with grease filled to 30% of its internal volume.

Table 1 Properties of grease

Grease	A	B	C	D	E	F
Base oil type	Ester A	Ester B				
Base oil viscosity at 40°C, mm²/s	26	34				
Thickener type	Li-12OH	Li-12OH/Li-capric acid				
Thickener concentration, %	12	5.5	7.5	12	13.5	13.5
Worked penetration	250	290	244	200	180	200
Dropping point, °C	190	198	202	202	204	200
Additive	○	—	—	—	—	○

2.2.3 Acoustic life test

We used a deep groove bearing ($\phi 8 \times \phi 22 \times$ W7) with grease filled to 30% of its internal volume for the acoustic life test. The bearing was rotated under an atmospheric temperature of 120°C, 29.4 N axial load, and 1 800 rpm inner ring rotation for a period of time, and then its vibration was measured with the Anderon meter. Acoustic life was defined by the time required for the Anderon value (high band) to exceed "8."

2.2.4 Bearing oil film formation test

We measured the separation rate to calculate oil film thickness so that the oil film formation characteristics could be examined inside the bearing during rotation. We used a deep groove bearing ($\phi 25 \times \phi 62 \times$ W17) with 30% of its internal volume filled with grease and rotated the bearing under an atmospheric temperature of 100°C, 29.4 N axial load, and 600 rpm inner ring rotation speed. The bearing with base oil only was filled with 0.006 g of the oil.

3. Results and Discussion

3.1 Yield stress of grease

We previously examined the relationship between the yield stress of grease using a Li-12OH thickener and torque and reported that the yield stress increased in relation to the combination with ester oil. The larger the yield stress, the higher the channeling property. Consequently, the amount of agitation inside the bearing decreased, resulting in lower torque[3]. In this study, we researched characteristics of grease, in which the new Li soap had a higher dropping point, to further reduce torque in relation to the commonly used Li-12OH.

Figure 1 shows the relationship between the amount of thickener and yield stress. We found that the Li soap grease, having the same amount of thickener as Li-12OH, exhibited a higher yield stress. The Li soap demonstrated a stronger capability to retain base oil with the thickener fiber compared to Li-12OH, which seemed to have a rigid grease structure.

Figure 2 shows the change in yield stress due to shear stress. We discovered that while applying shear force at 100°C for 24 hours, the yield stress of Grease A was reduced to approximately 1% of that at the initial stage, and the yield stress of grease F remained at around 40%, indicating little change in yield stress by shear force.

These results shows that the new Li soap can increase yield stress to a level higher than what Li-12OH is capable of, even with the same amount of thickener, and thus helps to reduce the change in grease flow by shear force.

3.2 Bearing torque performance of new Li soap

We also examined the relationship between the yield stress and torque of grease using the new Li soap. The results of our test are shown in Figure 3. Torque was measured under common compact motor conditions. Grease with higher yield stress tended to have lower rotation torque, and Grease E was confirmed to have approximately 50% less torque compared to Grease A.
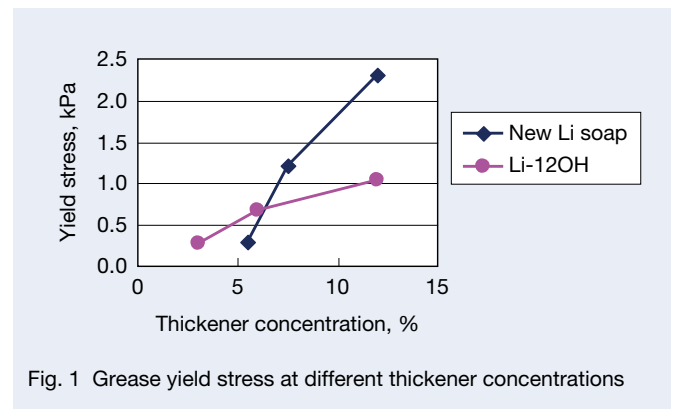

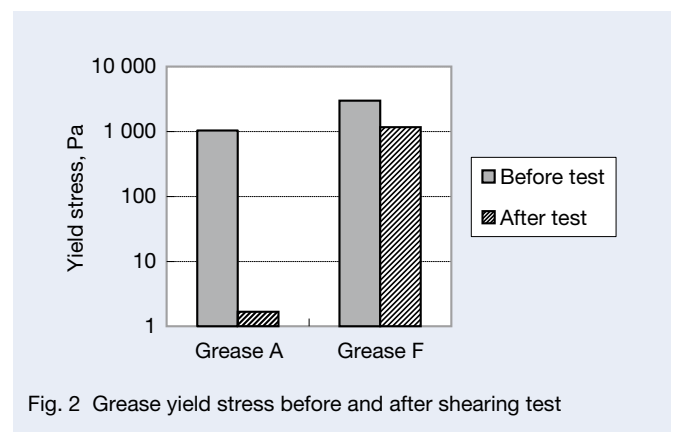Fig. 1 Grease yield stress at different thickener concentrations

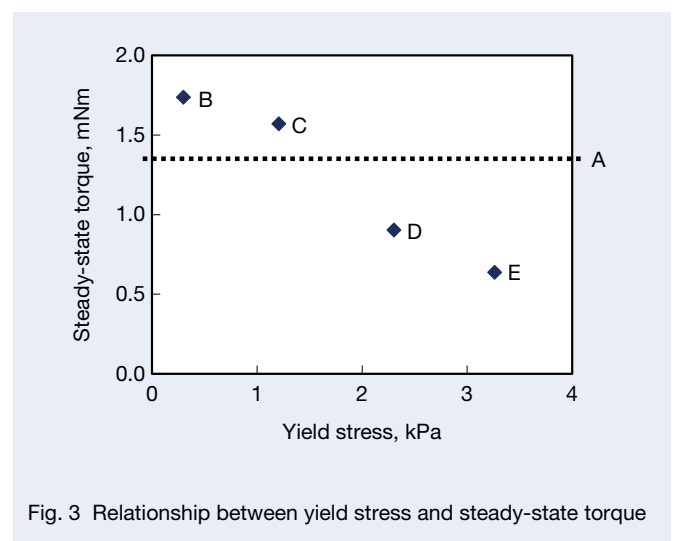Fig. 2 Grease yield stress before and after shearing test

Fig. 3 Relationship between yield stress and steady-state torque

3.3 Application in bearings for motors

After identifying the low torque property, we reviewed long-term quietness, which is also important for motor grease.

An acoustic life test was performed on bearings filled with greases A and F. While the time taken by the bearing with Grease A to a mark over 8 Anderons was approximately 2 000 hours, it was 5 000 hours for the Grease F bearing, which means that acoustic life with Grease F is more than twice that with Grease A. Figure 4 shows the oil film thickness inside the bearing measured under 100°C. Whereas Grease A exhibits a thinner oil film compared to the base oil, Grease F was confirmed to have thicker oil film than base oil. From the test, it is clear that quietness is also due to the new thickener, which has an enhanced fiber structure for reduced torque, and with less tendency to separate the base oil and thickener, allowing the grease to get caught on the friction surface and lubricate.
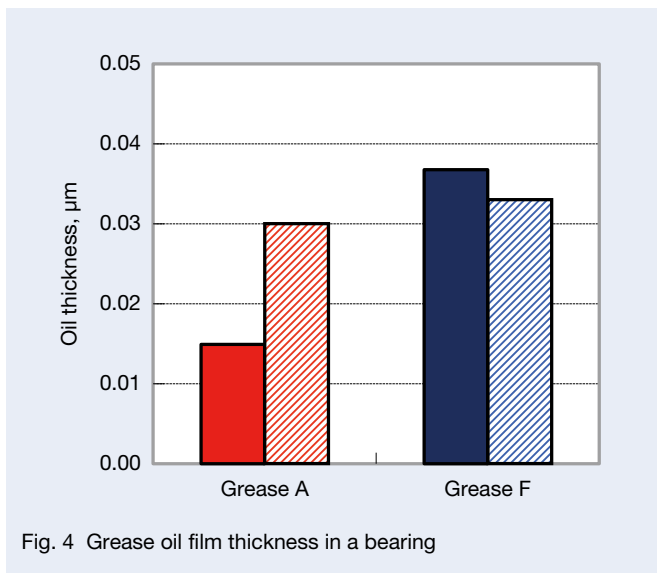
Fig. 4 Grease oil film thickness in a bearing

4. Summary

The following observations were made during our research into lowering grease torque.
- The new Li soap grease had a higher yield stress with the same amount of thickener as Li-12OH while the change due to shear force was also suppressed.
- The new Li soap grease reduces more torque compared to conventional Li-12OH grease.
- Long-term quietness with the new Li soap was improved by forming a stable oil film even under high temperatures.

References

1) Hishino, "Flow properties of lubricating greases and torque in rolling bearings (Part 2)," Journal of Japan Society of Lubrication Engineers 25, 8 (1980) 555–561.
2) I. Couronné, G. Blettner, and P. Vergne, "Rheological Behavior of Grease: Part I - Effects of Composition and Structure, Tribology Transactions," 43, 4 (2000) 619–626.
3) E. Oikawa, N. Inami, M. Hokao, A. Yokouchi, and J. Sugimura, "Bearing torque characteristics of lithium soap greases with some synthetic base oils, Proc. IMechE Part J," J. Engineering Tribology, 226, 6 (2012) 575–583.

Eri Watabe

Yujiro Toda

Atsushi Yokouchi

Water Resistant Technology for Grease and Application to Bearings

Noriyuki Inami, Michita Hokao and Atsushi Yokouchi
NSK Ltd.

1. Introduction

Carbon dioxide emissions are increasing with the worldwide growth in automobile production. Consequently, reducing CO_2 emissions to prevent global warming poses a critical challenge for the automotive industries, which in turn requires further suppressing bearing torque to save energy in automobiles. In addition, highway infrastructure in newly developing nations where there is skyrocketing demand for automobiles is insufficiently developed to handle massive rainfall, leading to concerns over premature bearing damage from water penetration due to excessive exposure to rain[1].

This paper reports on the results of a performance evaluation of bearings that involves prototyping a water resistant grease. The prototyping evaluation was directed to hub unit bearings because they are frequently exposed to water and require low torque.

2. Test Method

Water resistance and low torque properties as well as performance were verified through the following test.

2.1 Measurement of water dispersion state

Ion exchange water was evenly mixed into grease at 20 wt%, which was then sandwiched between cover glasses at a thickness of 20 µm to measure the maximum number of water particles in the grease with a microscope.

2.2 Measurement of oil film thickness and traction coefficient

The oil film thickness and traction coefficient of grease were measured using an EHL (elastohydrodynamic lubrication) tester and optical interferometry.

2.3 Element test of flaking life

A rolling four-ball tester was used and the time taken until flaking occurred on a steel ball was measured. Ion exchange water was evenly mixed into grease at 20 wt% for the test at the maximum surface pressure of 4.1 GPa and a rotation speed of 1 200 rpm.

2.4 Measurement of oxide film thickness

The oxide film thickness on the raceway surface was measured after a bearing test using an Auger electronic spectroscopy analyzer. A thrust ball bearing (51305) was used to analyze the raceway surface after running for 150 hours at a maximum surface pressure of 2.4 GPa and a rotation speed of 1 000 rpm. The oxide film thickness was defined as the thickness at which the oxygen peak became a background level is cleared while analyzing the depth direction of the raceway surface.

2.5 Water mixed bearing endurance test

The endurance property of a bearing was tested to confirm bearing service life under the condition with a water mixture. A deep groove ball bearing (6017) was used to measure the time until the occurrence of damage under running while supplying water at the radial load of 15.7 kN and a rotation speed of 1 000 rpm.

2.6. Torque test

Torque was measured under a condition equivalent to the straight-line travel of a vehicle with a hub unit bearing.

3. Grease Design

3.1 Water resistance grease technology

A sufficient level of lubrication without any mixed water in grease forms an oil film on the contact surface. The oil film becomes thinner, however, when water infiltrates into the grease, which is considered to be the cause of shorter service life as a result of metal contact and abrasion on the raceway surface or corrosion or flaking due to the contact of water and metal[1].

In order to extend service life under the condition with a water mixture, it is critical to prevent water that may have penetrated the bearing from reaching the contact surface and to protect the raceway surface when the water reaches the contact surface[2].

The state of water dispersion in grease was observed to confirm the impact on grease performance under the condition with a water mixture. Figure 1 indicates a correlation between the diameter of water particles in

grease and flaking life. The results show that the water particle diameter increases with the flaking life. It is possible that grease with larger diameter water particles tends to separate out the water so that it is not likely to be introduced to the contact surface, which in turn lowers the tendency to reduce flaking life.

In the case of thinner oil film due to an oil and water mixture, protecting the raceway surface with an inert oxide film may be effective. Figure 2 shows a correlation between the thickness of the oxide film on the bearing raceway surface and flaking life. The results show that the thicker the oxide film, the longer the flaking life.

In order to improve bearing service life under the condition with a water mixture, it can be considered to be effective to select a grease composite that separates water and forms a thick oxide film on the raceway surface.
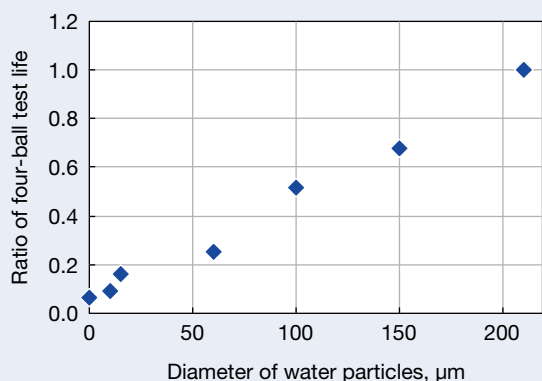

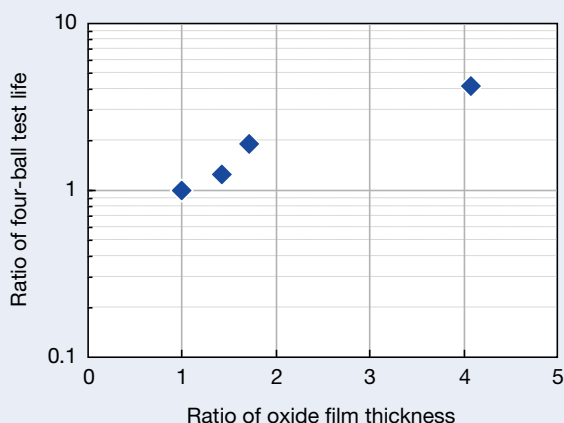Fig. 1 Correlation between water particle diameter and the ratio of life

Fig. 2 Correlation between oxide film thickness and the ratio of life

3.2 Low torque grease technology

Bearing torque is typically expressed by the formula (1) below, in which the viscosity term (the second term on the right side) becomes dominant in the high speed, low load region, and the load term (the first term on the right side) has a stronger impact in the low speed, high load region[3].

$$M = fWd_{m}(W/C_{0})^{c} + f_{0}\,d_{m}^{3}(vN)^{2/3} \qquad (1)$$

M: Bearing torque C_{0}: Static rated load
W: Load v: Lubricant viscosity
d_{m}: Diameter of bearing N: Rotation speed
     pitch circle f, f_{0}, c: Constant

Higher pre-load is applied to the hub-unit bearing to increase rigidity in addition to supporting the vehicle chassis while traveling. In addition, it may be used in a lower rpm region compared to typical bearings. Therefore, the load term is considered to be dominant for the torque of the hub-unit bearing, which means that selecting a grease with a superior friction property under lubrication would effectively lower torque.

The friction property of grease in the contact area is considered to be influenced by the friction property of oil film under a high surface pressure. Figure 3 shows the correlation between the viscosity-pressure coefficient and the traction coefficient of the base oil. The results show the traction coefficient increases with the viscosity-pressure coefficient. It can also be considered that the viscosity-pressure coefficient, as an index of the tendency to change viscosity as a result of a change in pressure, has a higher correlation with the traction coefficient due to a closer relationship with friction resistance in the contact area.

Selecting a base oil with a lower viscosity-pressure coefficient could be effective for reducing bearing torque under low speed, high load conditions.
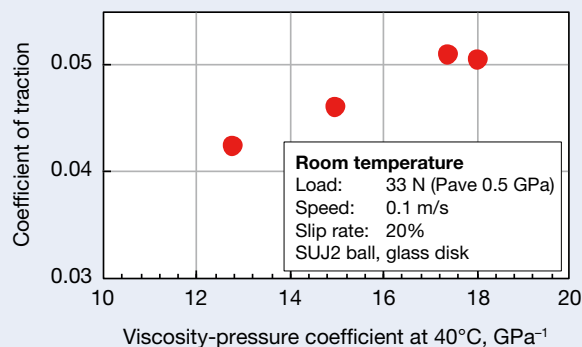

Fig. 3 Correlation between viscosity-pressure coefficient and coefficient of traction

4. Prototyping Grease and Results of Bearing Performance Evaluation

The results of the verification mentioned above were applied, and a grease (prototype) that would exhibit water resistance and reduce torque in the hub-unit bearing was prototyped. Water was separated to achieve a composition with a high tendency to form an oxide film in order to improve water resistance. A base oil with a lower viscosity-pressure coefficient was selected to lower torque.

Figure 4 shows the ratio of the friction torque of the hub-unit bearing. The ratio of the bearing friction torque is a ratio with the torque of the conventional grease as "1." It was confirmed that the torque became smaller for the prototype using the base oil with a lower viscosity-pressure coefficient under low speed, high load operating conditions.

Figure 5 shows the results of a bearing service life test under the condition of a water mixture. It was confirmed that the prototype extended bearing service life even with a water mixture, owing to a larger water particle diameter and achieving a composition with a strong tendency to form an oxide film.

5. Conclusion

The following facts were confirmed as a result of the performance evaluation of water resistance grease with extended service life while lower torque and a water mixture were taken into consideration.

- Enlarging water particle diameter in grease and achieving grease composition with a strong tendency to form oxide film extends bearing service life under the condition with a water mixture.
- Selecting a base oil with a lower viscosity-pressure coefficient lowers bearing torque under low speed, high load operating conditions.

References

1) K. Ueda, "Rolling Contact Fatigue Properties and Flaking Mechanism Under water Infiltrated Lubrication Condition," International Symposium on Rolling Elements Bearing, 2007.
2) N. Inami, S. Nakatani, J. Kuraishi, and A. Yokouchi, "Extension of bearing life by grease additives in a water containing condition," International Tribology Conference Hiroshima 2011 (2011) B2–06.
3) Japanese Society of Tribologists grease research meeting: Fundament and application of lubrication grease, Yokendo (2007) 122.

Fig. 4 Friction torque of bearing

Fig. 5 Bearing life test

Noriyuki Inami

Michita Hokao

Atsushi Yokouchi

Development of Bearing Units with Torque Sensors for Automotive Transmissions

Tohru Ueda and Tomoharu Saito
Future Technology Development Center

Abstract

A bearing unit with torque sensors that allows for smaller, lighter, and more efficient transmissions, such as automatic transmissions (ATs) and belt continuously variable transmissions (CVTs), has been developed. Pulse phase detection by two sensors and encoders is used for measuring torque from the torsion angle of the shaft in this development. The sensors are attached to the outer ring and the encoders are attached to the inner ring of the bearing. Due to the small relative displacement between the outer ring and inner ring of the bearing, a high-resolution torque measurement is achieved by reducing the gap change between the sensor and encoder while under the influence of torque and vibration. Furthermore, a compact design and simple harness structure for wiring makes it possible to position the two encoders next to each other on the encoder shaft and to mold the two sensors into one sensor case with the bearing.

1. Introduction

Fuel efficiency for transportation equipment has become critical due to the increasing urgency of environmental issues, such as global warming caused by the green-house effect of gas emissions, and energy challenges, such as the rapid depletion of fossil fuels.

Particularly in regard to the use of automobiles, despite the widespread application of more environmentally friendly technologies, such as HEV, EV, and high efficiency engines, the overall impact on the environment and energy is still severe due to the rapid expansion of automobile demand in developing nations. In addition, advanced nations are increasingly tightening fuel regulations[1, 2] and applying penalties for failing to meet fuel standards[1], and therefore making new technologies for further improvement of fuel consumption is a pressing task.

Automobile transmissions are required to be more compact and lighter while operating at a higher efficiency to improve fuel consumption. The majority of transmissions in the United States and Japan are automated components such as automatic transmissions (ATs) and belt-type continuously variable transmissions (B-CVTs)[3], for which improved efficiency has become critical. The step-type AT conveys driving power from the engine to wheels via planetary gears and changes speed by switching gears that transmit the driving power. The gears that transmit the driving power are selected and released by pressure contact and separation of a clutch using hydraulic pressure. On the other hand, a B-CVT conveys driving power via pulleys and belts and changes speed by changing the diameter of a pulley that contacts the belt by changing the distance of the pulleys that interface the belt. The pulleys are pressed against the belt by hydraulic pressure, similar to the clutch control of the step-type AT.

The insufficient hydraulic pressure that engages the clutch or the pressure that presses the pulley may cause slippage in the clutch or between the belt and pulleys, which results in a less effective transmission of driving power. However, excessive hydraulic pressure may cause a greater loss of energy at the pump that generates hydraulic pressure, which results in lower efficiency[4]. Also, higher hydraulic pressure settings require larger peripheral equipment such as bearings, and this creates a disadvantage for fuel consumption from the perspective of a more compact and lighter weight design. Consequently, hydraulic pressure must be as low as practicable within a range that avoids slippage for improving fuel consumption.

The optimal amount of hydraulic oil depends on driving torque. Hydraulic pressure must be set higher for greater torque and lower for smaller torque. Therefore, the optimal setting for the amount of hydraulic oil becomes feasible by enabling feedback on the accurate torque value to the hydraulic control with real-time detection, which may contribute to improving T/M efficiency as well as a more compact and lighter weight design.

Accurate torque value is also important information for engine control (E/G) and T/M control. Therefore, methods for measuring torque on the T/M shafts[5] and crankshafts of E/G[6] have been implemented. However, there is no actual example of practical application of torque sensors for T/M and E/G in mass-produced vehicles. NSK has started to develop a torque sensor for T/M and has mounted a sensor on the bearing inside a T/M for highly accurate torque measurement, although it is still at an experimental stage.

Here we introduce the most recent approach for T/M torque measurement[7–9] and the properties and performance of the newly developed bearing unit with torque sensor.
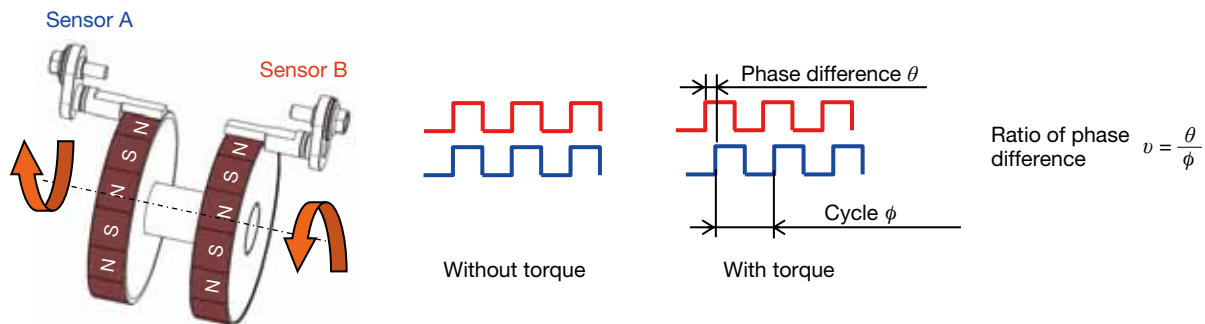
Fig. 1 Torque sensing mechanism

2. Measurement Principle

A pulse phase difference method was applied to measure torque for this effort. It uses hole sensors and magnetic encoders to measure torque based on the amount of torsion proportional to the torque. Figure 1 shows the principle of pulse phase difference torque measurement. In a typical pulse phase difference torque measurement, encoders are attached at both ends of the shaft and the sensors are placed at their respective positions facing the encoders. A pulse occurs when the N pole of the encoder passes right underneath the sensor as the shaft rotates. When encoders have been located at both ends with their phases aligned to the shaft, the sensors at both ends detect pulses with the same timing at zero torque and no shaft torsion; therefore, there is no phase difference. On the other hand, when the shaft is twisted by a generated torque, a pulse difference occurs according to the difference of the timing of the pulse detection of the sensors at both ends. The torque can be determined based on the phase difference since the phase difference, angle of torsion, and torque are proportional.

The hole sensor and the magnetic encoder are generally used to detect the wheel rotation speed of the hub-unit bearing with an ABS sensor, as shown in Photo 1[10]. This torque measurement represents the practical application of this technology.

Photo 1 Hub unit bearings with ABS sensors

3. Past Approaches to T/M Torque Measurement

NSK has developed a T/M torque sensor with two different structures (Units 1 and 2) for the purpose of evaluation. The counter shaft of an FF-car (front engine, front wheel drive) with a side-mounted engine was selected for measurement testing. We also selected the counter shaft, which is similar in many automatic transmissions for FF-cars with side mounted engines, because of its simple structure and relatively few components compared to other shafts.

3.1 Previously developed items: structure of Unit 1

Figure 2 shows the structure of Unit 1, which was the initial prototype. The Unit 1 encoders were simply mounted at both ends of the shaft for measurement, with sensors fitted on the aluminum test box (housing). In addition, when applying pulse phase difference torque measurement, higher shaft torsion improves resolution. In Unit 1, we increased torsion by decreasing the diameter of the central portion of the shaft within a range that would not result in breakage or plastic deformation.
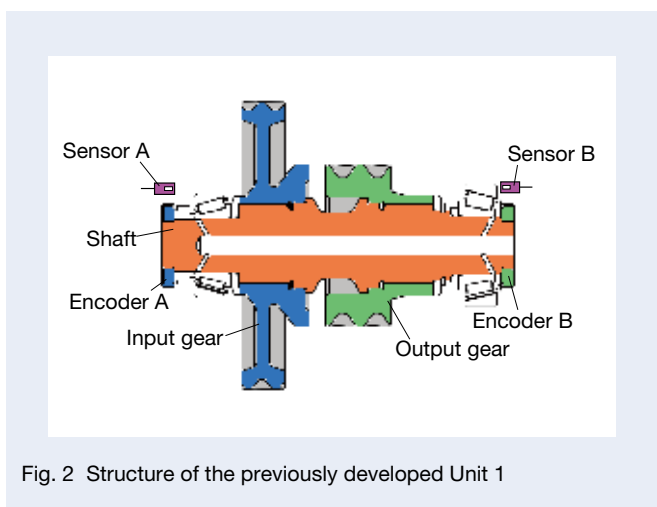

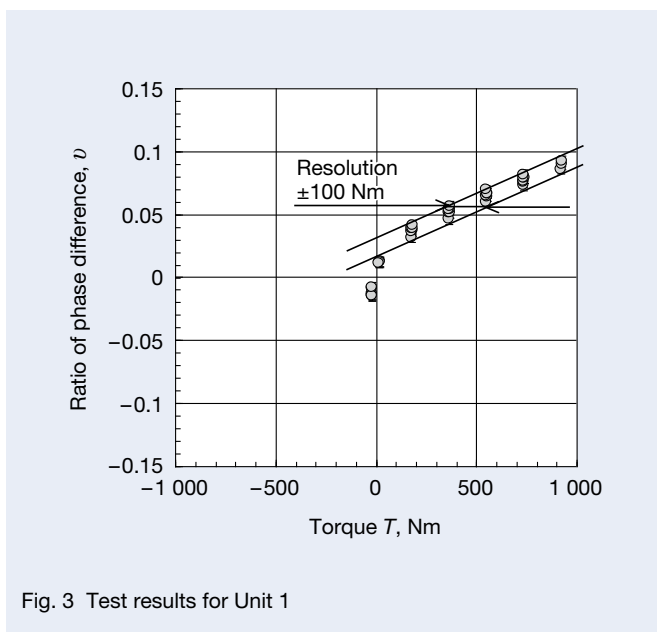Fig. 2 Structure of the previously developed Unit 1

Fig. 3 Test results for Unit 1

3.2 Previously developed items: evaluation results and discussion on Unit 1

Figure 3 shows the evaluation results of Unit 1. The horizontal axis in Figure 3 represents the value measured by a commercially sold torque gauge that is treated as a true value of torque, and the vertical axis represents the ratio of phase difference v (the value obtained by dividing the phase difference θ by the cycle of pulse ϕ) that was defined in Figure 1. Resolution was ±100 Nm (F.S. = 1 000 Nm), which means we were unable to achieve measurement with a sufficiently high accuracy.

Here are the reasons for reaching an insufficient resolution. The measurement value of the gain of Unit 1 obtained from the slope in the graph of Figure 3 was 7.02 × 10^{-5} (1/Nm). On the other hand, the gain obtained from the calculation of torsion of a simple shaft is 3.07 × 10^{-5} (1/ Nm). The actual measured value of gain was at least twice the calculated value, which indicates occurrence of a phase difference that is equivalent to or higher than the level of shaft torsion.

Figure 4 shows the reason that the actual measurement of gain became larger than the calculated value in the evaluation of Unit 1. As shown in Figure 4, encoders A and B at each end of the shaft are displaced in different directions against their respective sensors when the bearings at both ends of the shaft are displaced in different directions due to deformation of the aluminum test box as a result of the radial load applied to the bearings by the reactive force of gears. This means that a phase difference is generated to increase the measured gain due to the relative displacement of encoders A and B, even without any shaft torsion. Improving resolution therefore requires suppressing the generation of the relative displacement of two encoders due to deformation of the test box. In addition, as mentioned above, when applying pulse phase difference torque measurement, the larger the shaft torsion, the greater the improvement in resolution. Therefore, increasing shaft torsion may contribute to further improving resolution.

3.3 Previously developed items: structure of Unit 2

Using the results for Unit 1, we applied countermeasures to reduce any impact from deformation of the test box as well as any increase in shaft torsion. Figure 5 shows the structure of Unit 2, for which we placed the sensors and encoders that had been located at opposite ends of the shaft in Unit 1 at the same end to suppress impact from deformation of the test box. Encoder A, which had been located at the left end, as shown for Unit 1 in Figure 2, was relocated to the right side of the shaft on the encoder shaft parallel to encoder B. Displacement due to torsion at the left end of the shaft can be transmitted to encoder A, attached at the right end of the encoder shaft since the left end of the encoder shaft is fitted into the inner diameter of the left end of the input
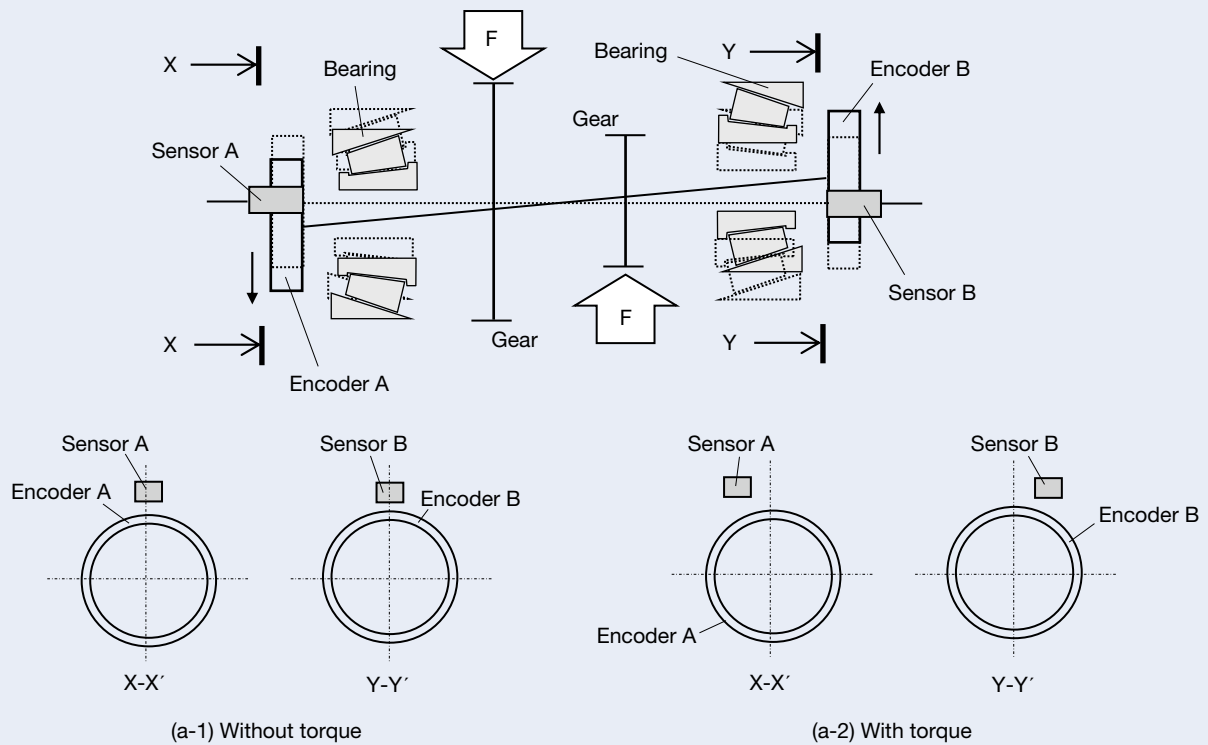
Fig. 4 Direction of relative displacement between the sensors and encoders caused by torque (Unit 1)

gear shaft. In addition, sensor A, located at the left end, was relocated to the right end parallel to sensor B, with both sensors integrated into a single enclosure. Having the sensors placed in parallel at the same end saved space and simplified the routing of the harnesses.

Figure 6 shows the reason that locating the sensors in parallel at the same end suppressed any impact from deformation of the test box. The parallel, same end layout of the two encoders, as shown in Figure 6, enables the direction and amount of deformation of the two encoders to be nearly identical from the deformation of the test box, even when the directions of the radial loads applied to the bearings by the reactive force of gears differs for the respective bearings at both ends of the shaft, similar to the case shown in Figure 4. Therefore, no phase difference is generated by any difference in the directions of deformation of the bearings at both ends since there is no relative displacement between the two encoders even when the test box is deformed. Moreover, the phase difference only indicates the amount of shaft torsion.
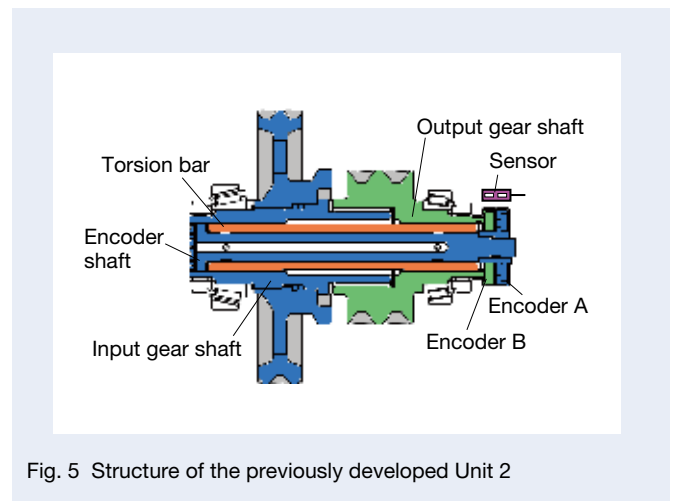
Fig. 5 Structure of the previously developed Unit 2

While we used an aluminum test box for this evaluation, aluminum T/M cases are typically used for actual T/Ms. In addition, recent T/M cases tend to be designed with thinner walls to reduce weight, making it imperative to develop countermeasures to reduce the impact of case deformation on measuring torque in actual T/Ms.

For a method for increasing torsion, we adopted a structure in which the gear shaft is divided into an input gear shaft and an output gear shaft, connected by a torsion bar, as shown in Figure 5.

3.4 Previously developed items: evaluation results for and consideration of Unit 2

Figure 7 shows the evaluation results for Unit 2. The resolution is ±27 Nm (F.S. = 1 000 Nm), an improvement of nearly four times the resolution shown in Figure 3. Table 1 compares the gain obtained from the measurement results shown in Figure 7 and that obtained from the calculated value of shaft (torsion bar) torsion, relative to Unit 1. Table 1 shows that the measured and calculated values of gains for Unit 2 are almost the same. For Unit 2, this means that the generation of a phase difference as a result of relative displacement between the two encoders caused by the deformation of the test box is suppressed, and that torsion is the sole contribution to a phase difference. In addition, for Unit 2 it can be observed that the measured value of gain is increased and the amount of shaft torsion is higher than that for Unit 1, even though the increase of gain caused by deformation of the test box is suppressed.

Figure 7 shows that a dead zone exists near zero torque, which is caused by a gap at the spline joint between the torsion bar and the gear shaft. The dead zone can be eliminated by closing the gap.
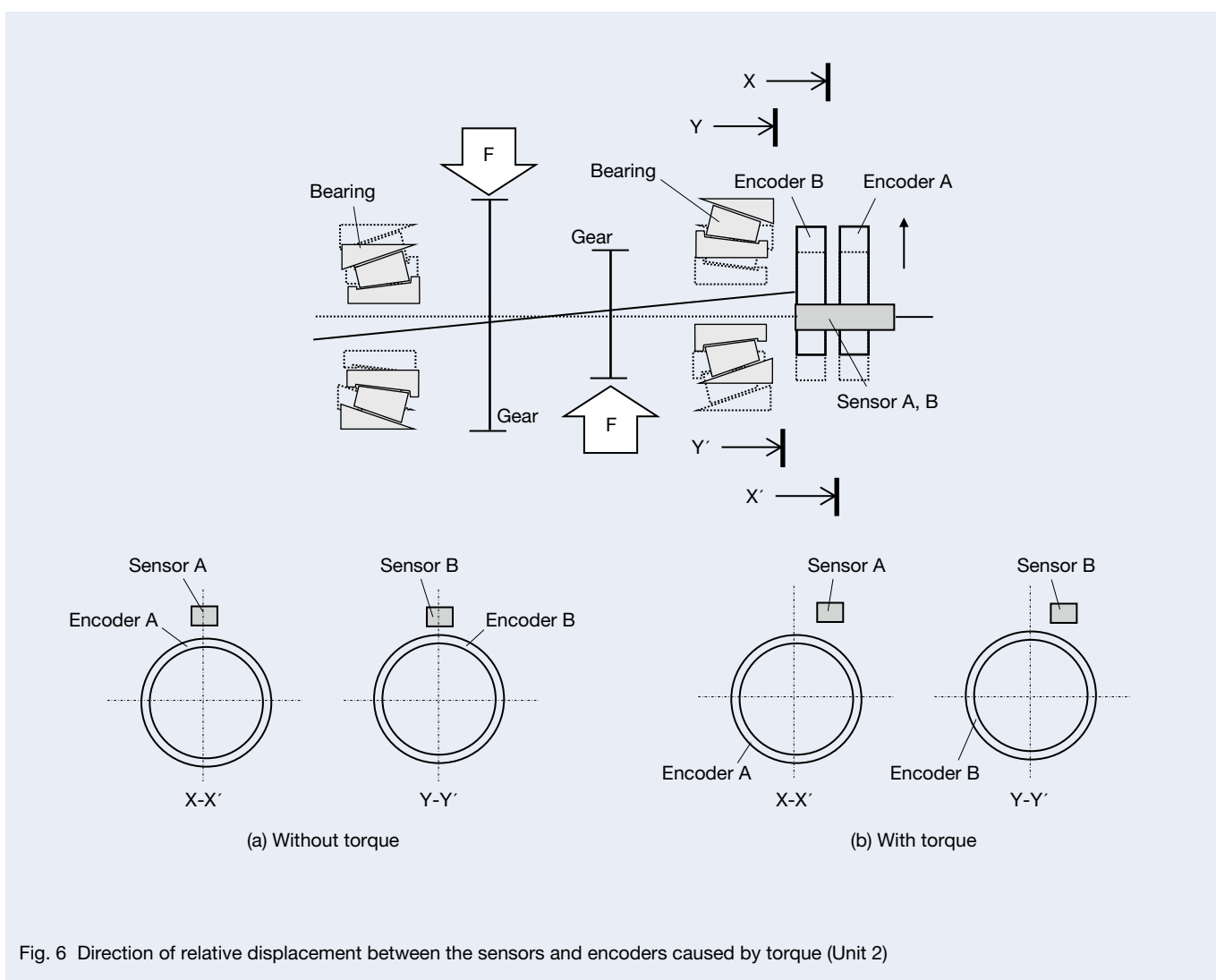

Fig. 6 Direction of relative displacement between the sensors and encoders caused by torque (Unit 2)

4. Features and Results of the Performance Evaluation of the Bearing Unit with a Torque Sensor

4.1 Features of the bearing unit with a torque sensor

Previously developed item: Based on the evaluation results for Unit 2, it has been clarified that a higher resolution measurement is possible when shaft torsion is larger. Nevertheless, it is difficult to ensure that shaft torsion in actual T/Ms will be the same as that for Unit 2 from the perspectives of strength and rigidity. In addition, the structure of Unit 2 using the torsion bar would increase the number of parts and lead to higher costs in actual implementation. Therefore, measuring torque at higher levels of shaft torsion is not practical.

It was imperative for a pulse phase difference torque measurement to improve sensing performance in order to measure torque with high accuracy using a shaft with lower torsion. Therefore, we dramatically improved sensing performance by reviewing sensor and encoder specifications for the newly developed product.

Figure 8 shows the structure of the new product. We used the same concept of parallel, same-side sensors and encoders that was applied to Unit 2 for the new product. We did this to provide it with a structure that would endure the impact of T/M case deformation and to save more space and simplify harness routing. In addition, assembling the sensor enclosure and the encoder on the outer ring and inner ring, respectively, of the rolling bearing with superior dimensional accuracy and less relative deformation between the inner and outer ring reduced fluctuation of the sensor gap and facilitated detailed management of the gap. While two sensors are integrated into a sensor enclosure attached to the outer ring, the design of the structure takes into account the need to prevent fluctuation in the distance between the two sensors due to temperature change and oil resistance in order to realize high accuracy torque measurement under actual T/M operating conditions.

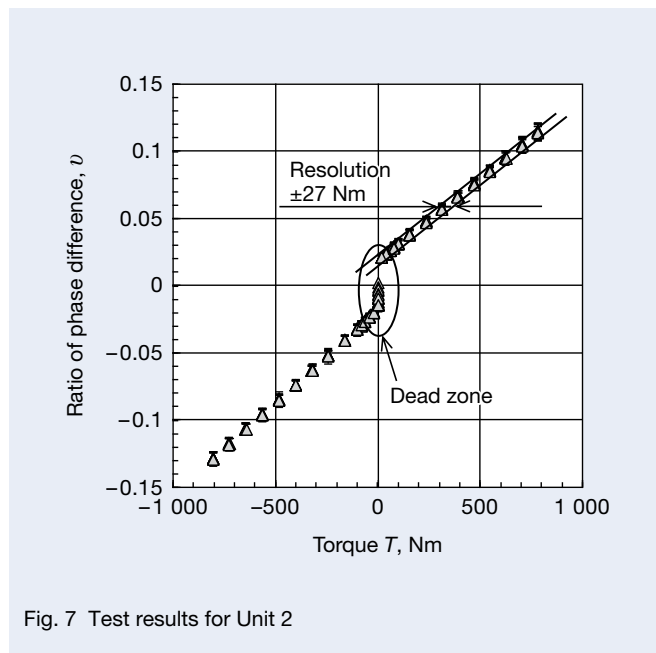Fig. 7 Test results for Unit 2
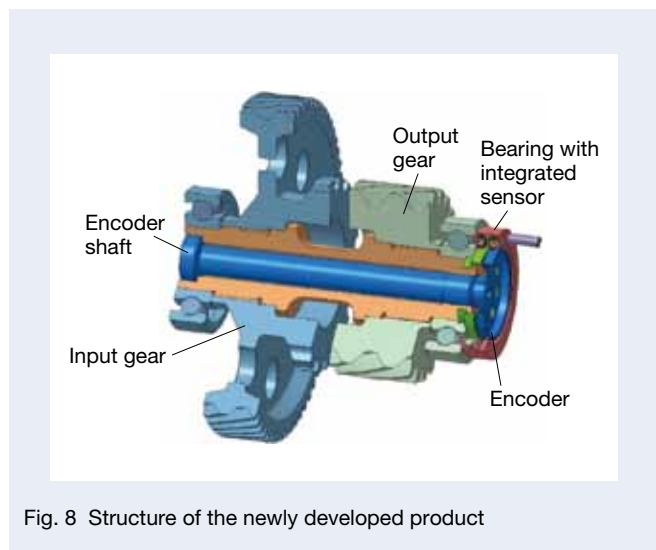

Fig. 8 Structure of the newly developed product

Table 1 Comparison of sensor gain between Unit 1 and Unit 2

	Unit 1	Unit 2
Measurement value of gain × 10^{-5} (1/Nm)	7.02	11.9
Calculated value of gain × 10^{-5} (1/Nm)	3.07	11.5

4.2 Evaluation method

Figure 8 shows the structure of the test rig and new product used for evaluation, and Figure 9 shows a cross-sectional diagram of the test box with the unit attached. The tester was a typical dynamo meter, on which the drive motor, the input side torque gauge, the test box, the output side torque gauge, and the load motor were placed in the proper sequence. The torque sensor unit was installed at a location where speed was reduced from the motor shaft and was structured in a manner that allowed for an increase of speed again after the driving power passed the sensor shaft to be returned to the motor shaft. The sensor shaft was designed with an allowable torque of ±1 000 Nm.

Rotation speed of the test shaft was set at 900 rpm, assuming the speed of the counter shaft of the C-segment vehicle driving at 30 km. Transmission oil was supplied at the rate of 5 l/min to lubricate the gears and bearings in the test box. Oil temperature was not controlled and was naturally between 55°C and 75°C at the exit of the box. We obtained data for the low torque zone in an interval of 20 Nm within a range of –100 through 100 Nm, and data for the high torque zone in an interval of 100 Nm within a range of –800 through 800 Nm. We reciprocally measured both the low and high torque zones three times to set the resolution as ±3σ of variation (three times the standard variation) from the least squares approximation line of the correlation of the torque measurement value of commercially sold torque gauges, regarded as a true value, and the measured torque value (ratio of phase differences).

4.3 Results of the performance evaluation for the bearing unit with a torque sensor

Figure 10 shows the results of torque measurement of the new product. Figure 10 (a) shows the results in the low
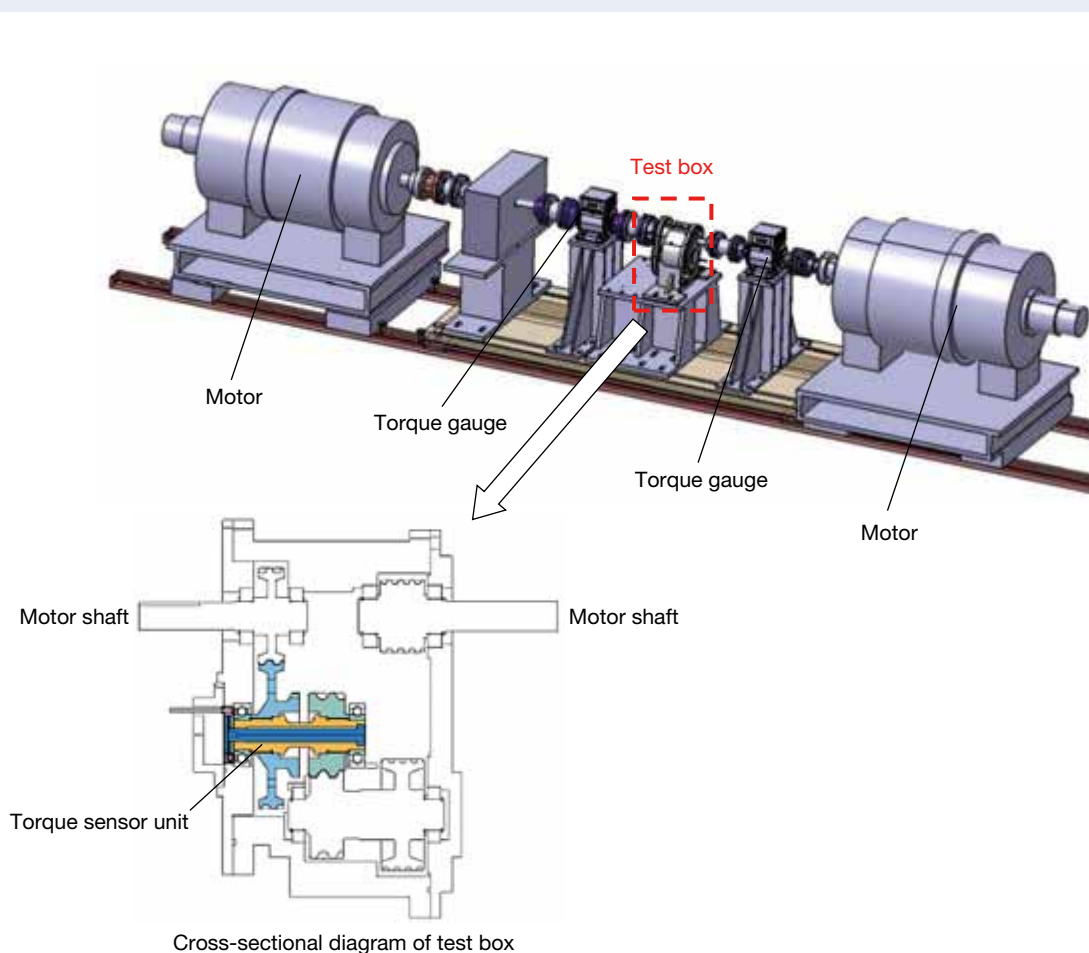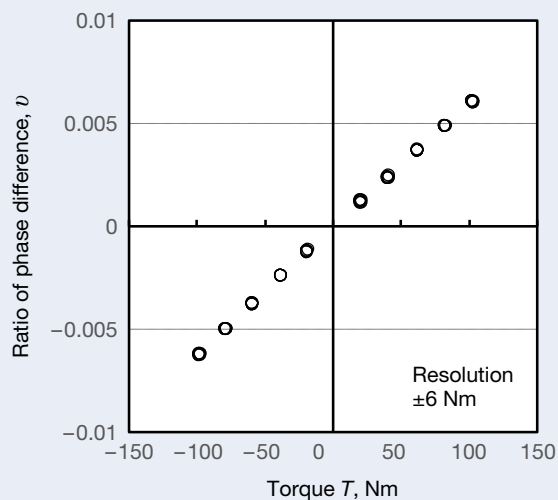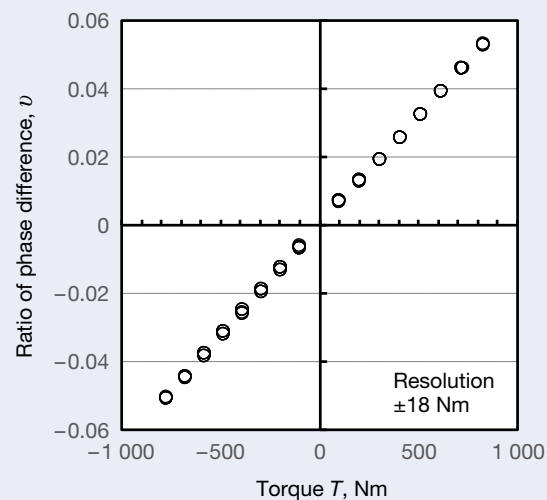

Cross-sectional diagram of test box

Fig. 9 Test rig for the transmission torque sensor

(a) Low torque zone (up to 100 Nm)

(b) High torque zone (up to 800 Nm)

Fig. 10 Test results for the newly developed product

torque zone, and Figure 10 (b) shows the high torque zone. As shown in Figure 10, we have achieved a resolution of ±6 Nm (F.S. = 1 000 Nm) for the low torque zone at or below 100 Nm, and that of ±18 Nm (F.S. = 1 000 Nm) even for the high torque zone up to and including 800 Nm. We presume that the high torque zone showed a degraded resolution compared to the low torque zone because of the run out of the encoder shaft on which the encoder is mounted in line with the tendency for a higher torque to generate greater test box vibration.

As shown in Figure 10, higher resolution torque measurement was enabled even in the shaft, without an excessively large level of torsion, through a structural fabrication that improved torque sensor sensitivity through integration with the bearings. This means that assembling a bearing with an integrated sensor + encoder and a shaft with an encoder onto a T/M shaft actually used in the market may enable us to realize higher accuracy torque measurement. We believe that the product we have developed is feasible since it enables torque measurement without any drastic structural change in the T/M and without any increase in the number of components.

5. Conclusion

NSK has developed bearing units with torque sensors that contribute to improving the efficiency of automated transmissions, such as step type ATs and B-CVTs. We expect that optimizing the pressure of pulleys and engagement of a clutch with hydraulic pressure will enable a driving power transmission with less loss based on the accurate torque value measured by the sensor. The torque sensor unit developed by NSK has the following features.

1. Torque measurement accuracy was improved by simplifying gap management between the sensors and encoders as well as by reducing relative deformation between the sensors and encoders caused by vibration and torque fluctuation by installing the sensors and encoders on the bearings.
2. The parallel layout of two sensors and encoders at one end of the shaft saved space and simplified harness routing.
3. We have achieved a resolution of 6 Nm within the low torque zone (up to and including 100 Nm) and of 18 Nm within the high torque zone (up to and including 800 Nm) with the structure described above (F.S. = 1 000 Nm).

Looking ahead, we will strive to achieve a practical application of the sensor described here by reviewing their responsiveness, oil resistance, durability, temperature property, and robustness.

References

1) "Current situation and forecast of market relating to electric automobiles 2015," (2015) 4, Fuji Keizai, Co., Ltd.
2) S. Furuno, "Global enhanced gas emission regulations and corresponding power train technology," Automobile technology, 67–9 (2013) 6–13.
3) "Motor Fan illustrated Transmission Bible," (2012) 26–27, San-ei Shobo.
4) M. Yoshida, K. Imai, H. Seiya, O. Sawada, and H. Yamashita, "Development of Large Capacity CVT Chain," Latest Technology of Power Train System 2013, (2013) 1–5.
5) Y. Fuji, R. Hogirala, and T. Greene, "MDI Magneto-Elastic Torque Sensor for Automatic Transmissions," 4th CTI-Symposium Automotive Transmissions North America, (2010).
6) Y. Seibu, H. Nonomura, A. Tsukada, S. Takeuchi, and T. Okumura, "Magnetic Torsion Torque Sensor for Automobile Engines," Toyota Chuo R&D Review, 31–2 (1996) 61–71.
7) T. Ueda, T. Saito, and T. Takehara, "Development of torque sensor unit for automatic transmissions," Monthly Tribology, 320 (2014), 18–20.
8) T. Ueda and T. Saito, "Development of torque sensor unit for transmissions," Paper for an academic lecture, 142–14 (2014).
9) T. Ueda and T. Saito, "Development of Torque Sensor Unit for Transmissions," Latest technology of power train system 2014, (2014) 6–10.
10) J. Sakamoto, "Trends and New Technologies of Hub Unit Bearings," NSK Technical Journal, 677 (2004) 2–10.

Tohru Ueda

Tomoharu Saito

Development of Automotive Transmission Thrust Needle Roller Bearings with Integrated Washer and Oil Flow Control

Masaki Sadamura and Yutaka Kondo
Automotive Bearing Technology Center

Abstract

Recently, further improvements of fuel consumption have been requested by automotive companies due to the strengthening of global environmental regulations and the rise of environmental awareness. For instance, in the case of transmissions, reducing weight, increasing compactness, decreasing torque loss, and optimizing the quantity of lubrication oil are ongoing goals.

Especially in automatic transmissions (ATs), control of the circulating oil flow enables reductions of stirring resistance and oil pump size. Therefore, demand has been increasing for oil flow control in AT components, including bearings.

In addition, a number of thrust needle bearings are used in ATs, and so demand has been growing for integrated thrust needle bearings to reduce assembly man-hours and improve work efficiency.

NSK has made improvements in the oil flow of thrust needle bearings used in automobile transmissions (especially ATs) to meet these demands. As a result, it has developed a thrust needle bearing with twice the amount of oil penetration (oil flow control) as a conventional product.

1. Introduction

Automotive companies have been asked to improve fuel consumption in the face of tightening environmental regulations worldwide and increasing public awareness of the environment.

For example, there is a growing trend to use higher efficiency transmissions, for which there have been advancements through efforts such as reducing size and weight, lowering torque loss, and optimizing lubrication volume. Demand has also increased for transmission bearings that are lighter, smaller, and with a decreased torque loss[1–4].

For automatic transmissions (ATs) in particular, controlling the oil flow inside allows for downsizing the oil pump and reducing agitation resistance. Demand has subsequently grown for oil flow control in AT components as a means of supplying optimal oil flow with the right volume to the right section.

Also, a number of thrust needle bearings are used in ATs (about seven bearings in FF types and ten bearings in FR types), and this is driving demand for the use of thrust needle bearings to control oil flow[1–3].

Demand is also growing for integrated thrust needle bearings (roller, bearing ring, and cage) to reduce labor and improve assembly line productivity for thrust needle bearings used in transmissions.

Here we report on a newly developed integrated thrust needle bearing with improved oil flow (penetrating amount of oil) compared to previous products.

2. Significance of the Integrated Thrust Needle Bearing with Oil flow Control

Photo 1 shows the external appearance of the new product. We have approximately doubled the penetrating amount of oil compared to previous products and achieved a 20% improvement in the internal radial clearance of the bearing, thereby contributing to improve the durability in regard to the breakage by eccentricity (radial offset) (Figures 1 and 2). These results were achieved by reviewing the following aspects of previous products.

2.1 Oil flow control by optimal design of a washer and cage

(1) Washer shape

We have achieved a structure with a larger opening area, which allows for smooth oil flow into the bearings, by reviewing and changing the washer profile from a full circumference bending (full curl construction) to a partial circumference bending (partial curl construction) (Figure 3).

(2) Cage shape

We adopted a structure that allows for smooth oil flow inside the bearings by narrowing the cage width in the axial direction and by adding small holes to cage pockets (Figure 4).

2.2 Improved the durability in regard to the breakage by eccentricity

We adopted a structure that partially retains bearing components (roller, washer, and cage) after reviewing and changing the shape of the curled section of the washer from a full circumference bending (full curl construction) to a partial circumference bending (partial curl construction) (Figure 3). As a result, we improved the internal radial clearance of the bearing to effectively improve the durability in regard to the breakage by eccentricity (radial offset), a common issue with integrated-style thrust needle bearings (Figure 2).

Photo 1 Thrust needle roller bearing with integrated washer and oil flow control

Test conditions
Oil: AT oil
Oil temperature: 80°C
Oil pressure: 5 kPa

Newly developed product

Conventional product

Combination of washer and cage with modified shapes doubles penetrating amount of oil compared to the previous product at low speeds
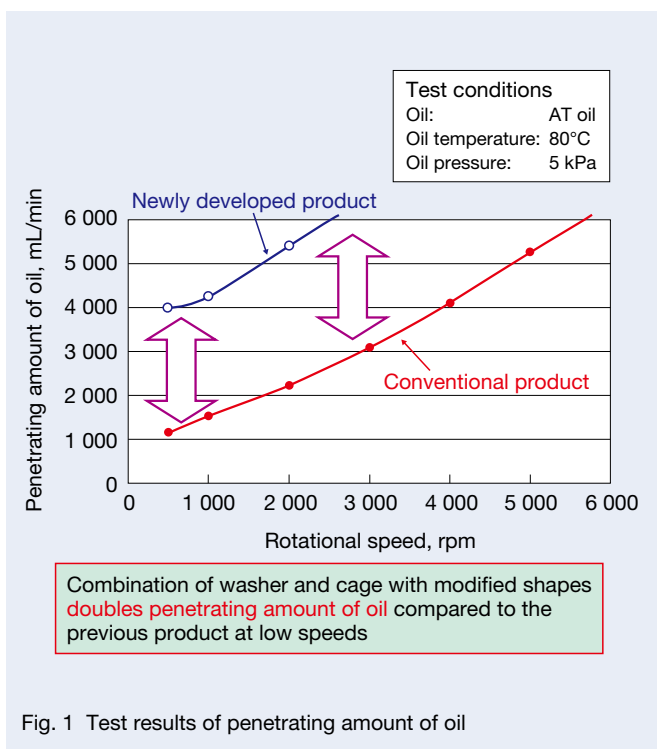
Fig. 1 Test results of penetrating amount of oil

Change from the conventional full curling to partial curling increases the amount of elastic deformation at the curl section, realizing an increased inner clearance.

Conventional product:
Full curl method

20% increase in inner clearance

Clearance of conventional product

Newly developed product:
Partial curl method

Clearance of newly developed product

(In regard to the breakage by eccentricity) Tolerance to shaft deviation improved by 20% owing to increased internal radial clearance
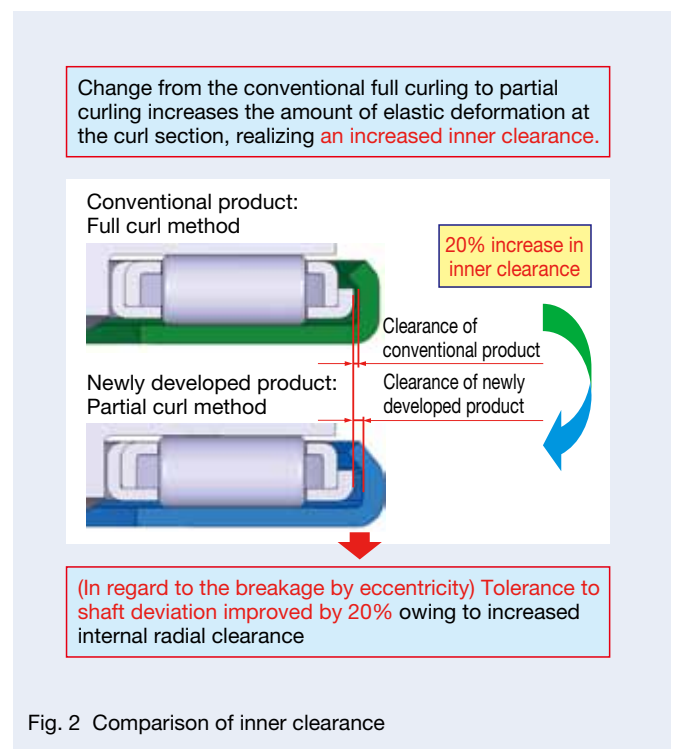
Fig. 2 Comparison of inner clearance

3. Examples of Application with ATs

The major AT components are shafts, clutches, brakes, and planetary gear mechanisms[3]. These components exhibit a relative rotation due to the difference in respective rotation speeds depending on the gear change stage, and this necessitates the use of a bearing that supports an axial directional load: a thrust needle bearing[3].

In addition, inside the AT, automatic transmission fluid (AT oil) is circulated as a hydraulic oil to operate clutches and brakes for changing gears, functioning as a lubricant to prevent heat seizure of rotating parts and as a coolant oil to reduce heat generated by components such as clutches, brakes, and torque converters. AT oil is mainly supplied from the shaft center and often passes through thrust needle bearings to reach the components. Therefore, an imbalance of oil flow in the thrust needle bearings disrupts the smooth supply of an adequate amount of oil to components such as clutches and brakes[3] (Figure 5).

This bearing enables the flow of an adequate amount of oil to the most suitable section, up to approximately double the amount of AT oil compared to previous products, by switching from the thrust needle bearings that have been traditionally used (Figure 5).

| Conventional bearing washer: Full curling | Newly developed product washer: Partial curling |

Fig. 3 Partial curling of the new bearing washer and full curling of a previous bearing washer

Conventional cage

Newly developed cage
Small holes
Narrowed cage width

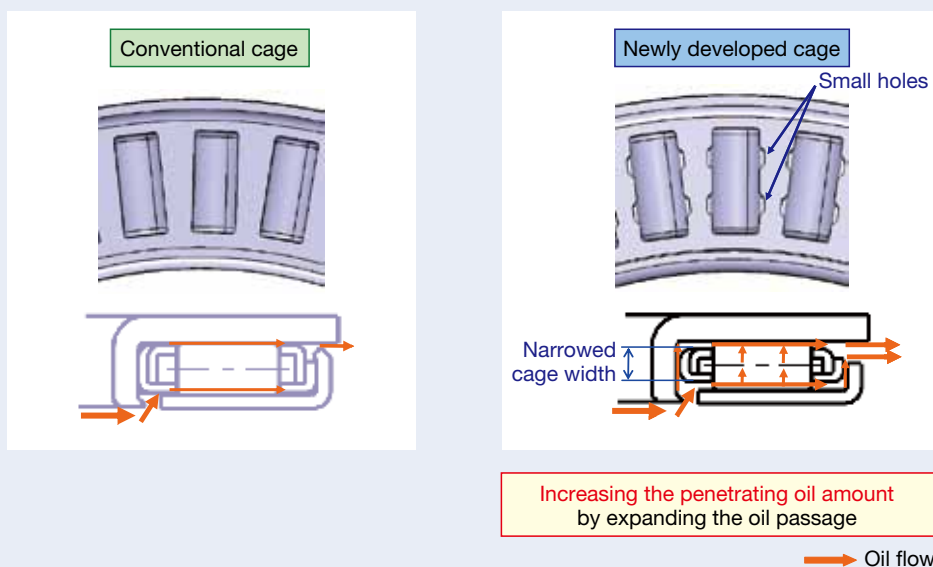Increasing the penetrating oil amount by expanding the oil passage

→ Oil flow

Fig. 4 Comparison of the amount of oil penetrating through a conventional cage and the newly developed cage
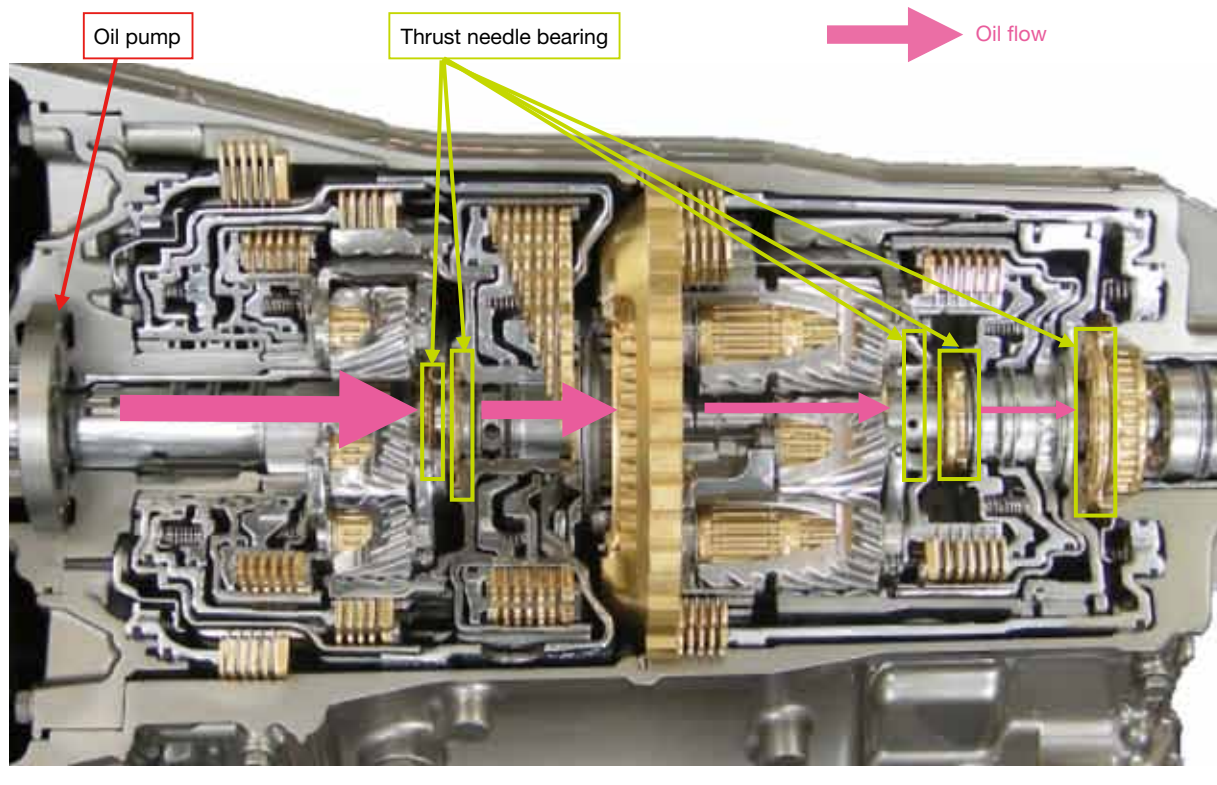
Fig. 5 Oil flow in an automotive automatic transmission

4. Conclusion

We have developed an integrated thrust needle bearing that can be used to control transmission oil flow. The bearing can allow for downsizing of oil pumps while ensuring that an optimal amount of oil flows to the appropriate section. This reduces component agitation resistance, and it also improves work efficiency by reducing the numbers of components and assembly labor hours as a result of integration in the transmission.

We look forward to meeting more user needs with this product.

References

1) T. Ootsubo and S. Kadokawa, "Trends and New Technologies of Automatic Transmission Bearings," NSK Technical Journal, 677 (2004), 46–53.
2) S. Masuda, H. Takemura, and Y. Shimizu, "Development of Thrust Needle Roller Bearing with Wear-Resistant & High-Strength Cage," NSK Technical Journal, No. 680 (2006), 42–47.
3) T. Ohno and H. Takemura, "Development of World's Thinnest Drawn Cup Needle Roller Bearings with Seal Ring—The Need for Improved Fuel Economy and the Application of Needle Roller Bearings," NSK Technical Journal, No. 684 (2010), 22–26.
4) K. Yamamoto and H. Takemura, "Development of Long-Life Planetary Shaft (SHX3 Steel) for Planetary Gears of Automotive Transmissions," NSK Technical Journal, No. 686, (2013) 52–57.

Masaki Sadamura

Yutaka Kondo

Development of Low-Friction Grease for EPS Worm Reduction Gear

Haruhiko Kiyota, Tetsuya Koike, and Takeshi Yamamoto
Steering R&D Center

Abstract

Electric power steering (EPS) systems are environmentally friendly products that help to improve the fuel economy of vehicles. EPS saves power as its motor rests when the vehicle is traveling straight. It offers intricate electronic control of its motor in response to various inputs, such as travel speed and road conditions, and thus provides a safer and more comfortable steering feel.

Smooth vehicle movement as the driver begins to turn the steering wheel and smooth steering wheel return are critical for achieving a comfortable steering feel. EPS friction is a key element in creating this smoothness, especially the friction of the reduction gear. NSK has developed an improved lubricity for a low-friction grease that avoids low-temperature fluidity deterioration in the reduction gear. Additives are incorporated in the grease to prevent an increase in viscous drag. The newly developed low-friction grease reduces the friction force of the reduction gear and thereby reduces the steering effort for the driver and improves the steering feel.

1. Introduction

The NSK Group has developed and manufactured an electric power steering (EPS) system as an environmentally friendly product that improves the fuel economy of vehicles as a means of protecting the environment (Photo 1).

Figure 1 provides an overview of a steering system using a column-type EPS. The basic configuration of this system consists of a torque sensor that senses the steering maneuver of the driver and vehicle motion transmitted from the tires, an ECU that calculates assisting force in accordance with the torque signal from the sensor, a motor that generates torque in accordance with ECU output, and a worm reduction gear that reduces and transmits the motor torque to the steering mechanism. This is a speed-sensitive EPS that takes into account vehicle speed and engine rotation data transmitted by the vehicle to the ECU[1].

While the EPS does consume low-level, stand-by power for sensing when the vehicle is travelling in a straight line with steering in neutral, no additional power is used until the electric motor for assisting steering force is engaged. This represents in improvement in fuel consumption compared to hydraulic power steering units that require constant hydraulic pressure, even when traveling in a straight line. It also affords a safe, comfortable steering feel for drivers due to the fine electronic control of the ECU in accordance with its sensing of the torque, speed, and frequency transmitted from the tires and vehicle engine correlating with travel speed and road conditions.

Steering force, however, is applied solely by the driver from the moment the driver begins turning the steering wheel until assisting torque is generated. This means that the mechanical friction of the mechanism significantly impacts the feel of steering in the range of movement before the electronic control applies effective motor assistance (Figure 2).

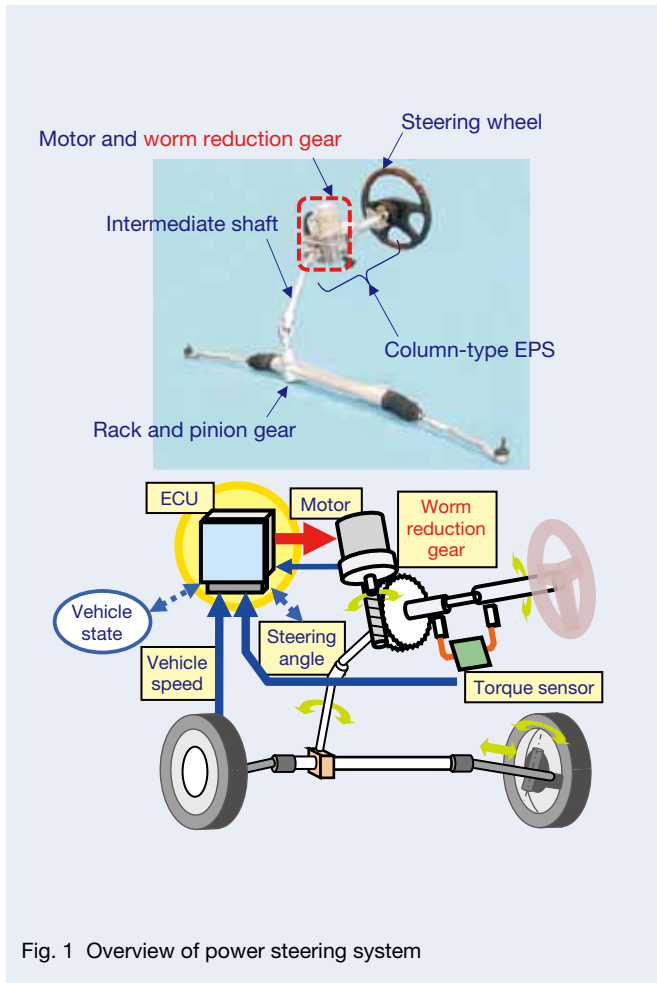Photo 1 Column-type electric power steering

Fig. 1 Overview of power steering system

Labels in Fig. 1: Motor and worm reduction gear; Steering wheel; Intermediate shaft; Column-type EPS; Rack and pinion gear; ECU; Motor; Worm reduction gear; Vehicle state; Vehicle speed; Steering angle; Torque sensor

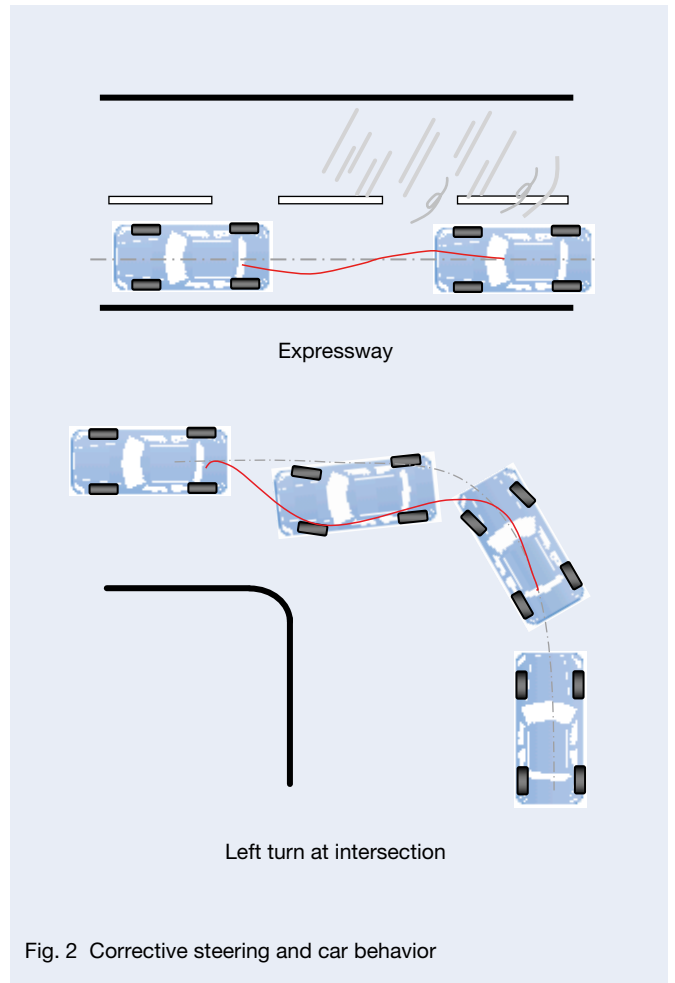
Expressway

Left turn at intersection

Fig. 2 Corrective steering and car behavior

- A sense of friction when the steering wheel is in a neutral position (during subtle steering corrections on sections of a straight road, such as on an expressway)
- A sense of friction when returning the steering wheel to its neutral position (the point at which the steering wheel automatically recovers to straight forward movement after having turned to the left or right, such as at an intersection)

NSK is working on an approach that affords an even more comfortable feel by reducing friction across the entire steering system, including that generated by the motor and worm reduction gear.

Here we introduce our development of a low-friction grease that improves lubrication at the gear teeth surface of the worm reduction gears, a core EPS component.

2. Characteristics of the EPS Worm Reduction Gear

NSK uses a worm reduction gear in the EPS because it is compact and provides a high reduction ratio for EPS (Figure 3). The wheel gear of the worm reduction gear is arranged on the steering wheel shaft that is moved by the driver, and the worm gear is directly connected in series to the motor shaft. In this configuration, motor torque assists the steering wheel shaft with a high torque reduced by the worm reduction gear. For the wheel gear, a resin material is used for quieter performance and a lower friction coefficient when gears are engaged, and steel is used for the worm to ensure strength (Photo 2).

The EPS is subject to repeated left and right turns as well as cyclic vibration applied to the wheel shaft from the tires due to uneven road surfaces. Since the gear is subject to conditions requiring continuous reversing, it can produce rattling and banging noises. To counter this tendency, the gears are assembled without any backlash.

Lubrication on the faces of the gear teeth engaged with
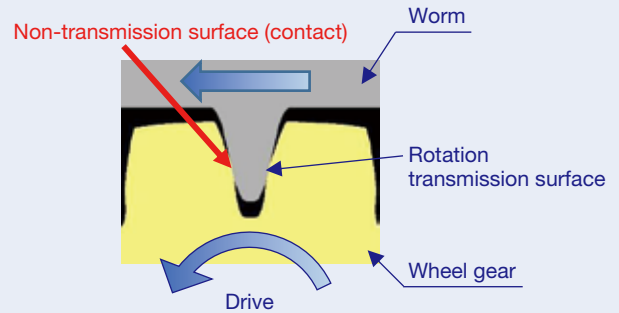
Fig. 3 Worm reduction gear

Fig. 4 Engagement contact of the worm reduction gear for EPS

the worm reduction gear involves a sliding lubrication in two directions of a flank line and a profile line, and a rolling lubrication at intermeshing datum height, which comprises a composite lubrication condition. The lubrication condition on teeth surfaces continuously changes, even under a steady rotational speed, and these changes repeat with each engagement. In addition, the impact of sliding motion in two directions as the major factor for this lubrication, along with the high gear reduction ratio, results in a higher sliding speed. Also, as already mentioned, the assembly has no backlash, and so the gear teeth opposite to the direction of rotation transmission also come into contact, as shown in Figure 4, which increases the likelihood of friction.

Photo 2 Configuration of the worm reduction gear for EPS

3. Features of Grease for the EPS Worm Reduction Gear

Automobiles are driven under conditions ranging from temperatures as high as an engine room to frigidly cold climates and therefore vehicle operating life must be taken into consideration. The properties of a grease suitable for such conditions must include durability, environmental resistance (high and low temperatures), high efficiency, and low resin corrosiveness. Therefore, the types of grease that have been adopted are composed with urea thickener, composite carbon hydride oil, and wax additives.

Conventional grease can exhibit a mixed lubrication state for lubricating the surface of gear teeth. Mixed lubrication involves a partial solid contact and lubrication with fluid oil film in other areas. However, the grease for the EPS worm reduction gear is subject to greater friction in room temperature due to the larger percentage of solid contact caused by the relatively lower viscosity of the base oil, which is intended for maintaining fluidity under low temperatures.

4. Goal of Low-Friction Grease

Lowering friction requires lowering the proportion of solid contact and securing adequate oil film on teeth surfaces. The general method includes securing oil film by increasing the viscosity of the base oil, which may simultaneously be subject to decreased fluidity under cold temperatures.

In this context, we examined a grease containing an additive that exhibits properties of a base oil without having to change the base oil itself. We did this so that an additive would support the oil film and decrease the solid contact of the mixed lubrication to reduce the friction coefficient.

Figure 5 shows a conceptual diagram of the behavior of grease in each lubrication state. The additive in the developed grease supports the base oil to prevent contact in areas likely to present a solid contact between both surfaces of gears in a mixed lubrication state. However, the additive does not exhibit this effect and does not disrupt fluidity since gear surfaces are not close to each other in the fluid lubrication zone. Therefore, there is less deterioration in fluidity other than an increase in the viscosity of the base oil under low temperatures. On the other hand, in a boundary lubrication state, in which a high load is applied, while the additive has no effect due to the absence of base oil on teeth surfaces, the wax provides some level of lubrication.

This means that we have developed a grease that achieves a lower friction coefficient under mixed lubrication conditions and maintains the same level of viscous drag during fluid lubrication, realizing low friction under all EPS operating temperature ranges.
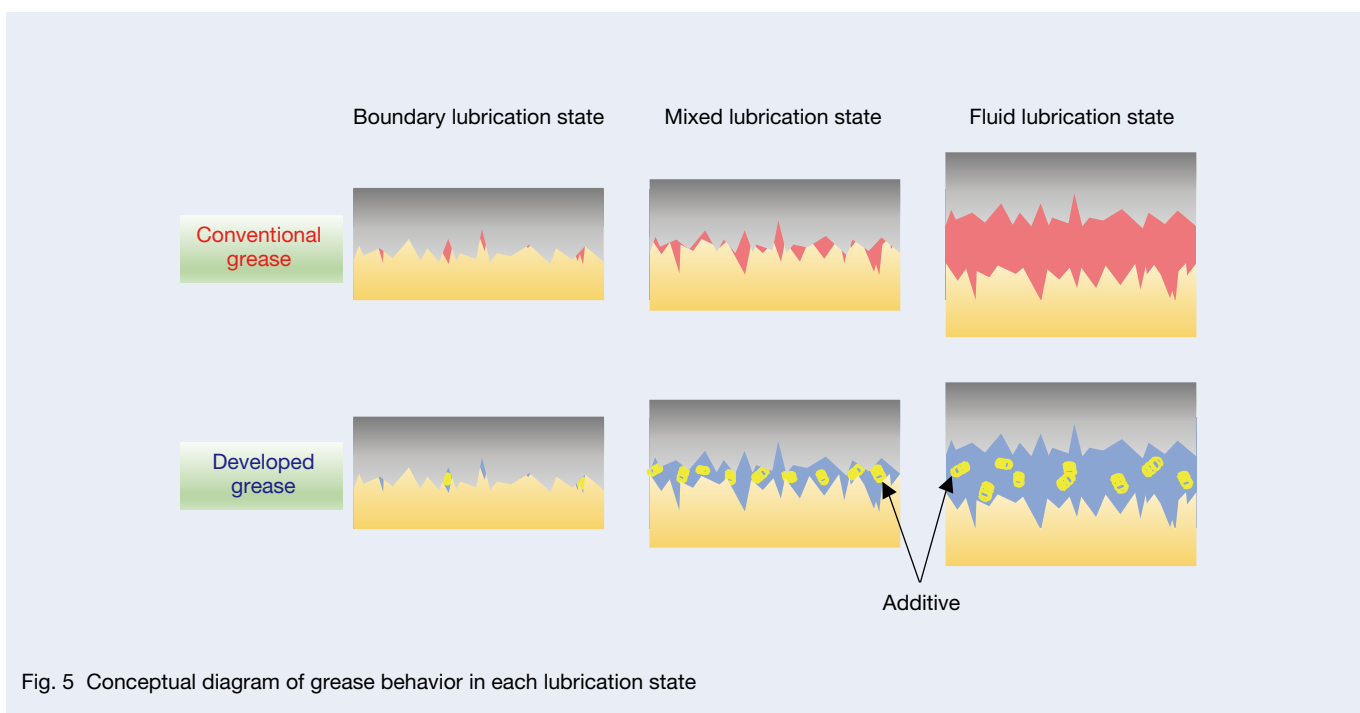

Boundary lubrication state   Mixed lubrication state   Fluid lubrication state

Conventional grease

Developed grease

Additive

Fig. 5 Conceptual diagram of grease behavior in each lubrication state

5. Verification of Friction Reduction Effect

5.1 Definition of friction

Friction in the development is defined as rotational torque during the reversed action of the worm reduction gear driven by the wheel shaft.

5.2. Method of experiment

Since the low friction grease was applied to lubricate gear tooth surfaces, we disconnected other EPS components, such as the motor, to avoid any impact from their rotational torque and left the worm in a corotation state. In addition, under ideal conditions, while friction should only be checked for gear surfaces, removing the bearings that support the gears is difficult. Therefore, the friction evaluated here is based on a combined rotational torque of the worm reduction gear unit and the bearings (Figure 6).

The specifications of sample worm reduction gears used for this test are shown in Table 1. To avoid individual variability, rotational torque was measured on both gears by first applying a conventional grease and then washing the gears and applying the developed grease. In addition, the pitch between the wheel gear and worm shaft was maintained at a constant distance for all tests.

Table 1 Worm reduction gear sample

Number of wheel gear teeth	37, 41
Number of worm threads	2
Gear ratio	18.5, 20.5
Wheel gear material	PA66GF25
Worm material	S45C

5.3 Experiment results and effect

5.3.1 Effectiveness for reducing rotational torque

Given the impact of velocity on grease viscous drag and oil film formation, we measured rotational torque at different rotational speeds. The results shown in Figure 7 indicate that rotational torque using the developed grease decreased at every rotational speed compared to the conventional grease, which confirms the effect of reduced friction. While this level of performance was about the same for 4 rpm and 10 rpm, the difference was relatively less at 1 rpm. This is because low speeds tend to inhibit oil film formation, as evidenced by the Stribeck curve in Figure 8, as a result of additives being less effective at a rotational speed of 1 rpm (Figure 8, A). On the other hand, it can be considered that the existence of abundant regions capable of securing oil film in mixed lubrication in the 4 rpm through 10 rpm range facilitated the significant effectiveness of the additives (Figure 8, B and C).
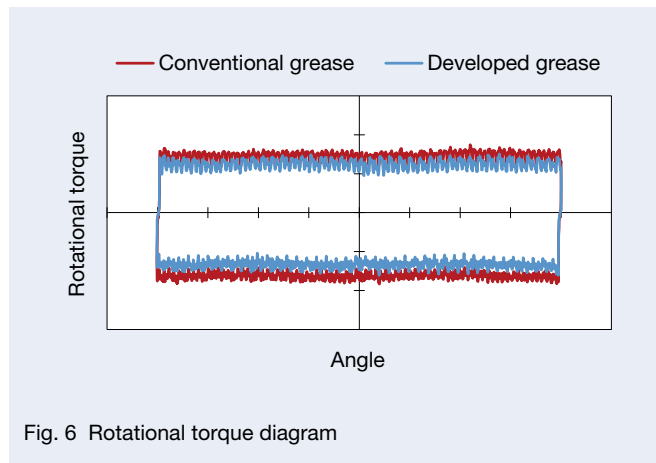

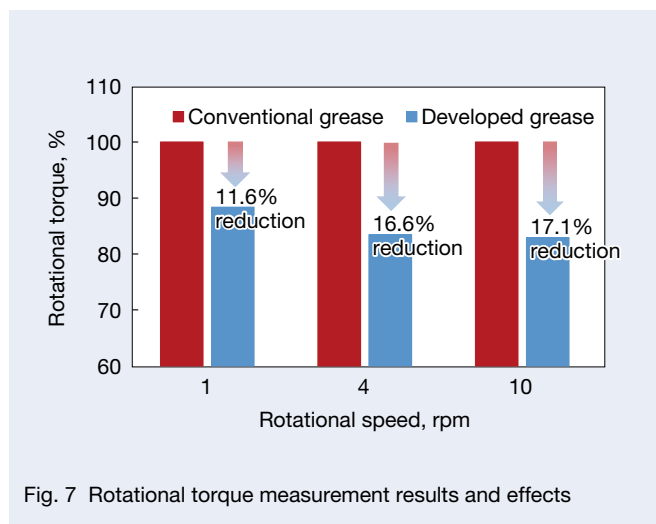Fig. 6 Rotational torque diagram

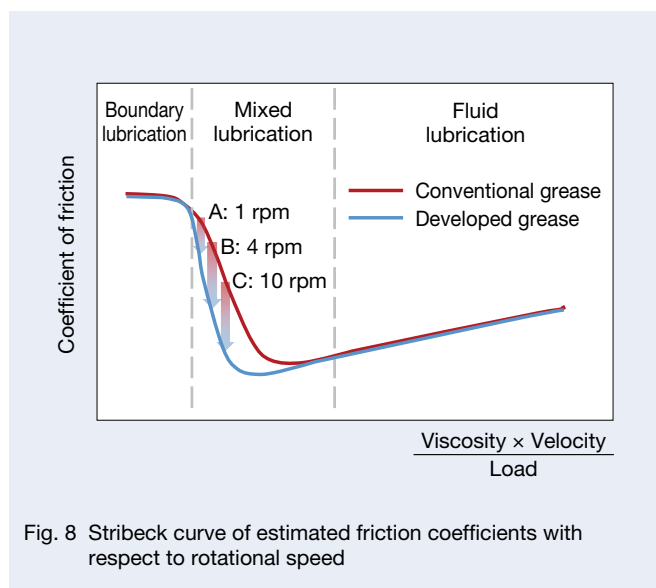Fig. 7 Rotational torque measurement results and effects

Fig. 8 Stribeck curve of estimated friction coefficients with respect to rotational speed
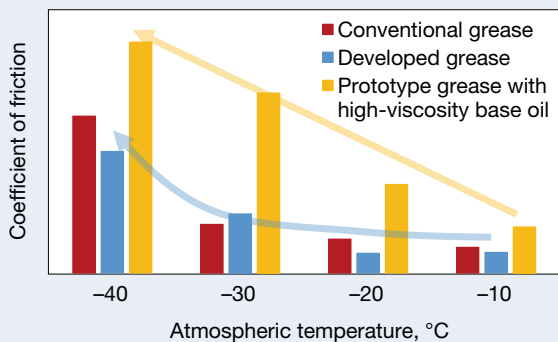
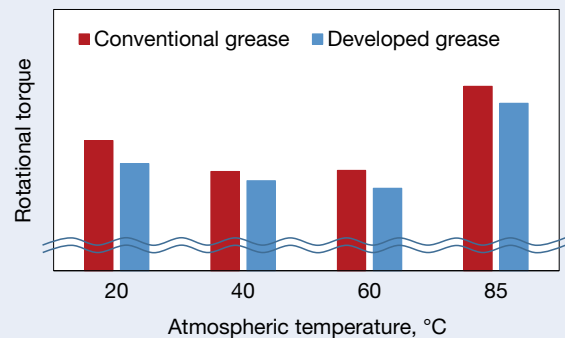Fig. 9 Rotational torque measurement results at low temperatures

Fig. 10 Rotational torque measurement results at high temperatures

5.3.2 Impact of rotational torque from atmosphere temperature

Since temperature also affects grease, we measured rotational torque at different atmospheric temperatures. We measured rotational torque with the worm reduction gear units placed in the tanks at preset atmosphere temperatures and allowed them to run for at least five hours.

Figure 9 shows the results of rotation torque measurement under low temperatures. Torque with the conventional grease and the developed grease are equivalent in that rotational torque gradually rises at −30°C and then increases at a different slope at −40°C. On the other hand, the prototype grease, which lends higher viscosity to the base oil for securing the formation of the oil film, already generated a large rotational torque at −10°C, which continued to rise in correlation with the change in temperature. This indicates that the grease using a base oil with just a higher viscosity can be considered to be in a fluid lubrication state. However, the developed grease can be regarded as being in a mixed lubrication state up to −30°C.

Figure 10 shows the results of rotational torque measurement under high temperatures. We have confirmed the friction reduction effect of the developed grease, even under high temperatures.

As already mentioned, we have confirmed that this developed grease effectively reduces friction under a typical EPS operating environment.

6. Conclusion

The low friction grease improved the lubricating properties of the worm reduction gear, contributing to an improvement in steering feel. EPS is expected to play an important role in the realization of automatic driving, at least partially, and perhaps fully automatic driving, with a vehicle total control system. The high performance of this type of system would require a speed reduction gear with low friction. NSK will continue making progress toward achieving more comfortable steering by utilizing NSK Tribology technology.

Reference

1) Y. Mitsuzaki, G. Hirose, S. Sekiya, and Y. Miyaura, "Electric Power Steering (EPS)," NSK TECHNICAL JOURNAL, 667 (1999), 14–22.

Haruhiko Kiyota

Tetsuya Koike

Takeshi Yamamoto

Development of Micro Manipulation System

Nobuaki Tanaka
Future Technology Development Center

Abstract

A manipulator is used to perform fine operations on cells and electronic components under a microscopic field of view. However, mastering the device requires extensive use and a skilled technique. Therefore, NSK developed a manipulation system that enables easier automation of operation by applying mechatronics.

The system is attached to a microscope and is composed of a three-dimensional motorized manipulator and a motorized sample stage. Except for replacement of the microscope's objective lens, the developed system is capable of all-electric operation. Operation is performed with one or more joysticks while looking at the camera image of the microscope that is displayed on the monitor.

To evaluate the usefulness of the system's capabilities, we collaborated with bioresearch institutes during its development. The system was used to produce confirmed offspring by ICSI using the egg cells of experimental animals.

We have started to sell this system to domestic and foreign companies, biotechnology research institutions, and electronic component manufacturers.

This product received the "MONODZUKURI life culture Institute Chairman Prize" of the Cho-MONODZUKURI Components Award from the MONODZUKURI.Nippon.Conference.

1. Introduction

A manipulator is a device used to perform micro-operations on cellar materials and micromechanical components under a microscopic field of view and is broadly used in biotechnology research at universities and research organizations and as well as in the development efforts of electronic component manufacturers.

Nevertheless, the history of using manipulators in devices to perform micro-insemination and generate living modified organisms is short.

In most cases, users separately purchase manipulators and peripheral devices such as a sample stage and make necessary adjustments before use because they are provided by different manufacturers. The equipment must also be operated separately, sometimes requiring the operation of five or six handles at a time due to the absence of any mechanical linkage between devices.

In addition, unless a special camera and display configuration has been set up, the user has to operate while looking through a microscope eyepiece lens and have the skill to manipulate multiple handles without looking at them. Obtaining this skill can take more than six months and thus only highly skilled technicians can conduct micro-insemination. Moreover, generating living modified organisms requires working with approximately 100 fertilized eggs while gazing through the eyepiece, which places severe physical stress on the technician.

Therefore, NSK has developed a unique manipulation system that facilitates highly accurate operation by incorporating a new automation technology and a technology that NSK has applied to its bearings, ball screws, and linear guides as well as mechatronics.

We have reached a solid prospect for commercialization of this system as a result of an evaluation of usability through joint research with the Central Institute for Experimental Animals (CIEA).

Here we report on the configuration, functionality, and results of the evaluation testing of the system.

2. Manipulation System

2.1 Basic configuration

The manipulation system shown in Photo 1 is attached to a microscope configured with an electric XYZ manipulator, electric sample stage, electric focusing system, electronic injector, piezoelectric actuator, electronics, piezoelectric amplifier, PC, and joystick.

Figure 1 shows the system set-up, in which an electric drive section is connected to the electronics and a PC is connected to the electronics and joystick. The piezoelectric actuator is connected to the electronics via the piezoelectric amplifier. Table 1 shows the component specifications.

2.2 Electric drive operations

The electric XYZ manipulator is installed on the side of the microscope for three-dimensional operations within the microscope's field of view along with installed micro-tools. While micro-tools of various shapes and materials can be used depending on the specific application, we used a thin-tip, hollow glass needle for the joint research with the CIEA.

The electric sample stage and the electric focusing system are installed on the microscope for adjusting the position of the object to be manipulated in the microscope's field of view. The electric injector, in concert with a thin
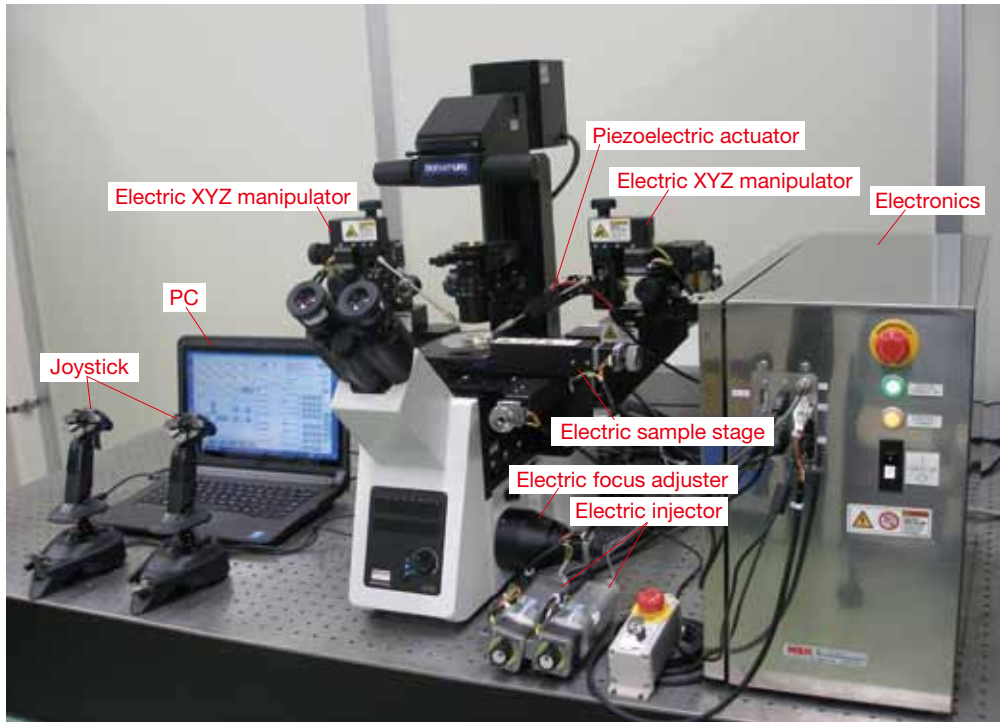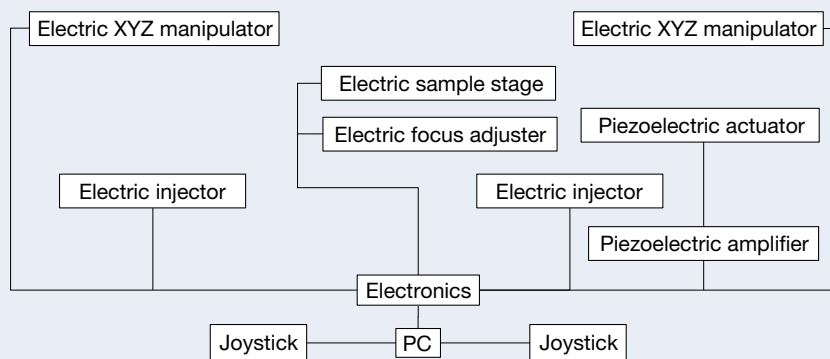

Photo 1 Manipulation system

Fig. 1 System configuration

Table 1 Specifications

	Electric XYZ manipulator	Electric sample stage	Electric injector	Piezoelectric actuator
Stroke, mm	20		1178.09 µl	5 µm
Resolution, µm	0.1		0.0039 µl/step	5 nm*
Maximum velocity, mm/s	5		5 rps	
Driving method	5-phase stepping motor			Piezoelectric element
Dimensions, mm	143 × 144 × 149	296 × 294 × 80	42 × 42 × 167	20 × 20 × 43.5
Weight, kg	1.5	1.5	1	0.13

	Electric XYZ manipulator	Electric sample stage	Electric injector	Piezoelectric actuator
Operation	USB joystick	USB joystick Keyboard Screen operation	USB joystick	USB joystick Screen operation
Control software	Used by installing a Windows PC			
Communication method	Serial Communication			
	Electronics			Piezoelectric amplifier
Dimensions, mm	250 × 400 × 500			320 × 350 × 149
Weight, kg	19			7.5
Power supply	AC100–125 V 50/60 Hz 3A			AC100–125 V 50/60 Hz 2A

*When using positioning application

tip, hollow glass needle micro-tool, is used to support an object to be manipulated, such as cells, and it is used for adjusting flow rate over the course of operation when injecting a solution, and it can be driven by pneumatic or hydraulic pressure.

The electric drive movements are produced by a stepper motor set for high resolution motion. For the XYZ manipulator and sample stage, the resolution is set at a micro-meter level. The manipulation system is configured for full electric drive operation except for adjusting the objective lens magnification.

2.3 Piezoelectric actuator

We used a piezoelectric actuator with an installed manipulator, as shown in Photo 2. NSK's proprietary nanopositioner[1] was incorporated into the configuration of the piezoelectric actuator. To apply subtle oscillations with a micro-tool, we used a piezoelectric actuator, which we have also used for the nanopositioner. The piezoelectric actuator is driven by applying voltage amplified by a control signal from the electronic components to the piezoelectric amplifier. The piezoelectric actuator is turned on and off using a button on the joystick. A voltage signal with a frequency on the order of kHz is applied to the piezoelectric element to perforate an egg cell with minimal damage.

Perforating egg cells with a piezoelectric actuator is conducted with a hollow glass needle with a thin, couple micrometer diameter tip, which is filled in advance with Fluorinert, as a micro-tool (Photo 2). Therefore, it is possible to perforate egg cells with minimal deformation (Photo 3).

2.4 Operation and control methods

A joystick is used to implement almost every task while the user observes an image captured by a camera mounted on the microscope and displayed on a monitor, as shown in Photo 4. This enables operators to work in a comfortable position and thereby reduces fatigue from long hours of operation.

Buttons on the handle of the USB joystick facilitate easy, highly accurate operation of the manipulator as well as the injector and piezoelectric actuator so that users do not need to leave the joystick even when operating equipment other than the manipulator.

The electric sample stage is operated by virtual buttons on the controller screen shown in Figure 2 and the PC keyboard. These operations, however, can also be done with an extra joystick if one is available.

Figure 2 shows the display screen of the control software, which can manage the drive speed and memorize and control the position of the sample stage. In addition, depending on specific applications, the manipulator can respond to different joysticks or OS that have been connected to control the system.

Remote operation from the microscope is possible if the necessary wiring is used.
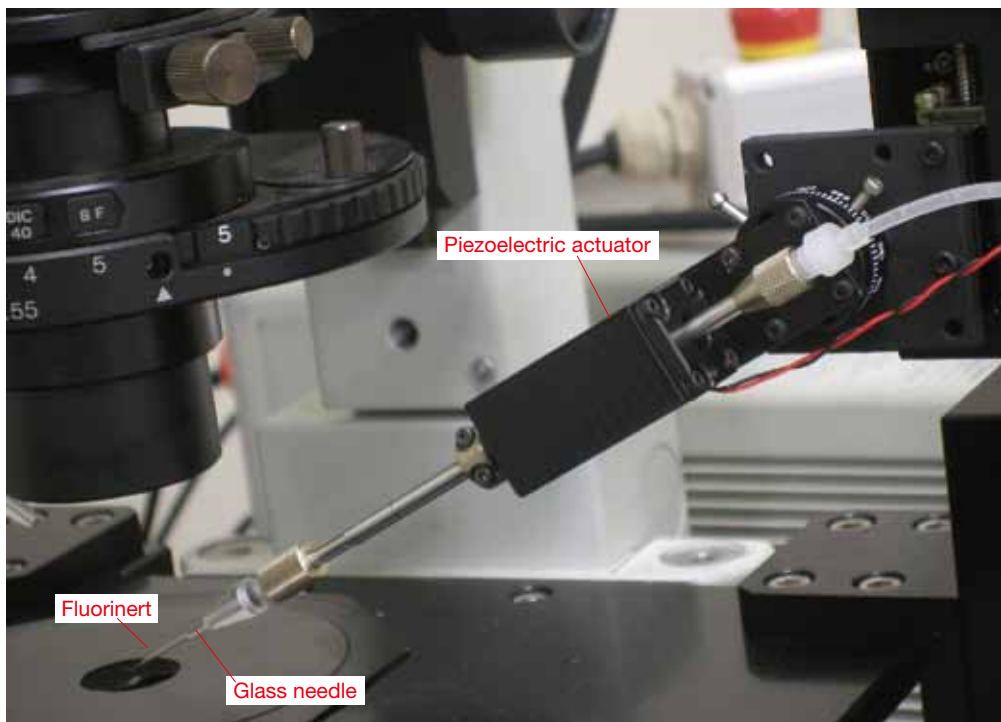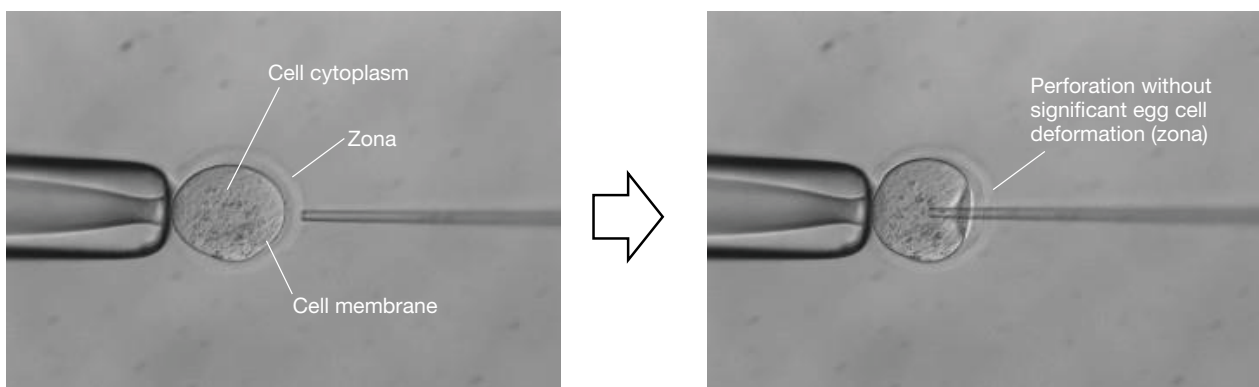

Photo 2 Piezoelectric actuator
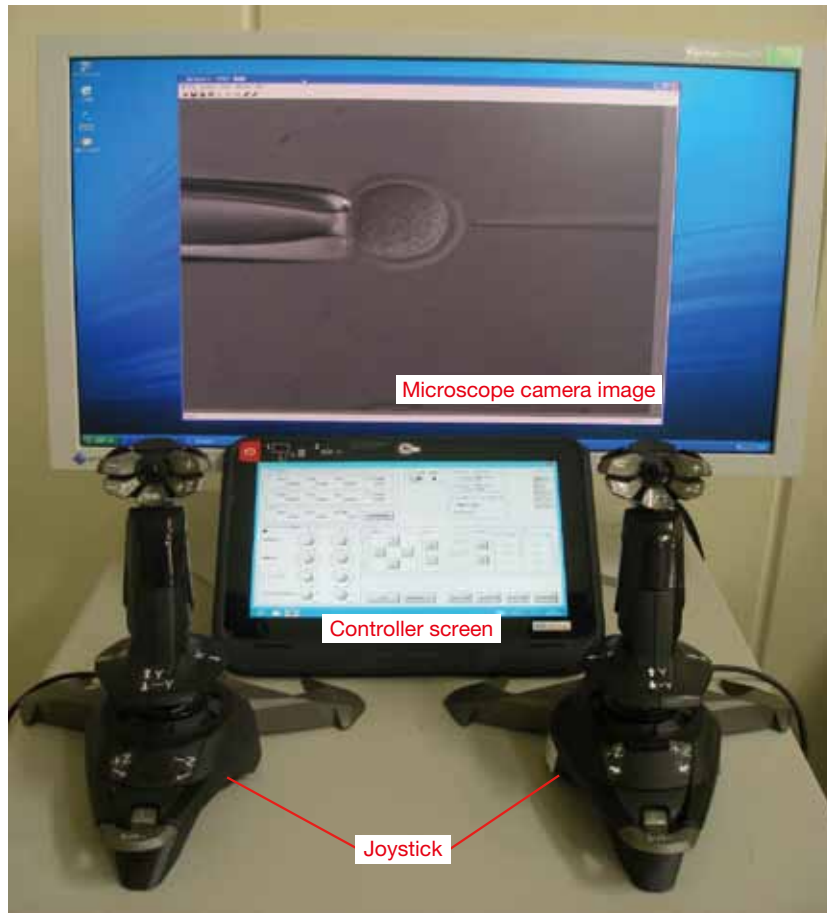

Photo 3 Perforated motion

Photo 4 Joystick operating environment

3. Automated Functions

The manipulation system is equipped with automatic functions, including image processing and sequencing. We used these functions to evaluate the manipulation of mouse egg cells during the joint research with the CIEA.

3.1 Image processing

When manipulating multiple egg cells must be performed in a single operation, eggs that have been manipulated should not be remixed with those that have not, and the relative position of the eggs spread out under the microscopes field of view must be carefully monitored. Recognizing the relative position of all the eggs spread across the sample stage is difficult because the high level of magnification creates a very narrow field of view through the microscope.

We have developed a means of identifying egg cells spread across the captured image. First, we record microscopic images while driving the same stage of a preset path (Figure 3A). Next, we generate the image data that enables composition and recognition of broad regions (Figure 3B). Then, we further process the images (Figure 3C).

Another function automatically positions the egg cells identified in the processed image within the field of view of the microscope and in accordance with joystick operation (Figure 3 D-1 to 3), and the function also automatically positions them for working with the fixed location of the glass needle (Figure 3 D-4).

The use of these functions does not require knowing the position of the egg cells throughout the culture medium, and it is possible to prevent the operation and non-operation of mixing egg cells.

In addition, as shown in Figure 3D, the injection operation can always be initiated from the same position by setting the glass needle location when first starting to work with an egg cell, as shown in "b" (Figure 3 D-4), and its location when directly operating on the cell, as shown in "c" (Figure 3 D-7), which facilitates the implementation of frequently repeated operations.
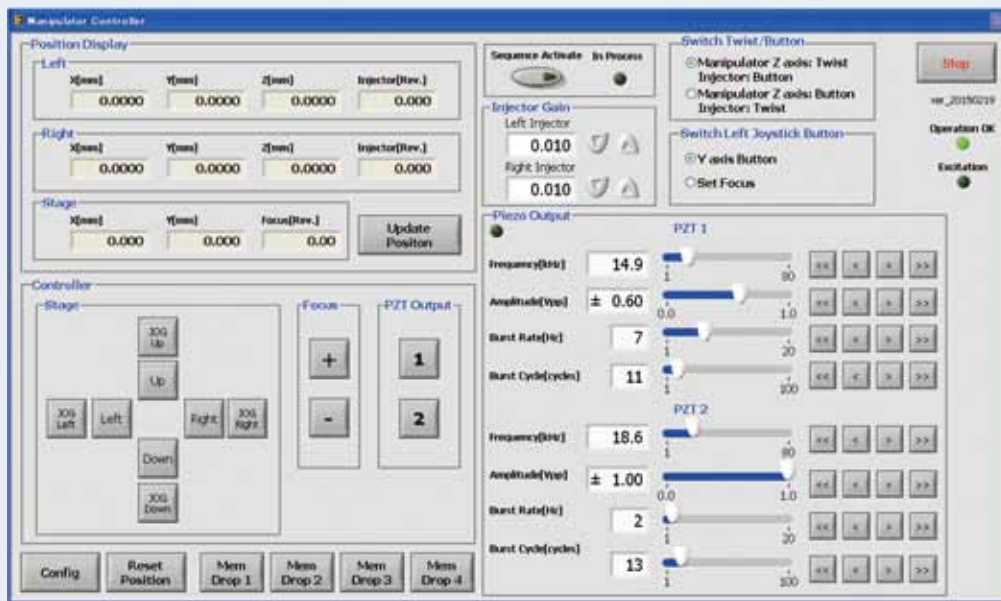
Fig. 2 Control screen

3.2 Sequencing

Moving back and forth between different spots within the field of view of the microscope is sometimes necessary, as is adjusting the position of a micro-tool to each spot for operating the manipulator. For instance, injecting a cell into an egg cell requires adjusting the glass needle position while traveling between the injection operation position and the cell collection position, as shown in Figure 4 A through C. In this case, the operation requires a high level of skill for the very complicated manipulation because the operator has to adjust the micro-tool position at a microscopic scale for each movement of the specimen stage while keeping track of the starting and ending positions. We took advantage of PC control over the manipulation system to develop a sequencing function for memorizing the position data of the driving axis and to travel to the memorized position. In situations that involve highly accurate positioning adjustment for complicated procedures, a series of actions can be implemented by pre-setting the sequencing operation with a combination of multiple commands for moving to the memorized position or to the specified position. Furthermore, the manipulation system is capable of sequentially driving multiple devices, including the manipulator and sample stage, since the single control software integrates all of these operations.

As a result, the automation of complicated tasks is possible, allowing traveling between culture medium 1 and culture medium 2 and the automated position adjustment of the glass needle in respective positions, using only the joystick, as shown in Figure 4 D.

4. Performance Evaluation Results

The evaluation test was conducted as joint research with the CIEA. Our research, using laboratory mouse egg cells, included these manipulations: DNA micro-injection to generate a living modified organism by injecting DNA into an egg cell, embryo-stem cell injection to generate a chimera animal by injecting an ES cell into a blastocyst, and ICSI for micro-insemination by injecting semen into an unfertilized egg.

4.1 Injection results

Table 2 through 4 show the results of the evaluation tests for DNA micro-injection, ES cell injection, and ICSI manipulation, from which we can confirm generations of offspring of a living modified organism, a chimera animal, and by ICSI, respectively[2)–4)].

The piezoelectric actuator is used to perforate egg cells in ES cell injection and ICSI manipulation. ICSI manipulation is believed to be particularly difficult due to the high risk of destroying an unfertilized egg. Instantaneous perforation is imperative for reducing damage and minimizing the deformation of the egg cell. The test results shown in Table 4 are roughly comparable with the use of traditional technology, which confirms the usefulness of the new piezoelectric actuator.
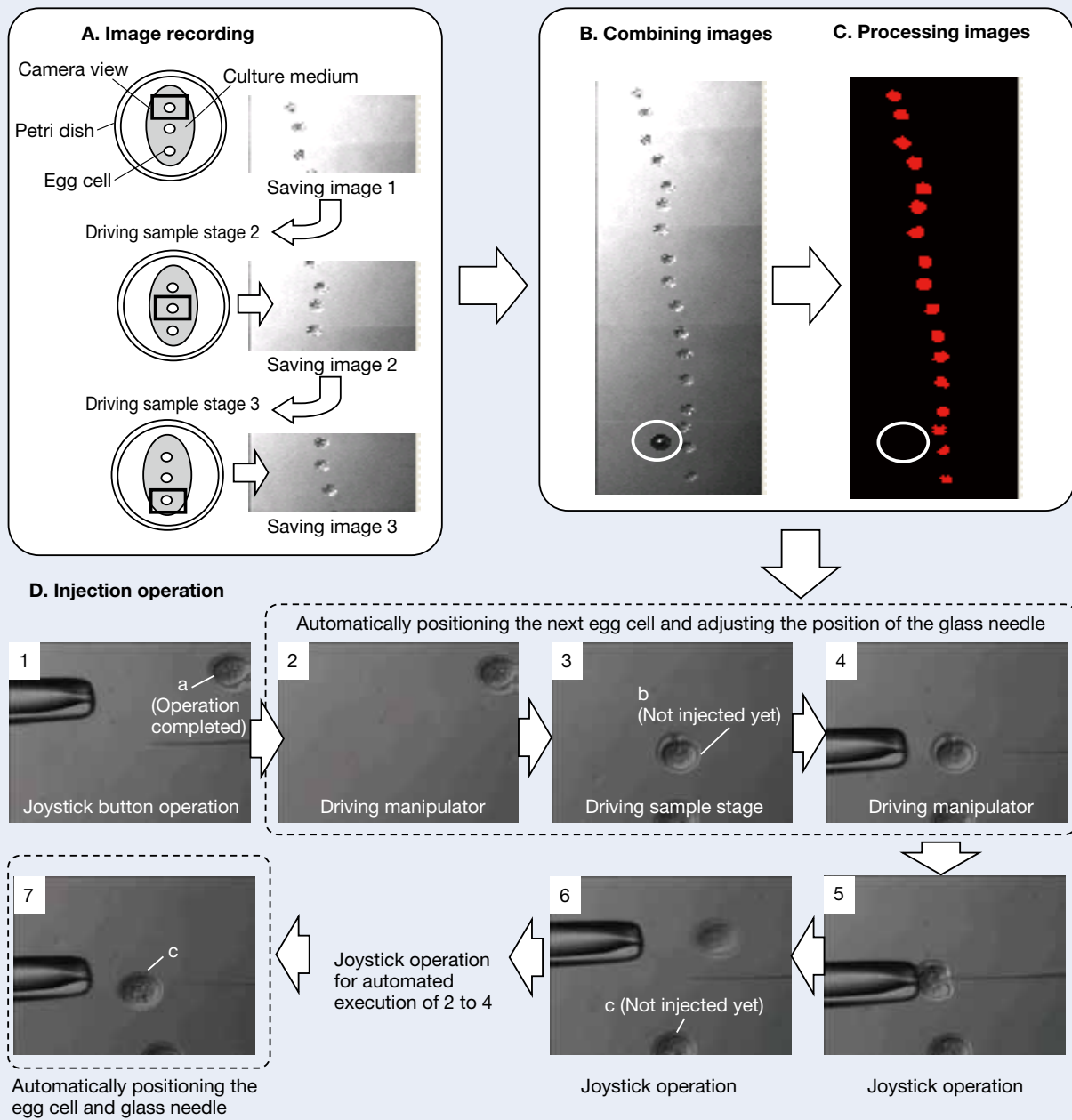
Fig. 3 Image processing

Table 2 Results of DNA micro-injection

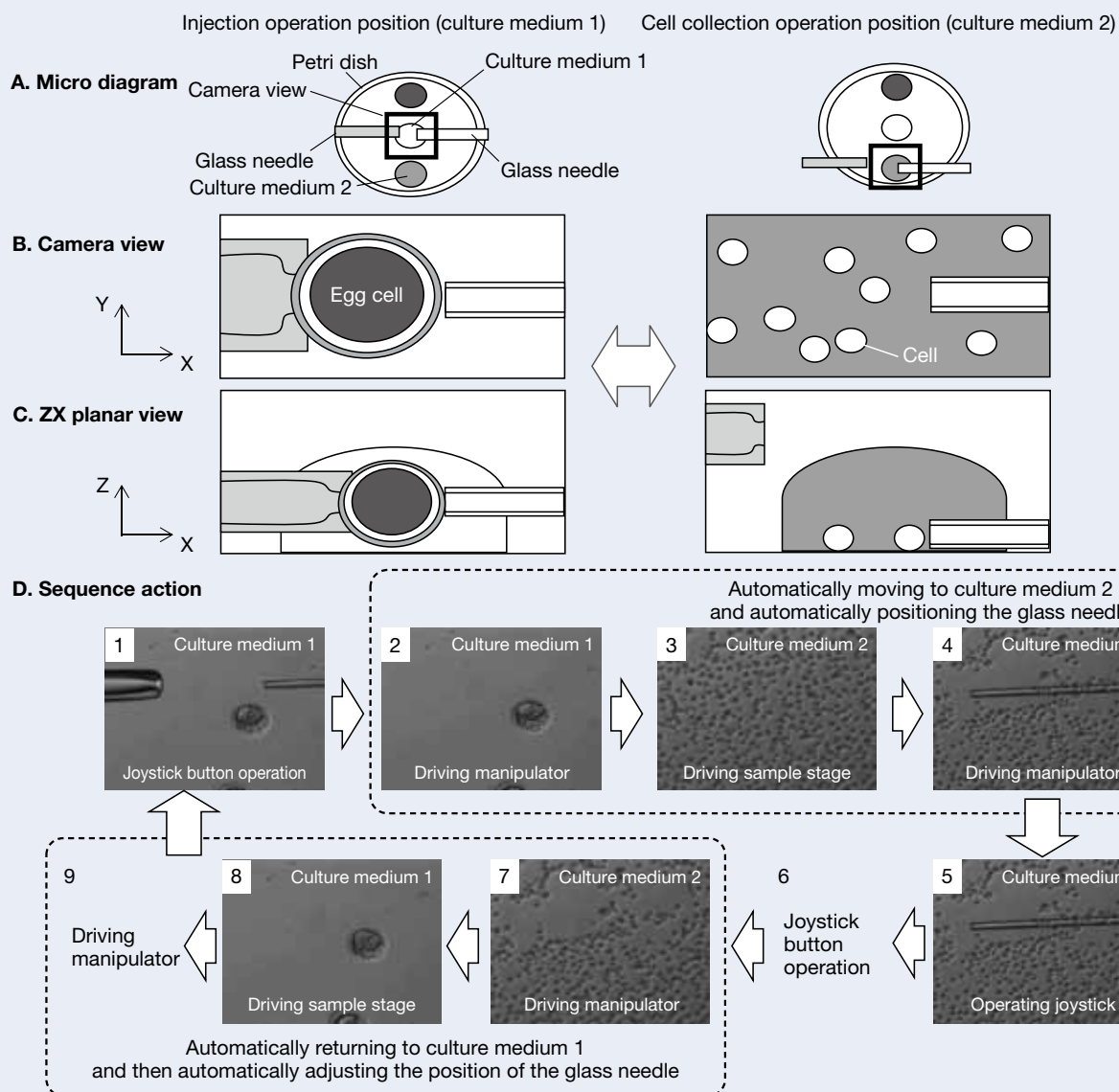| 2.6	Fertilized egg mouse system	Injection			Offspring					Transgenic mouse	
		Operated embryo	Survived embryo	%	Number of moving embryos	Number of implanting instances	%	Number of offspring	%	Tg number of positives	%
pEGFP-N1	C57BL/6J	115	109	94.8	94	61	64.9	39	41.5	3	2.6

Fig. 4 Sequence function

Table 3 Results of ES cell injection

ES cell	Blastocyst mouse system	Injection						Offspring		Chimera mouse			
		Operated embryos	Transplanted embryos	Number of implanting instances	%	Number of fetuses	%	Number of fostering instances	Number of weaning instances	Population	%	Number of GT	%
129 system MM8	C57BL/6J	122	122	80	65.6	40	32.8	34	26	17	13.9	17	13.9

Table 4 Results of ICSI

System name		Injection			Culturing				Offspring				
Female	Male	Operated embryos	Survived embryos	%	0.5 (2 PN)	%	1.0 (2 cells)	%	Transplanted embryos	Number of implanting instances	%	Number of fetuses	%
Jcl:BDF1	Jcl:BDF1	94	77	81.9	68	88.3	66	97.1	66	50	75.8	34	51.5

4.2 Evaluation results of image processing

The image processing function accurately recognized the used egg cell, as shown in Figure 5. In addition, the image processing function proved to be capable of automatically positioning an egg cell to a default location for subsequent operations under the field of view of the microscope while simultaneously adjusting the position for the initial operation of a glass needle.

To evaluate the usefulness of this function, we video-recorded the injection manipulation and measured the time required for manipulating a single egg cell. The results shown in Figure 6 confirmed that use of the image processing function did indeed reduce the operation times per injection by the following amounts: approximately 8% in DNA micro-injection operation, approximately 18% in ES-cell injection operation, and 26% in ICSI operation, thereby improving operational efficiency.

4.3 Evaluation results of sequencing

We confirmed that the sequencing function developed is capable of being used in an operation that involves different locations for injection and for collecting cells to be injected (ES cell injection operation, ICSI operation), and that a series of injection operations were successfully completed.

To evaluate the usefulness of this function, we recorded the injection manipulation on video and measured the time required for sequencing. The results shown in Figure 7 confirmed that sequencing reduced operation time by approximately 60% compared to that of not using it, thereby improving operational efficiency.

5. Conclusion

The manipulation system is a mechatronic product that integrates newly developed software technology with a mechanical system configuration that combines NSK products, including bearings, ball screws, and linear guides.

We were able to demonstrate the feasibility of the system through this particular joint research effort. The system can be adapted to such applications as collecting microscopic foreign substances as a preprocessing stage of composition analysis in addition to biotechnology. It also complies with international standards (CE marking and European Harmonized Standards), confirmed by overseas standard compliance inspections from a certification agent, and can therefore be used in overseas markets as well.

We will continue the joint research with the CIEA and proactively disclose the results to the public. At the same time, we will endeavor to improve the performance of the manipulation system in order to contribute to the advancement of biotechnological research.
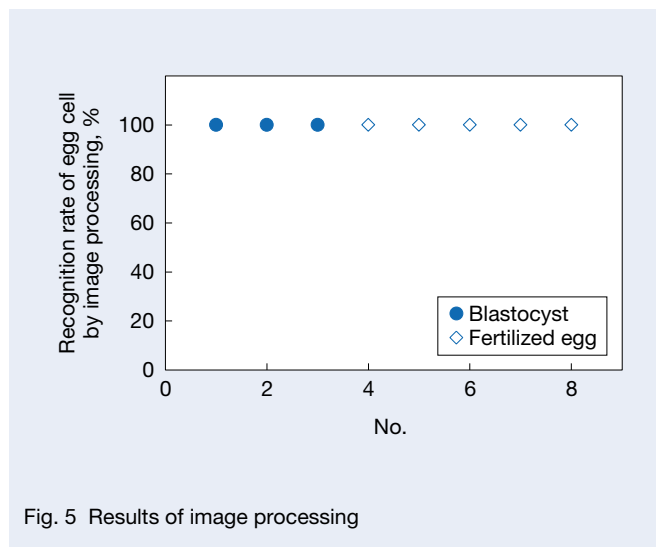

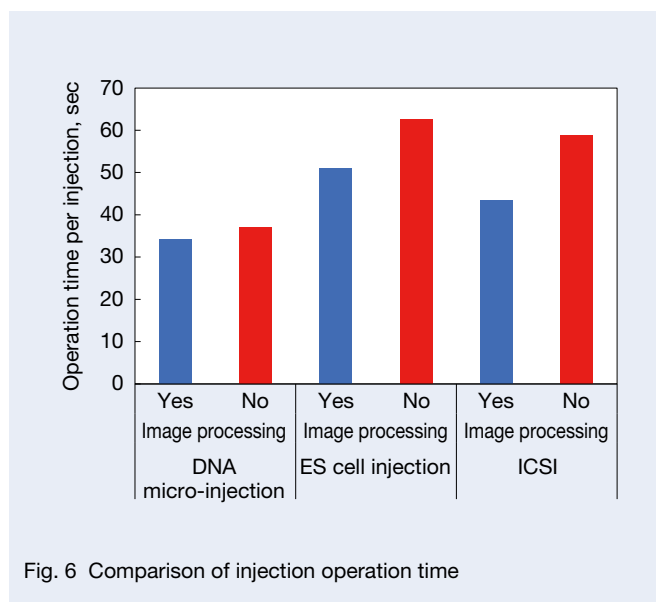Fig. 5   Results of image processing
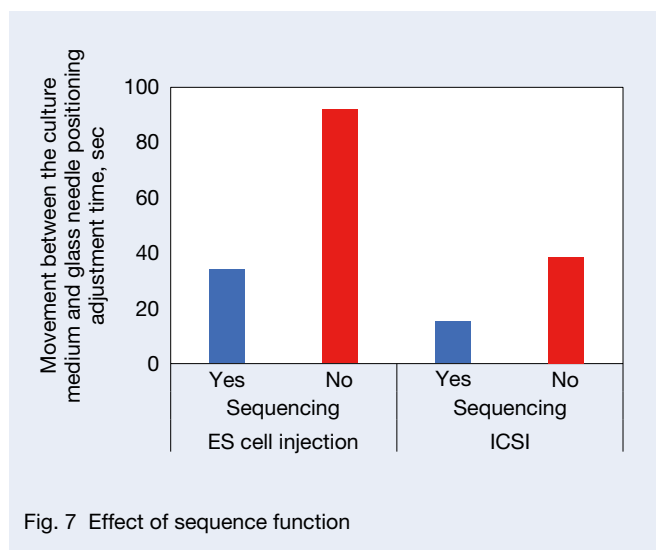

Fig. 6   Comparison of injection operation time

Fig. 7   Effect of sequence function

References

1) N. Tanaka, "Development of Nanopositioner," NSK Technical Journal, No. 680 (2006), 29–35.
2) T. Kamisako, N. Tanaka, A. Sato, K. Endo, H. Sakai, R. Ito, and T. Eto, "Production of transgenic mice using an electrically operated manipulator," Lecture Abstract from the 44th General Meeting (2010) 101, Japan Association for Experimental Animal Technologists.
3) T. Kamisako, N. Tanaka, S. Ida, K. Endo, K. Hioki, M. Ito, and T. Eto, "Development of semi-automatic manipulator and its usability - 2," Lecture Abstract from the 58th General Meeting (2011) 192, Japan Association for Laboratory Animal Science.
4) T. Kamisako, N. Tanaka, K. Hioki, and T. Eto, "ICSI operation using semi-automatic manipulator," Japan Association for Experimental Animal Technologies, the #60 general meeting lecture summary, (2013), 217.
5) K. Endoh, K. Mochida, N. Ogonuki, M. Ohkawa, A. Shinmen, M. Ito, N. Kashiwazaki, and A. Ogura, "The Development Ability of Vitrified Oocytes from Different Mouse Strains Assessed by Parthenogenetic Activation and Intracytoplasmic Sperm Injection," Journal of Reproduction and Development, 53–6 (2007), 1199–1206.

Acknowledgments

Nobuaki Tanaka

Strategy for Frictional Behavior Control in Ball Screws

Satoru Arai
Linear Technology Center

Abstract

This paper reviews a strategy for controlling frictional behavior in ball screws installed onto precision feed drive systems. The strategy applies technological development for consistency of frictional characteristics. In order to verify the performance of consistent frictional behavior in a ball screw, an accuracy evaluation of circular interpolation motion with two orthogonally oriented axes was carried out on a unique feed drive system originally developed for this experimental investigation. The new strategy has successfully contributed to obvious stability and repeatability of motion delays caused as quadrant glitches in reverse motions and has also led to fewer trajectory errors in circular interpolation motion. With a function of a servo controller, the consistent quadrant glitches are compensated in all places on the ball screw shaft. Therefore, a ball screw with consistent frictional behavior can provide a feed drive system with potential advantages for future production systems. The consistency of the frictional characteristics of ball screws realizes the other advantage of less heat generation. This reduction in temperature rise has been observed in various levels of the practical ball screw feed drive system.

1. Introduction

Ball screws emerged as a critical mechanical element of feed drive systems at the dawn of the NC machine tool age more than fifty years ago. Ball screw technology evolved over time in response to demand for faster speeds to improve productivity and for greater accuracy to increase added value.

In this article, we introduce technical development toward higher functionality by focusing on the friction characteristics of ball screws, for which there has recently been expectations of additional value.

2. Ball Screw as a Configuring Element of Feed Drive Systems

Figure 1 shows the configuration semi-closed of a feed drive system for a machine tool as a typical example of a feed drive system. Basic elements include a ball screw and bearings to support the ball screw shaft, a support bracket to integrally hold the bearing on the machine base, and a table with associated guides (e.g., linear guideway) and a servo motor.

Applying a feed drive system as an object of control requires a frequency response feature to avoid resonance as well as stable properties of friction. Stable properties of friction are also needed as an object of control for a ball screw, an essential configuration element of the feed drive system, with torque as an index.

The controllability of servo motors is significantly impacted by change in the torque of the ball screw and bearing elements of the feed drive system and change in friction generated by the covers enclosing the guideways and the feed drive system. A change in friction is likely to generate significant error, typically during acceleration or reverse motion of the feed drive system. Delays in motion, known as quadrant glitches, are particularly associated with change in frictional characteristics during reverse motion.

A quadrant glitch may leave streaky traces on the surface of the workpiece that has been machined by an interpolation motion of multiple axes on a machine tool. This can cause significant deterioration in machined surface integrity in applications that demand highly accurate machining. A lot of research has therefore been focused on clarifying this phenomenon as a practical subject in the overlapping area of machine design and control system design. It has been clarified that the non-linear spring characteristics of rolling elements[1] influence the mechanism that delays actual motion against the commanded value, and that examining the impact of centripetal acceleration[2] is also necessary.

NSK also has carried out various evaluations to clarify the quadrant glitch phenomenon caused by a ball screw. The results of NSK's evaluations correlated with the occurrence of the second quadrant glitches with the difference in the preloading method of the ball screw[3] through an explanation of a change in torque characteristics during reverse motion on an off-set lead, preload-type ball screw is caused by the existence of a region, in which there is a change in the number of contact points between balls and thread grooves.
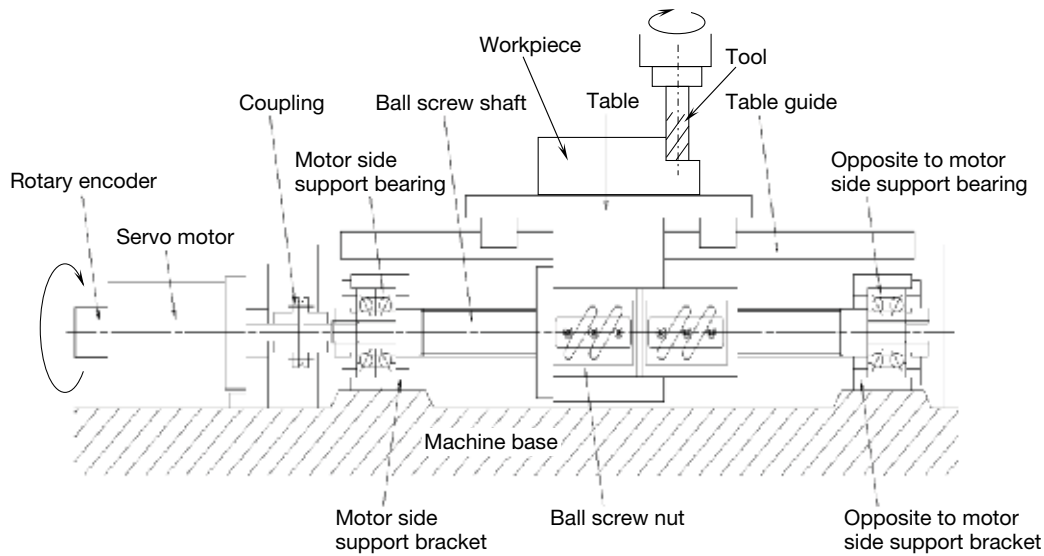
Fig. 1 Feed drive system with ball screw

On the other hand, the magnitude of the quadrant glitch in the actual feed drive system is also influenced by the design and configuration of the machine itself, in addition to the frictional factor. Therefore, deducing the type of motion error based only on stable properties of frictional components is difficult. In this context, a quadrant glitch is typically corrected by adjusting the action of a compensator that is capable of generating a correction signal to address the quadrant glitch after mechanical and control system parameters are identified[4].

Motion errors represented by quadrant glitches are inevitable[5] as long as a machine is configured with frictional components and an elastic body. However, being able to stabilize the motion error may simplify compensation through correction signals. The challenge is posed by the instability of friction. Therefore, NSK has suggested a measure to improve the effectiveness and accuracy of the quadrant glitch correction function in the control system using an approach to improve the frictional component; that is, to ensure consistency of the frictional characteristics of ball screws at any axial position on the screw shaft.

3. Motion Controllability of the Ball Screw

3.1 Friction characteristics and control factors

Understanding how torque and friction influence ball screw performance is critical for controlling the change in friction caused by ball screws.

The following formula (1) shows how the standard torque of a ball screw with pre-load is calculated.

$$T_{p0} = k \frac{F_{a0} \cdot l}{2\pi} \qquad (1)$$

T_{p0}: Standard torque, N·cm
F_{a0}: Pre-load, N
l: Lead, cm
k: Torque coefficient of ball screw

The relationship expressed in the formula (1) indicates that ball screw torque depends on the pre-load and lead.

Figure 2 shows the relationship between factors that impact the frictional characteristics of ball screws. Previous NSK evaluations explained that friction characteristics in general have a complex dependency on such factors as the preloading method, contact condition between balls and grooves, the surface finishing condition, the material, and the lubrication state. These influences are considered to affect the torque coefficient of ball
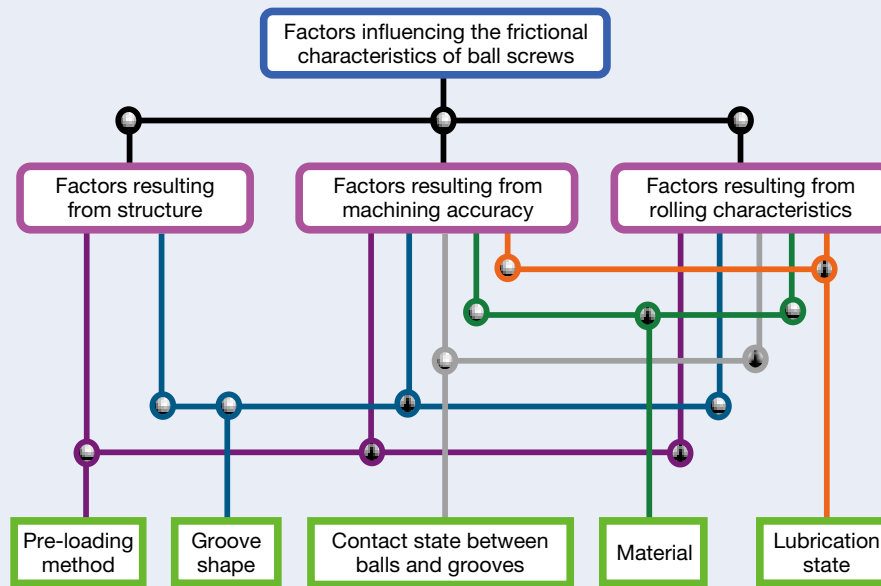
Fig. 2 Factors influencing the frictional characteristics of ball screws

screws, as shown in the formula (1).

The reduction of changes in the frictional characteristics of ball screws stabilizes the torque fluctuation amplitude in particular, and it also controls the contact and lubrication states between balls and grooves.

3.2 Highly precise motion error evaluation mechanism

Figure 3 shows the highly precise motion error evaluation mechanism that was developed for investigating the frictional characteristics of a ball screw feed drive system.

The device is configured with a full-closed loop numerical control function for the feed drive systems in two orthogonally oriented axes. Various features have been applied to constrain the influence of error factors, such as Abbe's error, which is inevitable in machine configurations. Its effectiveness was confirmed by a correlation of the evaluation results of contouring accuracies measured with three different methods (grid encoder on the table, linear scales for respective axes, and an externally installed laser measurement system).

In addition, this device facilitates the evaluation of motion error under various conditions, including the addition of pre-tension to the screw shaft of the ball screw and mounting the linear scales in different positions.
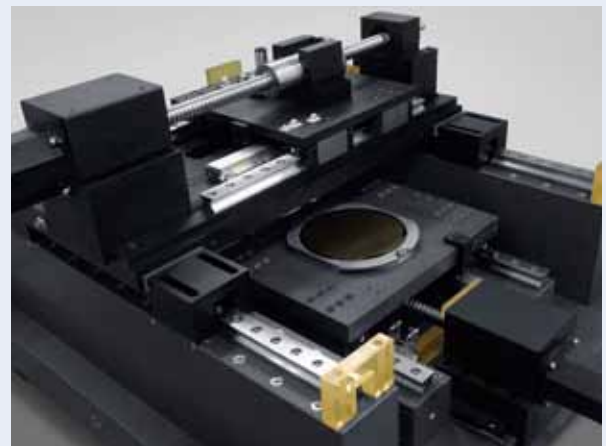

Fig. 3 Precision ball screw feed drive system for evaluating motion error

3.3 Evaluation results of motion error

Figure 4 shows the results of evaluating motion error over time against the target position on the aforementioned evaluation mechanism with a ball screw (Y-axis) in a conventional specification grade (JIS-C5) and a ball screw (X-axis) in a specification reflecting stabilized frictional characteristics (shaft diameter: ϕ40 mm, lead: 12 mm) as the objects of evaluation.

The target position of the circular interpolation motion of the two orthogonally oriented axes of R10 mm at a feed rate of 480 mm/min is given as a command value for evaluation with a shifting center position of motion at every 50 mm for each object ball screw. A circular interpolation motion with two orthogonally oriented axes is quite common for highly precise counter milling using tools such as ball end mills. A highly precise machining

(i) Evaluation results at three positions on ball screw in conventional specification

(ii) Evaluation results at three positions on ball screw in stabilized frictional characteristics
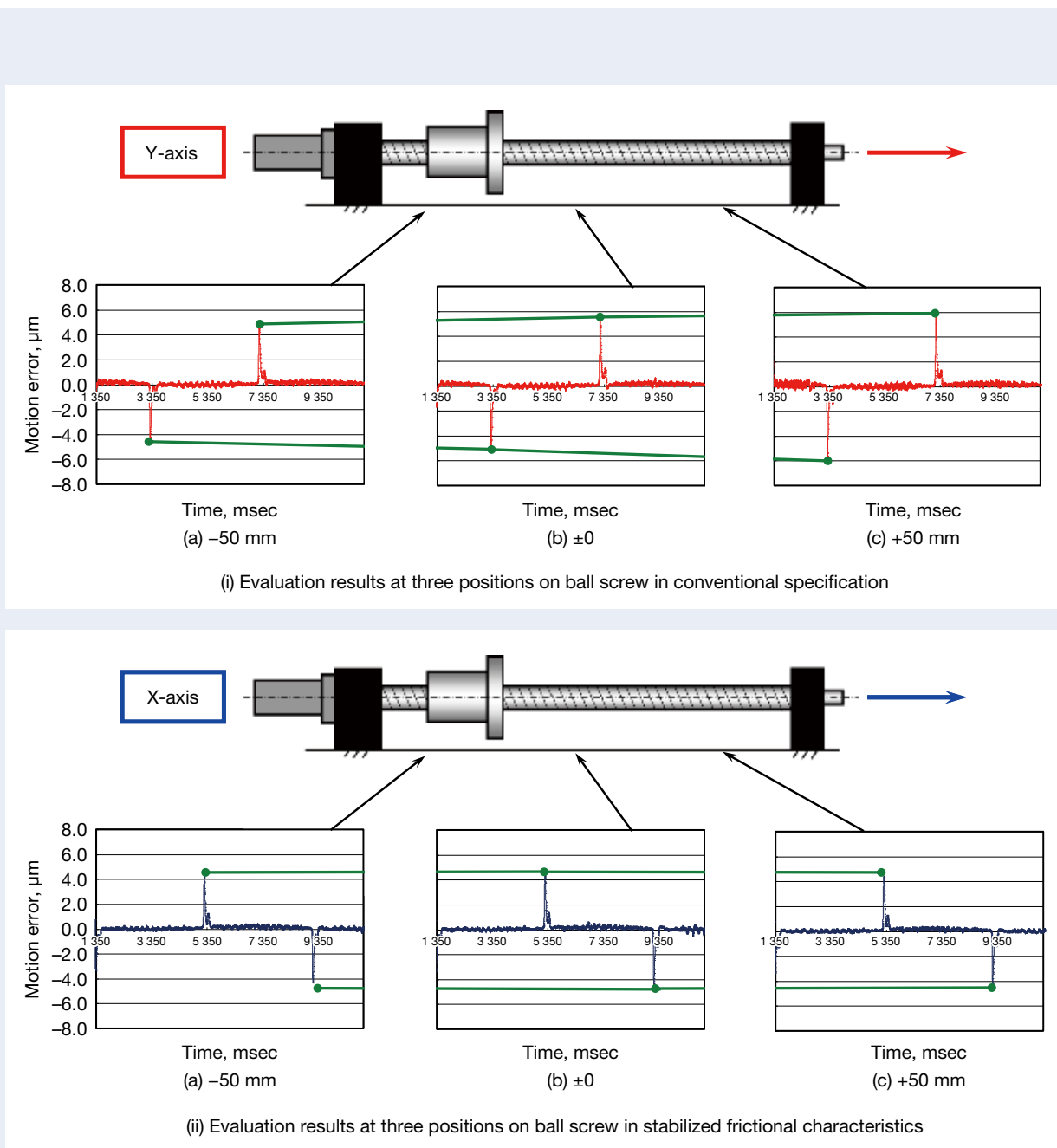
Fig. 4 Circular interpolation motion errors with two orthogonally oriented axes: in time scale

center, such as that used for die mold machining, which requires a high surface quality, is likely to be subject to accuracy evaluation during circular interpolation motion in order to confirm its influence while accelerating, decelerating, or operating in reverse.

A circular interpolation motion with two orthogonally oriented axes includes two reverse motions per cycle on each feed drive system. Thus, two quadrant glitches per axis were observed, as shown in Figure 4. This suggests that while the height of the quadrant glitch varies with the change in position on a conventional ball screw (Y-axis), the corresponding height remained constant on a ball screw in a stabilized frictional characteristic (X-axis) at any position.

Figure 5 shows the evaluation results of motion errors summarized in the X-Y coordinate roundness graph to clearly indicate this tendency. For simple descriptive purposes, the evaluation results are laid out with the X-axis representing the ball screw in a stabilized frictional characteristic and the Y-axis reflecting a conventional specification. The shifting center positions in each axis have been set wider than in Figure 4 to more closely simulate actual applications.

The figure suggests that the quadrant glitches of the X-axis ball screw in stabilized frictional characteristics appear as essentially identical shapes at every position compared to the Y-axis in the conventional specification. The figure also suggests that at the circular interpolation motion region other than that representing reverse motion, while the direction of the Y-axis for the conventional ball screw shows variation in motion errors, the X-axis for the ball screw in stabilized frictional characteristics has less variation in motion error at any given position.

While motion errors in reverse operation mainly discussed as a representative of ball screws tends to become obvious, the aforementioned result implies that stabilizing the frictional characteristics of ball screws has a greater effect in light of mitigating the variation of errors at the circular interpolation motion region.

Figure 6 shows motion errors during the circular interpolation motion of the two orthogonally oriented axes on the graph depicting roundness while changing the feed rates in four steps at the same axial position. The results of the evaluation with the ball screw in stabilized frictional characteristics on the X-axis and the conventional ball screw on the Y-axis are identical to the aforementioned cases. This reveals that there is an influence of centripetal
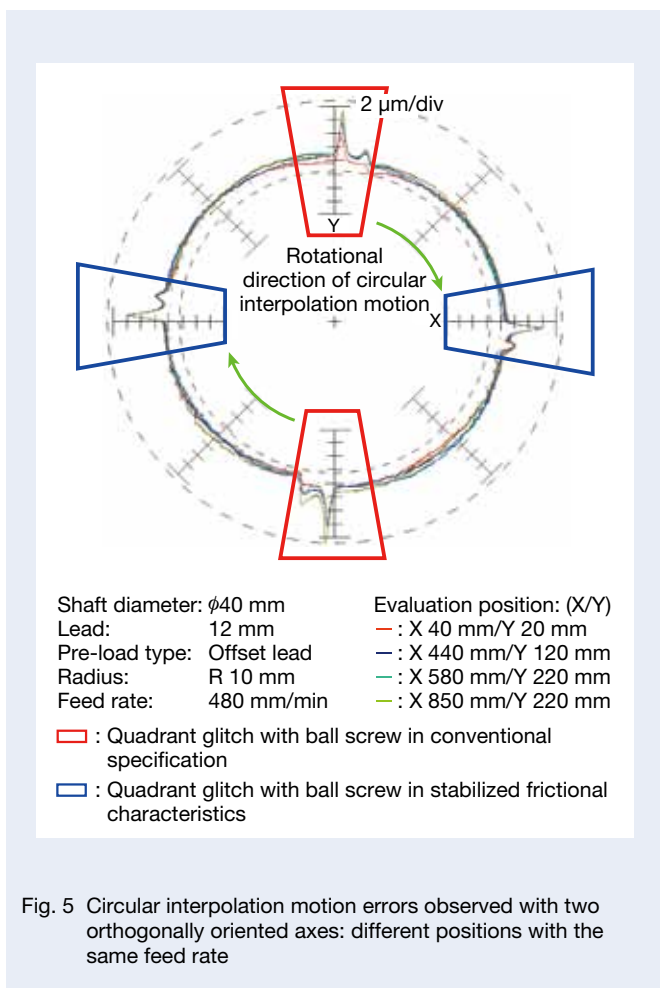

Shaft diameter: φ40 mm   Evaluation position: (X/Y)
Lead: 12 mm   — : X 40 mm/Y 20 mm
Pre-load type: Offset lead — : X 440 mm/Y 120 mm
Radius: R 10 mm   — : X 580 mm/Y 220 mm
Feed rate: 480 mm/min — : X 850 mm/Y 220 mm

☐ : Quadrant glitch with ball screw in conventional specification

☐ : Quadrant glitch with ball screw in stabilized frictional characteristics

Fig. 5 Circular interpolation motion errors observed with two orthogonally oriented axes: different positions with the same feed rate

Shaft diameter: φ40 mm   Feed rate
Lead: 12 mm   — : 120 mm/min
Pre-load type: Offset lead — : 240 mm/min
Radius: R 10 mm   — : 480 mm/min
Feed rate: 480 mm/min — : 960 mm/min
Evaluation position: (X/Y)
X: 120 mm/Y: 135 mm

☐ : Quadrant glitch with ball screw in conventional specification

☐ : Quadrant glitch with ball screw in stabilized frictional characteristics
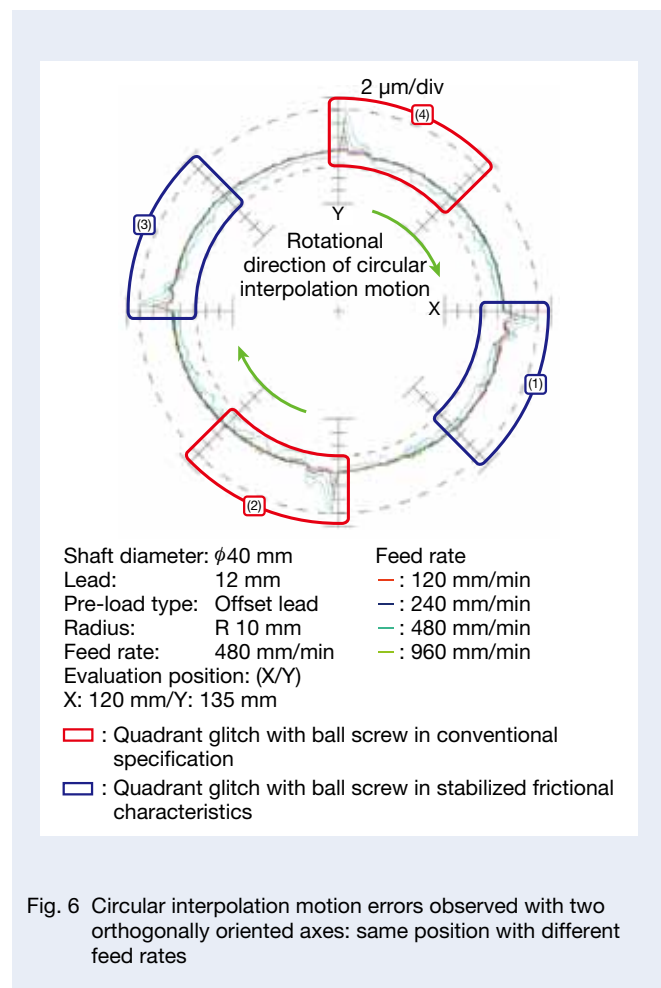
Fig. 6 Circular interpolation motion errors observed with two orthogonally oriented axes: same position with different feed rates

acceleration (influence of friction force generated by rolling elements and inertial force due to mechanical structure) from the increasing height of the quadrant glitches at high feed rates. However, its extent is relatively lower on the ball screw in stabilized frictional characteristics on the X-axis compared to the Y-axis representing the conventional ball screw, and furthermore geometric repeatability during reverse motion in both positive and negative directions is also higher in the X-axis.

In addition, a relatively higher contouring accuracy was also observed for the ball screw in stabilized frictional characteristics on the X-axis, in regard to the error at the circular interpolation motion region; that is, a tendency toward a smaller fluctuation of motion errors in (1) and (3) of Figure 6 compared to those of (2) and (4). The setting of the control system parameters when the two types of ball screw are assembled in the feed drive system are known to be identified in almost the same conditions. Therefore, the phenomenon observed here can be considered as a result of smaller potential motion delay, which appeared as a quadrant glitch when the motion reversed under identical control system conditions, and occurred for the ball screw in stabilized frictional characteristics on the X-axis.

With the aforementioned results, it can be confirmed that the ball screw in stabilized frictional characteristics on the X-axis exhibits consistent motion controllability in light of the quadrant glitch and contour control. The feed drive systems incorporating ball screws in this specification are capable of consistently correcting quadrant glitches under reverse motion regardless of position, even when identifying the system parameters to compensate the quadrant glitch at any position. Furthermore, since these feed drive systems also correct potential motion error during reverse motion, a higher contouring accuracy can be achieved, even in the region of the circular interpolation motion.

4. Mitigating Ball Screw Heat Generation

While the effect of stabilizing the frictional characteristics of a ball screw contributes to improved motion controllability, this also has a certain potential on mitigating the heat generation of the ball screw.

The formula (2) expresses the amount of heat generated by the ball screw itself.

$$Q \propto nT \qquad (2)$$

Q: Amount of heat generated per unit time, kJ/h
n: Rotational speed of ball screw, rpm
T: Friction torque, N·cm

The amount of heat generated by a ball screw depends on rotational speed and torque. Therefore, measures for stabilizing frictional characteristics, such as by reducing torque fluctuation amplitude and adequately controlling the contact states and lubrication states between ball and grooves, which improve motion controllability, may also effect the mitigation and stabilization of heat generation, which ball screws potentialy cause.

Figure 7 shows the tendency of a thermographic evaluation, which reveals areas of temperature rise. These two ball screw feed drive systems are in the same configurations and in the same setting motion cycle. In this layout, the conventional ball screw system is at the left and the ball screw in stabilized frictional characteristics is at the right. For the evaluation, both ball screws are set up in the same pre-loading and stiffness conditions.

The evaluation results suggest that the tendency of heat is lower on the ball screw in stabilized frictional characteristics than on the conventional ball screw. The tendency of temperature rise within the stroke of motion on the ball screw can be regarded as coinciding with the tendency of heat generation because there is the proportional relationship between the value of temperature rise of the ball screw and the amount of heat generation.

Figure 8 shows the recorded change of positioning errors due to the heat generated by the ball screws.

The feed drive system used for the evaluation is configured with a fixed support on the servo motor side and a simple support on the opposite side of the servo motor, under semi-closed loop control. Therefore, the linear expansion of the ball screw shaft due to heat generated by the ball screw itself is likely to appear as a positioning error on the opposite side of the servo motor. Thus, the positioning accuracy in terms of amount of positioning error on the opposite side of the servo motor at a point 1 200 mm apart from the motor side is measured with a laser length measuring system.
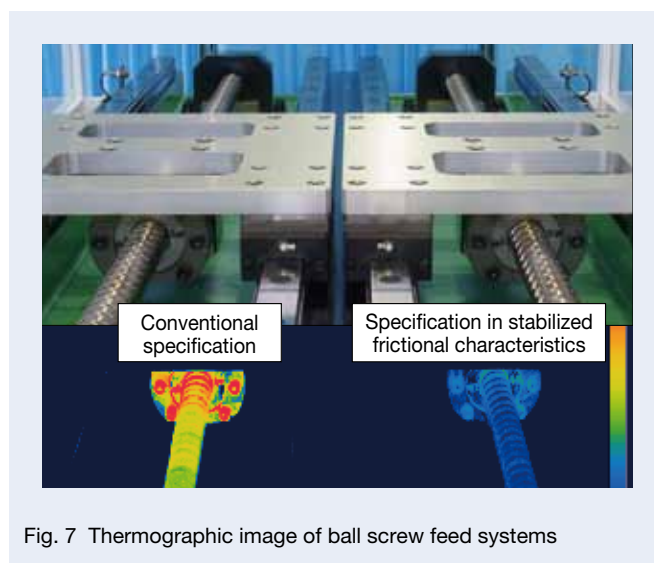

Fig. 7 Thermographic image of ball screw feed systems

• **Evaluation specification**
· Shaft diameter: φ40 mm
· Lead: 20 mm
· Pre-load type: Offset lead
· Average rotational speed: 241 rpm
· Maximum rotational speed: 246 rpm

· Table stroke: 1 200 mm from fixed support side
· Time constant: 0.2 sec
· Dwell time: 0.1 sec
· Lubricant: LRL3 grease

→ : Positioning error of conventional specification ball screw μm at 1 200 mm
■ : Positioning error of stabilized friction characteristics specification μm at 1 200 mm
— : Nut temperature rise on conventional specification ball screw, °C
— : Nut temperature rise on stabilized frictional characteristics specification ball screw, °C
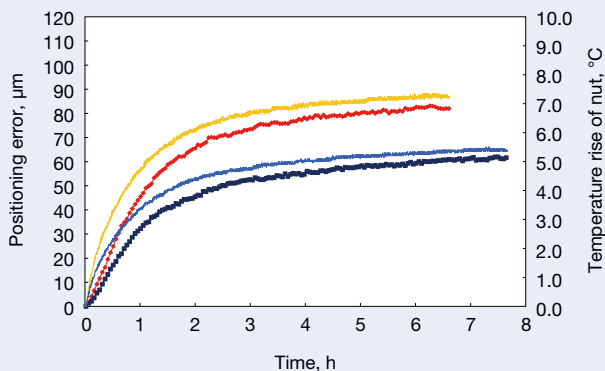
Fig. 8 Temperature rise and positioning error in ball screw feed systems

The figure indicates that, whereas the positioning error saturates at 82 μm with a 7.2°C temperature rise at the nut on the conventional ball screw, the positioning error drops to 62 μm with a 5.4°C temperature rise at the nut on the ball screw in stabilized frictional characteristics. This suggests that the tendency of temperature rise in the ball screw and the magnitude of the positioning error due to the linear expansion of the ball screw shaft are essentially proportional, and that the stabilized frictional characteristics of ball screws may contribute to improving the positioning accuracy of the feed system.

Several methods have been explored as countermeasures against the heat generation of ball screws, including a method of forced cooling inside the ball screw shaft by internal circuit to reduce the linear expansion of the ball screw shaft and a method of forced cooling the nut to cool the heat source itself [6]. The results discussed in this article suggest that the strategy to stabilize frictional characteristics should be assessed as a new countermeasure for heat generation, even when forced cooling is difficult to adopt due to various restrictions.

Conclusion

This article explores the strategy and impact of stabilizing the frictional characteristics of ball screws. Dramatic social change across the world is driving unprecedented innovation and development in industry. NSK is committed to further integrity and higher performance of motion by proactively envisioning the nature of future demand for ball screws, such as consistency of frictional characteristics in ball screws, and will thereby contribute to the evolution of the production market.

References

1) J. Otsuka, "From ancient wooden screw to ball screw with infinite application expansion (20)—Non-linear spring stiffness of ball screw influencing ultra-precision positioning," Vol. 66, No. 6, June issue (2014), 499–509.
2) R. Sato, M. Tsutsumi, and K. Nagashima, "Dynamic behavior of feed drive systems around quadrant changes in circular motion," Journal of the Japan Society for Precision Engineering, Vol. 72, No. 2 (2006), 208–213.
3) K. Miyaguchi, M. Ninomiya, Y. Watanabe, S. Arai, M. Sawamura, and Y. Kakino, "A study on the friction torque variation of a ball screw at motion direction change / Friction torque variation due to the change in ball contact points." Journal of the Japan Society for Precision Engineering, Vol. 68, No. 6 (2002), 833–837.
4) T. Higuchi, H. Kunisada, Y. Kunii, R. Sato, and M. Tsutsumi, "Compensation of quadrant glitches with two peaks in circular motions of machining centers." Transactions of the JSME (version C), Vol. 78, No. 788 (2012–4), 1211–1220.
5) S. Arai, "Design points of ball screw positioning mechanism on the basis of the structural design view of machine tools," Machine Design, Nikkan Kogyo Shimbun, Vol. 58, No. 8 (2014), 128–133.
6) K. Miyaguchi and S. Arai, "State of the Art Ball Screw Trends for Machine Tool Application," Journal of SME – Japan, Vol. 2, August (2013), 13–18.

Satoru Arai

High-Reliability Clutch Release Bearings for Emerging Markets

Manual transmissions have predominated during the rapid evolution of motorization in emerging countries, leading to an increase in the use of clutch release bearings. Road construction and maintenance, however, are still at the development stage, and so cars are often operated on poor road conditions. This has led to increased demand in these countries, more than in developed countries, for clutch release bearings with improved water resistance allowing for a greater exposure to external muddy water.

Here we introduce an NSK-developed clutch release bearing with improved water resistance (Photo 1) that also maintains a friction characteristic equivalent to those of conventional clutch release bearings.

1. Structure and specifications

Figure 1 shows cross-sectional views of a conventional bearing and the newly developed bearing.

Compared to the conventional bearing, the newly developed bearing has non-contact lips on both seals, which are stronger than the original ones, and newly installed non-contact lips at two locations of the seal on the gear box side. In addition, a new drain groove is installed at the outer diameter of the sleeve to further prevent the ingress of foreign matter, such as muddy water, into the bearing.

In our evaluation and verification of the water resistance of the newly developed product, we used actual vehicle components, assuming the ingress of muddy water into the clutch cover (Figure 2).

The new lips at two locations suppressed the ingress of foreign matter, and even if muddy water were to enter into the bearing, the new drain groove mitigates against the accumulation of muddy water close to the bearing, dramatically improving overall water resistance (Figure 3).

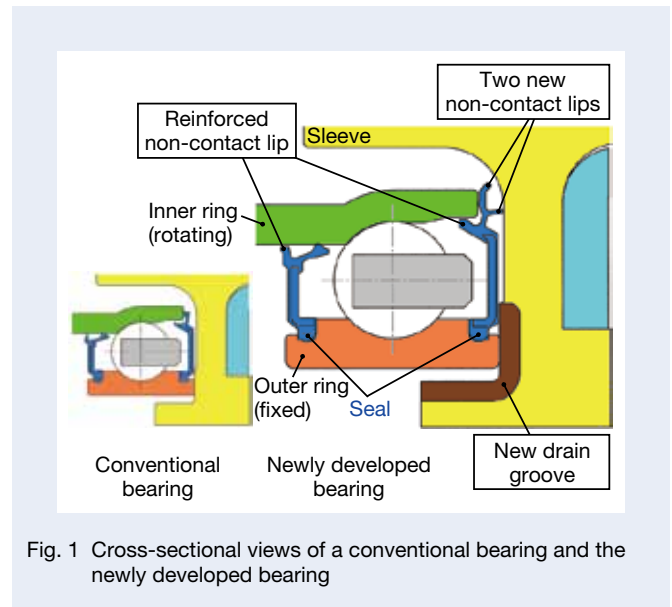Photo 1 High-reliability clutch release bearing for emerging markets

Fig. 1 Cross-sectional views of a conventional bearing and the newly developed bearing
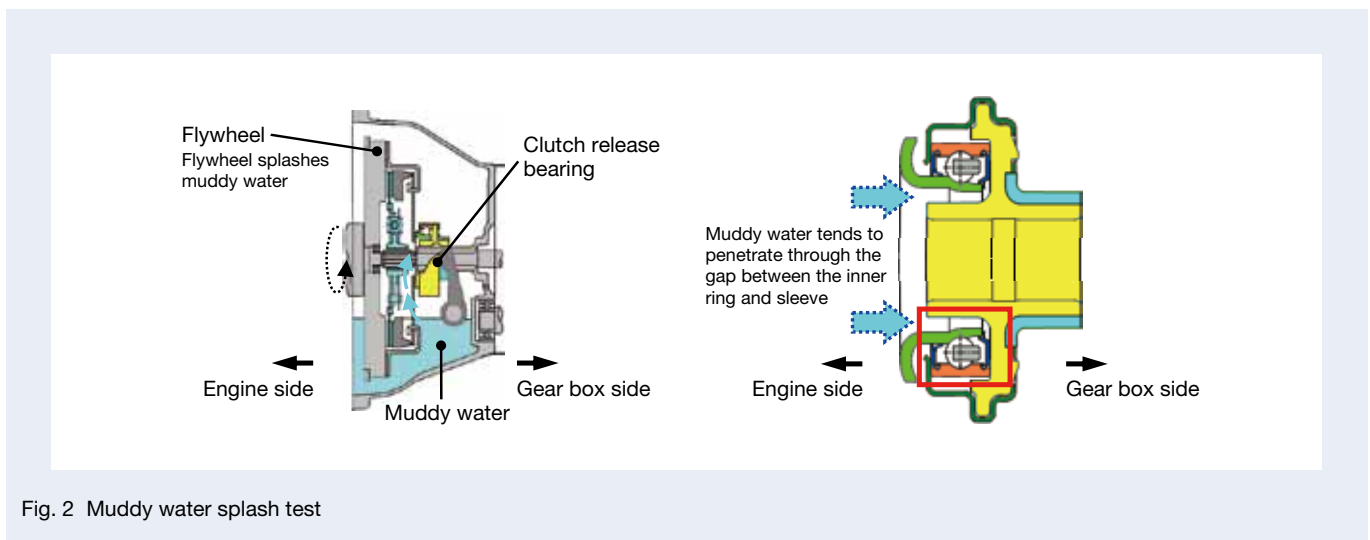
Fig. 2 Muddy water splash test

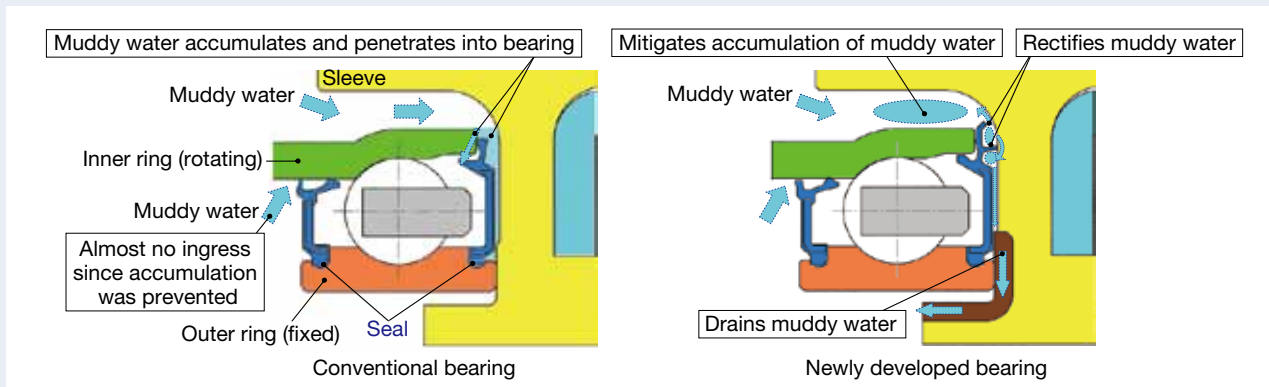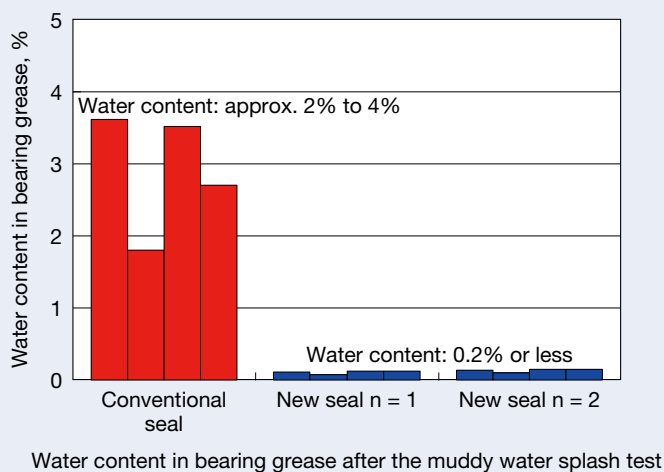Fig. 3 Strong points of the newly developed bearing

Water content in bearing grease after the muddy water splash test

Bearings after the muddy water splash test

Fig. 4 Results of muddy water splash test

2. Effectiveness of the Newly Developed Product

Figure 4 shows the results of the comparative muddy water resistance test, in which the amount of muddy water penetrating into the newly developed bearing was dramatically reduced.

Figure 5 shows the results of a comparative friction measurement, with the friction of the newly developed bearing equivalent to that of the conventional product.

3. Summary

We anticipate growing demand for clutch release bearings with improved endurance in emerging countries, where the percentages of vehicles with manual transmission are high.

NSK will remain focused on maintaining and improving the endurance of clutch release bearings for use under poor operating conditions.
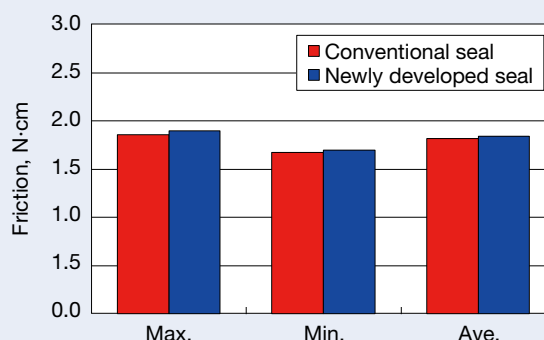

Fig. 5 Friction measurement results

Compact, Lightweight Planetary Needle Bearings

The recent worldwide push to lower automobile fuel consumption has led to the urgent need for more compact, lighter weight transmissions capable of higher efficiency performance. This is driving the trend toward using lower viscosity lubrication oil in smaller quantities. Consequently, planetary gear in transmission mechanisms are expected to be operated under harsh conditions with less lubricant.

NSK has developed compact, lightweight planetary needle bearings (Photo 1) with a resin cage that address the need for smaller, lighter weight transmissions requiring less oil.

1. Configuration, Structure, and Specifications

The recent trend toward planetary pinions capable of higher rotational speeds and revolutions has created demand for cages that are stronger and more durable. NSK has already marketed related products using a chrome molybdenum steel cage featuring an "M" shape cross section to accommodate planetary pinions that operate at high-speed revolutions.

For the new product, our goal was to develop a low-speed revolution planetary pinion that would not require a high-strength, high-durability cage (Figure 1). We achieved a compact, lightweight planetary needle bearing by using a resin for the cage material and incorporating an optimal, analysis-based design with proven durability.

2. Features

These superior characteristics were achieved by using a resin for the cage material and optimizing the cage shape:

(1) Lighter weight
(2) More compact
(3) Added function to control lubricant volume (lower viscosity and a smaller amount)

Photo 1 Compact, lightweight planetary needle bearings (new bearing on right)
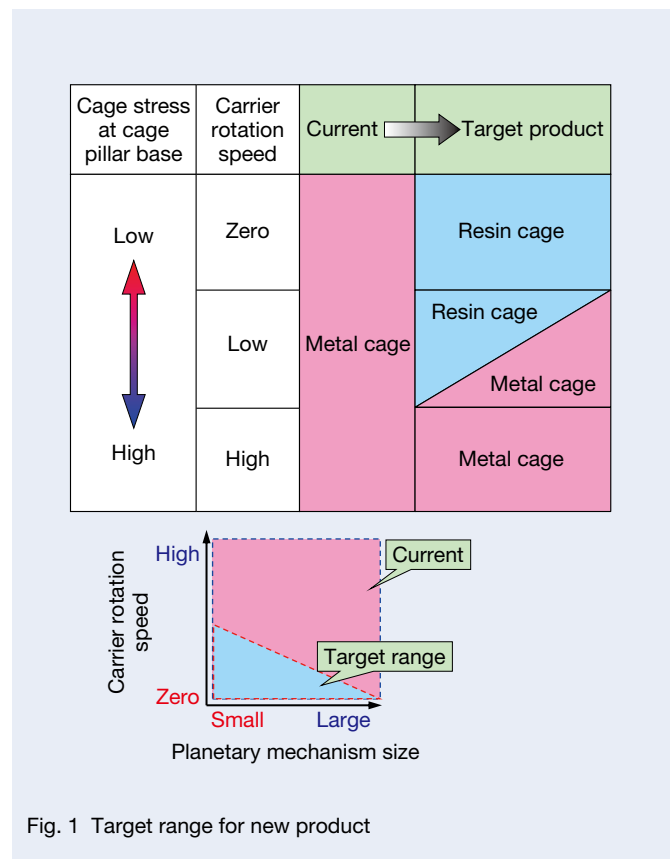

Fig. 1 Target range for new product

Table 1 compares specifications of a conventional metal cage with those of the new resin cage. Using a resin for the cage instead of metal reduces its strength; however, applying careful analysis to optimize the cage shape can reduce cage stress by approximately 66%.

The durability verification test demonstrated that the resin cage can manage up to 60% of the carrier rotation speed range of a metal cage.

Using a resin cage over a current metal cage enables the use of lighter weight bearings with the same dimensions. For example, using a $\phi 16 \times \phi 22 \times$ W20 mm bearing can reduce weight by 25%.

Moreover, the number of rollers used in a metal cage is constrained by the inability to significantly vary the thickness of pillars (extremely thinner or thicker) due to press workability. Resin cages, however, are produced by an injection molding process, which allows for greater freedom in the design of cage pillars and the setting of the number of rollers. Therefore, it became possible to set the optimal number and length of rollers for required cage strength to reduce bearing width by up to 10% while maintaining the same level of bearing capacity.

Furthermore, injection molding supports a variety of cage shapes, such as making discharge grooves to control the amount of lubrication oil that passes through the bearing, leading to a more effective use of small quantities of lubrication oil (Figure 2). An oil pooling feature would also improve lubrication oil retention to curb seizure and abrasion under low viscosity, low quantity oil conditions.

3. Applications

This product is optimal for the low revolution speed of planetary pinions that do not require a high-strength, high-durability cage, and will contribute to the creation of transmissions that are smaller, lighter, or that use less lubrication oil.

4. Summary

NSK will encourage the use of its new needle bearing as an optimal component that satisfies planetary pinion requirements such as high strength and lighter weight.

Table 1 Specifications of current and newly developed products

	Current product	Developed product
Material	High-strength metal	Glass-filled nylon
Cage type	"M" shape type (uniform thickness)	Straight type (thicker, reinforced columns)
Heat resistance temperature	240°C	150°C
Cage stress at cage pillar base under carrier rotation	66% stress reduction	
Weight ratio (cage + roller)	1	25% lighter 0.75

Representative results of measured amount of penetrating oil

Oil feed pressure: 0.02 MPa
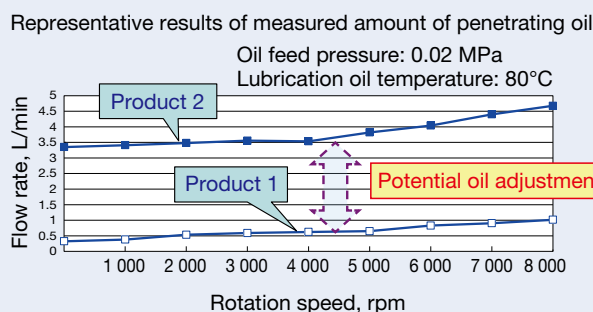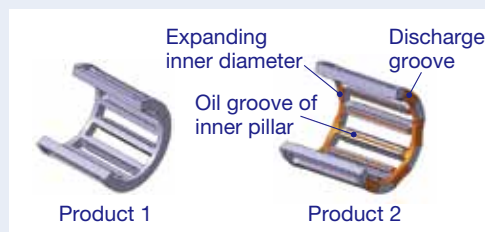Lubrication oil temperature: 80°C

Fig. 2 Example of a discharge groove for lubricant

Idler/Tensioner Bearings with High-Speed Capability and Excellent Sealing Performance

In developing countries that have experienced rapid growth in the use of automobiles, demand has increased for bearings with high sealing performance for tensioners and idlers (Photo 1) around engine accessory belts that operate in wet or dusty environments. These bearings must satisfy the high-speed resistance specifications required for smaller pulleys.

1. Construction, Structure, and Specifications

Accessories around an engine, including the alternator, air compressor, and water pump, are driven by belts with a tension that must remain constant by using a tensioner or an idler based on belt layout. These tensioners and idlers use pulleys with built-in bearings so they can maintain belt tension.

Located in the front of the engine compartment, these accessories may be exposed to water, dust, and muddy water during vehicle operation. The increasing use of automobiles in emerging countries under harsher conditions, such as dirt roads, necessitates that bearings demonstrate a higher sealing performance.

At the same time, the current worldwide trend toward small engines has led to reduced pulley diameters to fit belts in and around downsized engines, which, in turn, has boosted the speed increasing ratio. Bearings must therefore also meet high-speed resistance requirements.

Bearings for tensioners and idlers are fitted with contact seals to prevent the ingress of water and dust from outside as well as grease leaks from inside the bearing. Seals have movable parts at the tip, referred to as lips, which include the main lip moving against the inner ring, a dust lip to prevent ingress from outside, a grease lip to stop grease leaks, and a neck that supports the lips.

These new ball bearings deliver both excellent sealing performance and high-speed capability and were achieved by optimizing the seal lip shape.
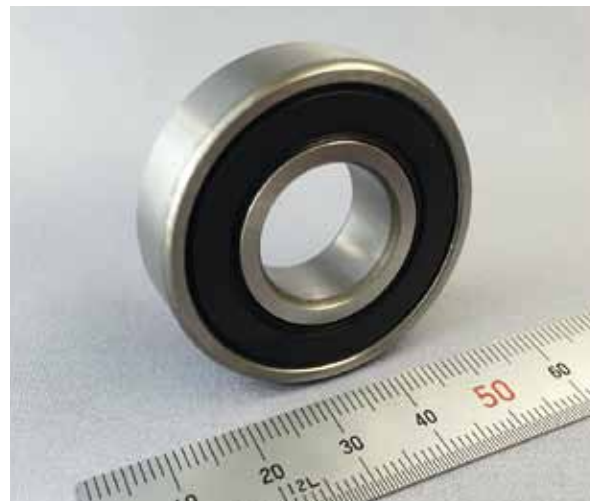

Photo 1 Idler/tensioner bearings with high-speed capability and excellent sealing performance
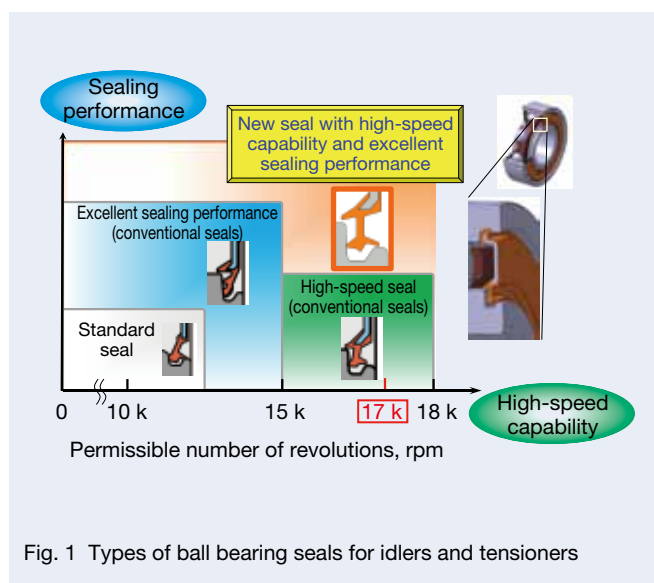

Fig. 1 Types of ball bearing seals for idlers and tensioners

2. Features

While NSK had separately produced high sealing performance seals and high-speed seals, we could create the new seals with excellent sealing performance and high-speed capability by improving existing high-speed seals (Figure 1).

Features (Figure 2)
(1) High-speed capability: Equivalent to existing high-speed seals
(2) Excellent sealing performance: More than twice the sealing protection of that of a conventional seal

Development goals
- Adopt a shape that optimizes the barycentric position of the seal lip, thereby reducing the influence of centrifugal force on the seal lip, which increases at high-speed rotation
- Enhance neck flexibility to reduce change in reaction force
- Narrow the gap in the dust lip to form a labyrinth between the seal and bearing part (inner ring), thereby preventing the ingress of foreign matter

Figure 3 shows the results of a sealing performance test, in which we sprayed muddy water onto the rotating bearings installed on a test bench that simulates an accessory belt drive, and the test results indicated that less water had penetrated into the bearings than when using the conventional seal.

3. Applications

The product can be used in bearings for tensioners and idlers to meet increasing demand for durability at high speeds and excellent sealing performance.

4. Summary

We will respond to the needs of customers by introducing these bearings into the market and expanding the product line.
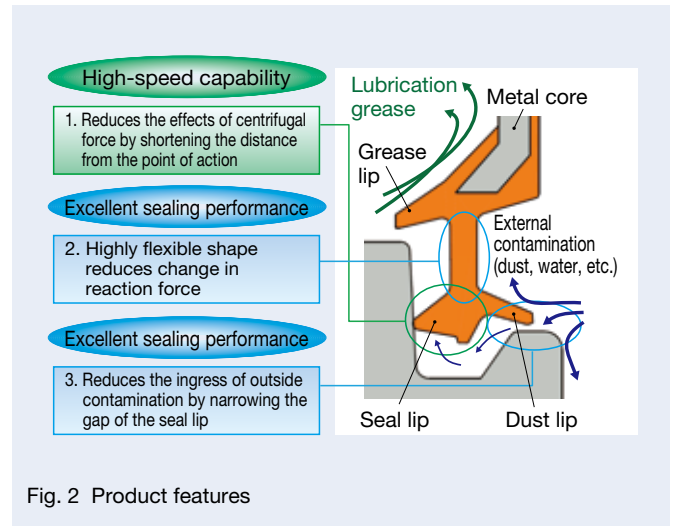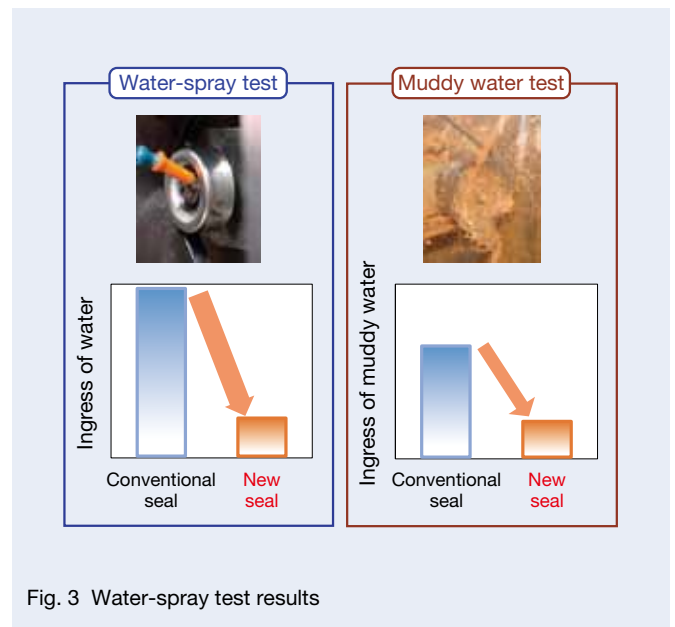

Fig. 2 Product features

Fig. 3 Water-spray test results

Dental Air Turbine Bearings

Dental air turbine bearings (Photo 1) reach speeds of 400 000 rpm and therefore require regular maintenance and replacement, leading to increased demand for longer bearing life. In addition, after each use, the bearings are exposed to cleaning solutions, high pressures, and high temperatures during the sterilization process, and so they have to demonstrate outstanding corrosion resistance and durability.

To meet these needs, NSK has developed long-life, low-vibration, and highly corrosion resistant bearings. We have also created a wide variety of products for this series to ensure interchangeability with the various bearing dimensions, types, and shapes available on the market.

Photo 1 Dental air turbine bearings

1. Features

(1) 1.5 times the life (Figure 1)

Air turbine bearings must maintain super-high speeds to enable precise treatment. The life of these bearings must therefore be viewed differently compared to other common types of bearing life, such as rolling fatigue life. For this reason, we introduced RPM life, which defines the end of bearing life as the point at which an initial RPM falls below a given threshold due to bearing failure. Consequently, design and dimensional control of bearing cages are crucial for extending RPM life. We achieved 1.5 times the life of a conventional bearing after developing an optimum design based on analysis and verification along with strict dimensional control supported by an advanced processing technique.
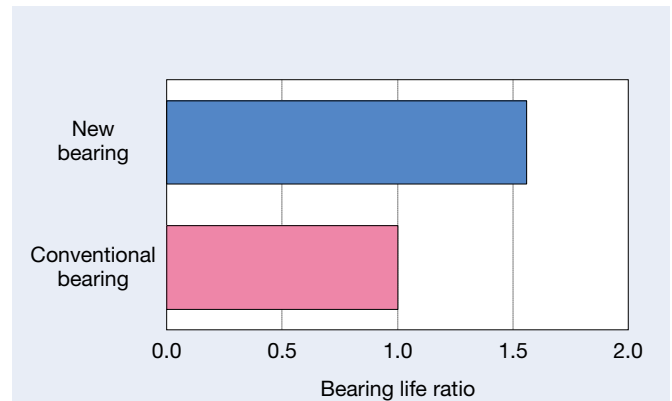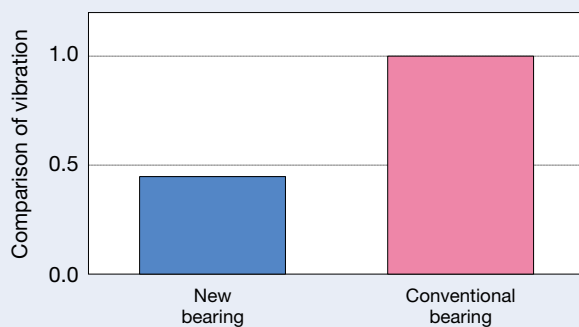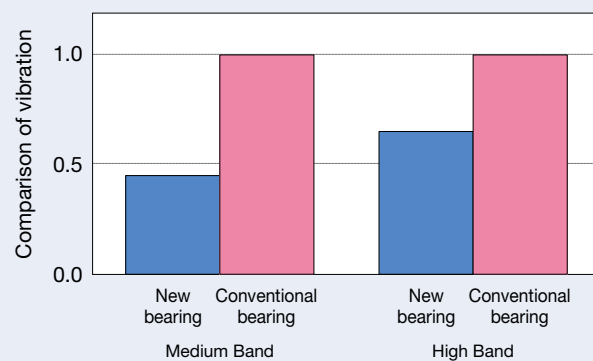

Fig. 1 Bearing life ratio (based on number of revolutions)

(a) Vibration acceleration in axial direction

(b) Anderon value

Fig. 2 Vibration level

(2) Half the vibration level (Figure 2)

Vibration generated by a bearing impacts both the cutting ability of an air turbine fitted in endodontic equipment and the dentist's delicate sense of touch during treatment. We reduced the vibration level in the new product by half compared to the conventional bearing by improving the processing accuracy of the inner and outer rings and the ball bearings.

(3) 10 times the corrosion resistance (Figure 3)

Various cleaning solutions are used to wash air turbines, in some cases including strongly alkaline liquid. In addition, air turbines are normally exposed to high-temperature sterilization (up to 135°C) and/or high-pressure steam environments. Bearings must also endure cleaning and sterilization processes. We therefore strengthened the corrosion resistance by using a high-corrosion resistant material developed by NSK.

(4) Wide range of dimensions, types, and shapes (Figure 4)

Our extensive product line-up includes 43 bearing types (e.g., deep groove ball bearings, angular bearings, and integral bearings) and outside diameter shapes (straight, flange, groove, and specialized flange) for use in a wide variety of air turbines.

2. Applications

The products are for air turbines in dental instruments.

3. Summary

The dental air turbine bearings can extend the maintenance interval of bearings, ensuring a safer and more reliable cleaning and sterilization process and contributing to a clean, comfortable treatment environment.

We are committed to developing safer products for society.

Test conditions
· Anodic polarization curve measurement test (JIS G 0579)
· Test solution: 5% H_2SO_4 water solution
· Sweep speed: 20 mV/min
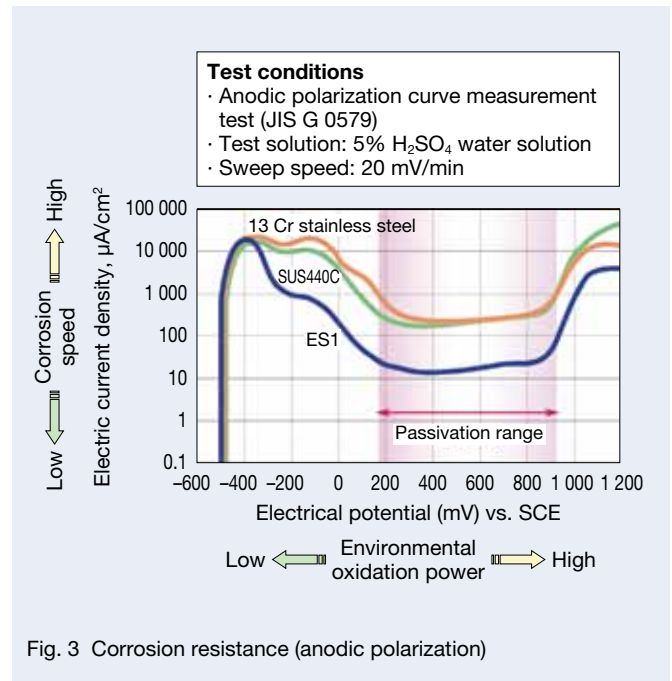
Fig. 3 Corrosion resistance (anodic polarization)

(a) Bearing types

Deep groove   Angular   Integral angular   Integral + shield angular

(b) Outer shapes

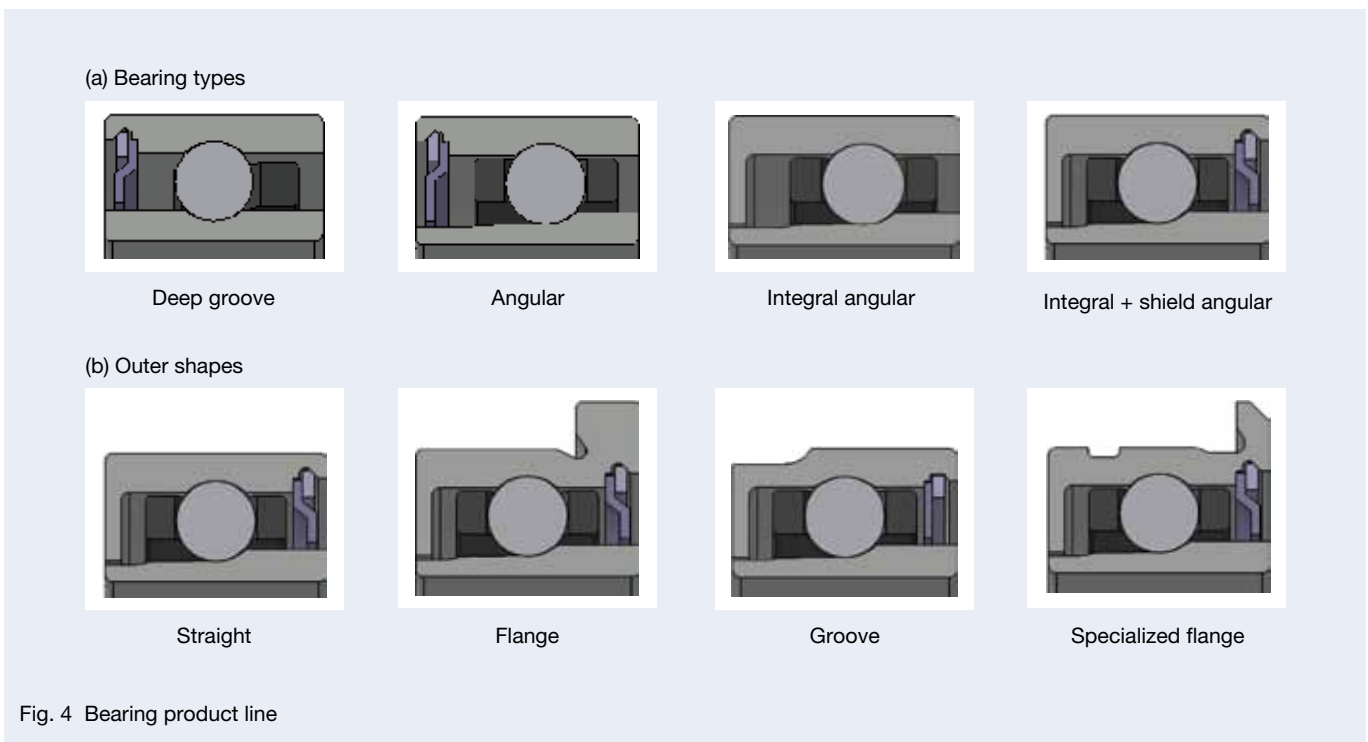Straight   Flange   Groove   Specialized flange

Fig. 4 Bearing product line

Long-Life, Sealed Four-Row Tapered Roller Bearings for High-Speed Rolling Mills

Growing populations and improving standards of living in emerging countries are creating unprecedented demand for tinplate products used for food and beverage containers. This type of tinplate is very thin, and its coil weight is lighter than that of other sheet metals, such as those for automobiles, and requires boosting the rolling mill speed to achieve higher productivity. Higher speed revolutions, however, expose the bearings used in rolling mills to the following challenges, which can result in early damage.

(1) Early deterioration due to the heat generated in the bearing seal lip allows the ingress of cooling water into bearings, which may lead to poor lubrication resulting in abrupt occurrences of early flaking and seizure.
(2) Early deterioration of grease due to heat generated in the bearings may lead to poor lubrication, resulting in abrupt occurrences of early flaking and seizure.

NSK developed long-life, sealed four-row tapered roller bearings for high-speed mills (Photo 1) to prevent these problems and ensure stable operation in a high-speed environment.

1. Features

(1) Seal providing lower heat generation and higher sealing performance
• Seal with lower heat generation is made of a special resin (PTFE) with a low-friction factor and incorporated into the rubber seal lip through integrated molding (Figure 1)
• Low-heat generation and high sealing performance can be maintained for an extended period, even during high-speed operation (Figure 2)

(2) Lower heat generation in the bearings
• By substantially reducing roughness on the tracking surfaces of inner and outer rings and on the rolling elements, the bearings generate less heat (Figure 3). Consequently, the occurrence of lubricant deterioration due to heat generation is significantly reduced.

(3) Extended service life with NSK's proprietary super TF bearings
• Use of super TF bearings, a proprietary NSK product featuring a new material and applying a heat treatment method, significantly extends the service life of the receway and rolling element surfaces, which can be adversely affected by foreign particles and poor lubrication (Figure 4).

Photo 1 Long-life, sealed four-row tapered roller bearings for high-speed rolling mills

Special seal for low-heat generation and high sealing performance

Fluoroelastomer   PTFE (polytetrafluoroethylene) resin

Fig. 1 PTFE seals

Speed: 2 300 m/min equivalent

Seal lip temperature, °C

160°C   50% reduction   80°C

Conventional seal   Special seal

Speed: 2 300 m/min equivalent

Water ingress rate, %

After 500 hrs. elapsed

78%   80% reduction   16%

Conventional seal   Special seal

Fig. 2 Heat generation and seal performance test results

Reduced friction on both rolling and
sliding surfaces

Surface roughness: High ⇨ Friction: High
(thin oil film)

Surface roughness: Low ⇨ Friction: Low
(thick oil film)

Surface roughness significantly reduced
by optimizing processing conditions

Speed: 2 800 m/min equivalent

20% reduction

115°C

90°C

Fig. 3 Low heat generation of bearing

Field test under conditions of foreign particles
and insufficient oil film formation

2 × life

1

2

Conventional
bearing

Super TF
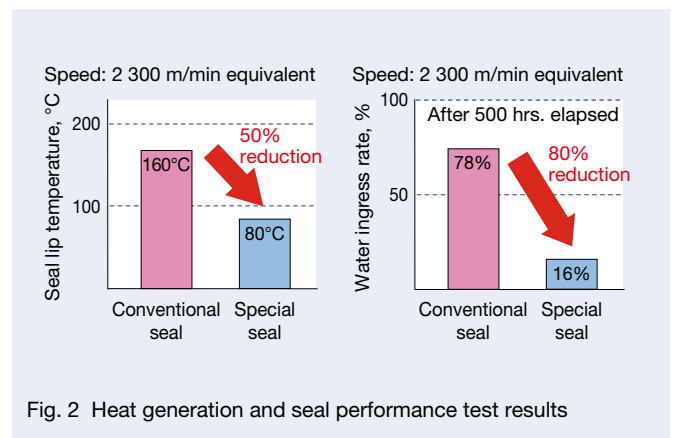bearing

Fig. 4 Field test results

2. Applications

While these new bearings are primarily used to support tinplate production by high-speed mill barrel rolls, they can be also used to support other mill rolls operating under harsh environments under which seals suffer early damage caused by ingress of cooling water and mill scale.

3. Summary

The long-life, sealed four-row tapered roller bearings for high-speed mills are expected to extend bearing service life by two to five times as a result of lowering the heat generated by the seals and bearings to constrain heat-induced lubricant deterioration and delivering enhanced performance against water ingress and insufficient oil film formation, thus improving the productivity and stable operation of rolling mills.
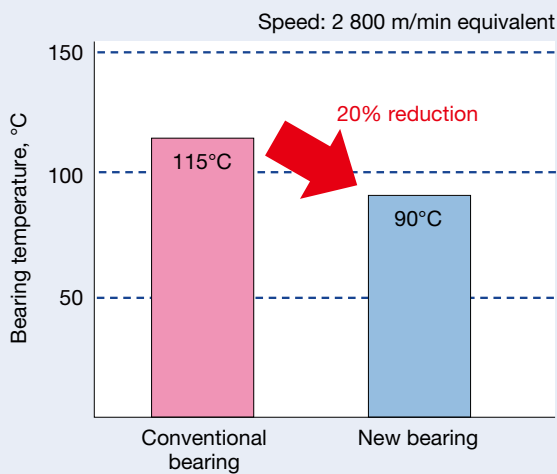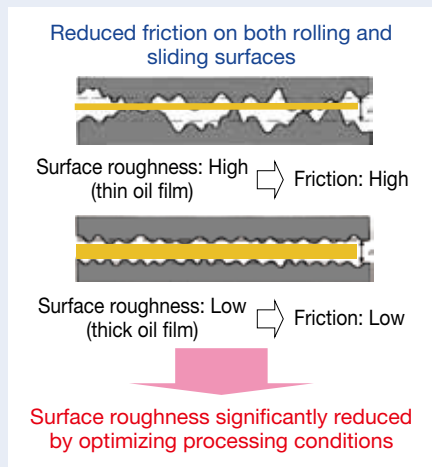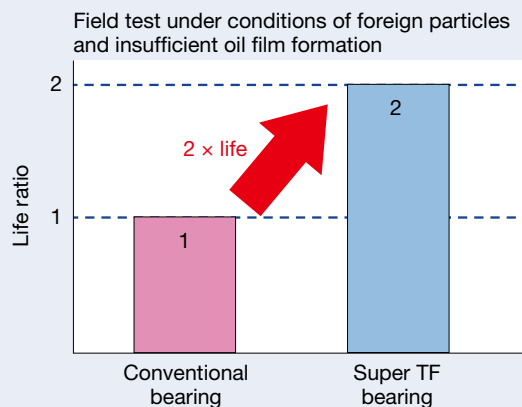
NSKTAC03 NSKHPS Angular Contact Thrust Ball Bearings for Ball Screw Support in High-Load Drive Applications

Increased demand for energy-saving solutions and oil-less components in injection molding and press machines for high-precision automotive plastics and large LCDs have induced a trend toward switching from hydraulic drive systems to electric drive systems, which include rotary motors and ball screws. Bearings used for ball screw support must provide improved reliability for higher productivity and operate under higher load conditions. In response, NSK has developed NSKTAC03 NSKHPS angular contact thrust ball bearings for ball screw support in high-load drive applications (Photo 1).

Photo 1 NSKTAC03 NSKHPS angular contact thrust ball bearings for ball screw support in high-load drive applications

1. Bearing Specifications

Our new products have improved both the dynamic load rating and the critical axial load as a result of optimizing the interior design of the bearings. The product line includes bearings with ϕ15 mm to ϕ120 mm bore diameters (with plans to increase the diameter up to ϕ180 mm) as well as a special bore diameter series with only the bore diameters downsized (Figure 1).

2. Features

(1) Rolling fatigue life is extended by 1.3 times compared to that of the older series owing to the modified initial contact angle and NSKHPS technology (Figure 2).

(2) Critical axial load is increased by 1.5 times compared to that of the older series. This is due to the elevated groove shoulder and optimized interior design (Figure 3). As a result, the number of bearing rows in the load application side can be reduced, allowing for the use of smaller parts surrounding the bearings (Figure 4).

(3) The special bore diameter series, which features a smaller bore diameter, while the other parts have remained the same size, allows for a more compact end of screw shaft with unchanged load capacity (Figure 5).

(4) The new bearings can replace products in the older series without the need for modification of the surrounding design, as the mounting dimensions are the same.

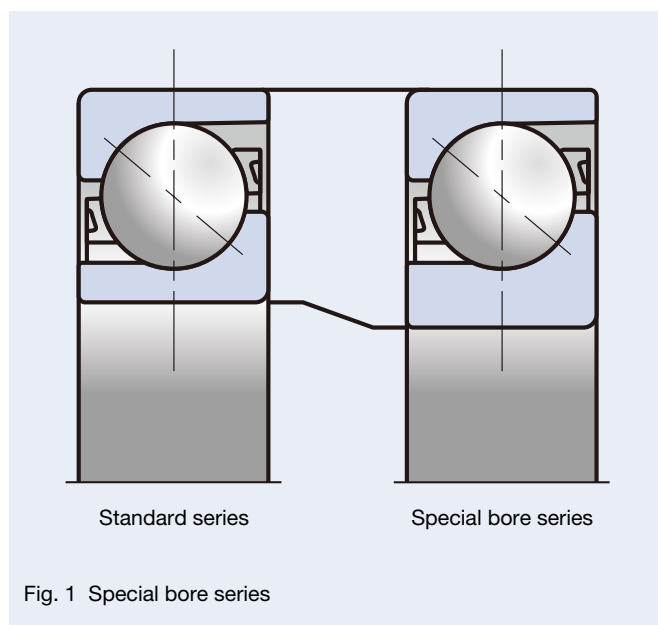Standard series   Special bore series
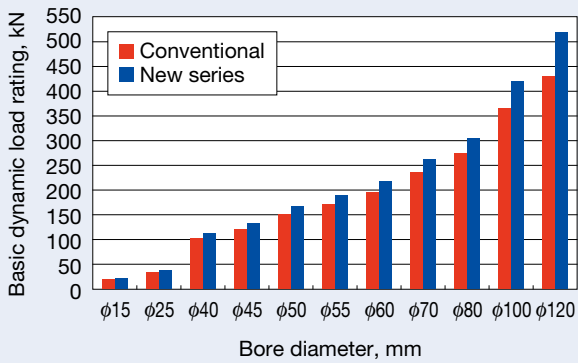
Fig. 1 Special bore series

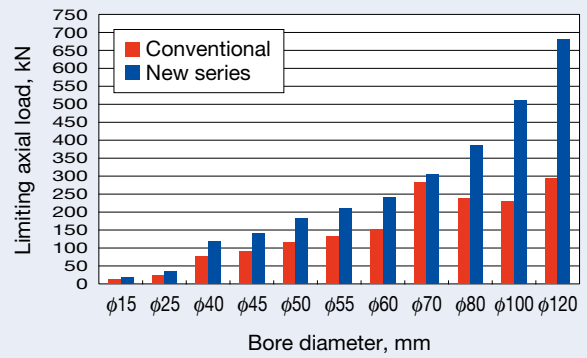Fig. 2 Comparison of basic dynamic load rating

Fig. 3 Comparison of limiting axial load
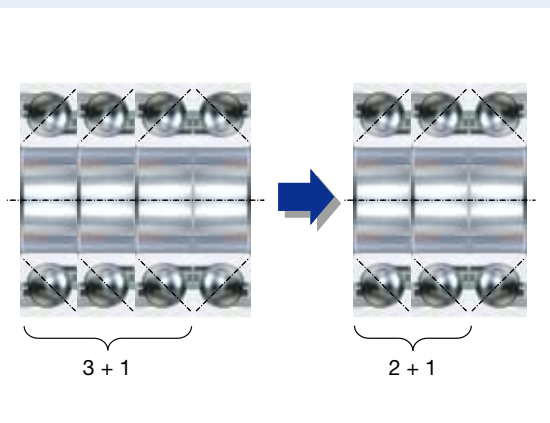
Fig. 4 Example of bearing row reduction

3. Applications

The new bearings are useful in injection molding and press machines that process high-precision plastic parts. Beyond their suitability for replacing conventional products, they also meet the needs for higher loads and downsized machines.

4. Summary

Compared with the previous series of angular contact thrust bearings for ball screw support in high-load drive applications, the new products have extended rolling fatigue life by approximately 1.3 times and increased critical axial load by 1.5 times. These functional improvements have allowed for reliable operation of equipment under high loads, which boosts productivity.

Fig. 5 Example mounting of special bore diameter series

Ball Screws with Minimal Grease-Splatter L1 Seals

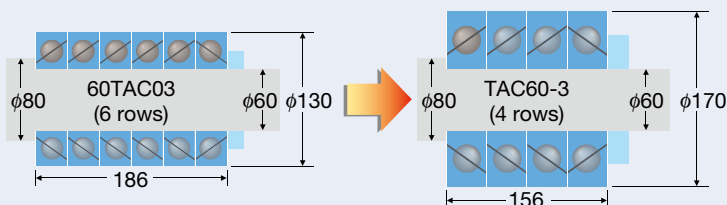The rotation of a ball screw shaft inevitably splatters grease, and devising effective countermeasures to control this issue has presented challenges. Avoiding grease-splatter contamination around the periphery requires the machine user to run equipment until the splatter of the filled grease decreases or to wipe off excess grease around the screw shaft. In some cases, an additional cover is necessary around the ball screw shaft to prevent contamination.

These issues have a direct impact on productivity and production cost, as well as a particularly strong impact on electronic chip mounting systems, semiconductor production equipment, and food processing and medical equipment, which require extremely clean operating environments. In addition, more grease splatters when the rotational speed of the ball screw is increased to shorten takt time.

To improve the situation, NSK achieved an industry first by developing ball screws with the aim of reduced grease and commercialized them as Ball Screws with Minimal Grease-Splatter L1 Seals (Photo 1).

1. Constitution

Centrifugal force generated by the rapid revolution of the ball screw shaft causes the splattering of grease from the shaft (Figure 1). Moreover, when ball screws are shipped, their nuts are usually filled with grease, and excess grease discharged from the nuts tends to easily adhere to the ball screw shaft, which can lead to splattering from the shaft as well.

L1 seals have been designed to prevent splattering by:

(1) Preventing the pooling of grease on the surface of the ball screw shaft; and
(2) Preventing grease leakage from the nut.

To prevent the pooling explained in (1), excess grease on the ball screw shaft is drawn into the nut through the slits and thread ridge that was incorporated in the seal (Figure 2). To prevent the leakage explained in (2), excess grease in the nut is collected inside the seal unit. Since the seal itself does not rotate, grease on the seal does not splatter.

Also, the design of L1 seals has minimized the clearance between the seal and ball screw shaft so that no seal torque is generated. As a result, the surface of the ball screw shaft continuously maintains such a thin grease film that splatter does not occur. This eliminates the need to wipe off excess grease around the ball screw shaft and is expected to produce a much better lubrication level comparable to that of contact seals.

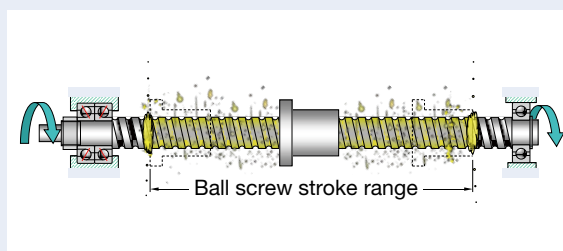Photo 1 Ball screws with minimal grease-splatter L1 seals
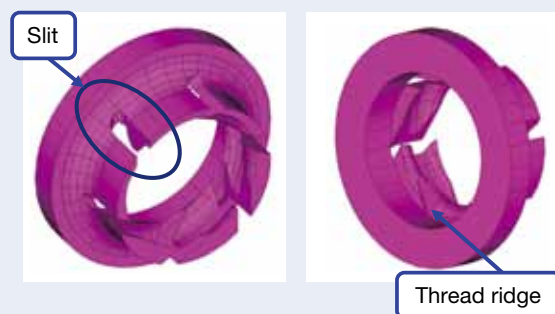

Fig. 1 Cause of grease splatter from ball screws

Ball screw stroke range

Slit

Thread ridge

Fig. 2 L1 seal structure

2. Features and Specifications

(1) Significantly reduces grease splatter

Owing to its new design for reduced splatter, L1 seals have significantly cut down the amount of grease splatter from the rapidly rotating screw shaft. According to the results of a comparative test (Figure 3), the L1 seal has produced one-tenth of the splatter compared to a conventional seal. This indicates that the new seals will contribute to maintaining clean conditions inside workpiece products and equipment.

(2) Adopts a non-contact seal

L1 seals do not generate seal torque because they are fitted with a small clearance between the seal ridge and ball screw shaft. Conventional seals that splatter a relatively small amount of grease used to be all contact seals. L1 seals are the first non-contact seals that reduce splatter.

(3) Includes a seal cover as a standard component

L1 seals are equipped with a cover to prevent grease dripping.

(4) Can be fitted onto standard ball screws

Ball screws with minimal grease splatter L1 seals can be fitted onto NSK standard inventory ball screws, such as Compact FA Series and High-speed SS Series ball screws, and thus allow quick delivery.

General product specifications are as follows:

Lubricant: General grease, low-dust grease, and grease for food processing equipment
Environment: Ambient room temperature
Applicable ball screws (Table 1): Compact FA Series (ϕ15–ϕ25 mm) and High-speed SS Series (ϕ32 mm)

Fig. 3 Grease splatter comparison

3. Applications

The L1 seals are suitable for use in electronic chip mounting systems, semiconductor equipment, food processing, and medical equipment that require extremely clean operating environments.

4. Summary

Ball screws with minimal grease splatter L1 seals now feature the shaft diameters of ϕ15 to ϕ25 mm, and ongoing enhancements for the product line are planned.

Table 1 Product line-up

Shaft diameter / Lead	5	10	20	25	Series supported
15	◯	◯	◯		
20	◯	◯	◯		Compact FA
25	◯	◯	◯	◯	
32	◯	◯			High-speed SS

TOUGHCARRIER

Development and widespread use of electrical equipment and jigs have led to increased application of electrically driven actuators in automobile production facilities and general industrial machinery. When actuators are used for these purposes, the moment force on the load position is in most instances offset from the guides, requiring a higher load bearing capacity than that of conventional MONOCARRIER actuators.

NSK has developed the TOUGHCARRIER single axis actuator for use in these environments (Photo 1).

1. Features

• Increased load capacity in the guides

As shown in Figure 1, the guide mechanism of the TOUGHCARRIER is fitted with rollers instead of balls. The change from point contact to line contact allows for a wider contact area, which disperses contact surface pressure. As a result, the dynamic load rating is more than tripled (extending service life by more than ten times) and the static load rating is more than doubled (Figures 2 and 3), and thus the load capacity of the guide section has been improved.

2. Construction, Structure, and Specifications

As shown in Figure 4, the TOUGHCARRIER is marketed as a standard TCH Series consisting of three model sizes, which incorporate NSK K1 lubrication units as standard equipment.

Optional accessories, similar to those offered for the MONOCARRIER, include a cover unit, a motor bracket, a sensor rail, and a sensor unit (Figure 5), which can be selected for mounting onto the main body.

3. Applications

The new products are suitable for carriage equipment used in automobile production facilities and general industrial machinery, where guides are exposed to excessive moment load.

4. Summary

The TOUGHCARRIER is a higher load capacity, single-axis actuator. NSK plans to extend the line-up of optional units for components such as reverse motor mounts in response to market demand for downsized equipment.
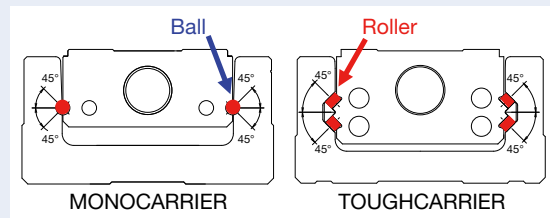

Photo 1 TOUGHCARRIER

Fig. 1 MONOCARRIER and TOUGHCARRIER structures
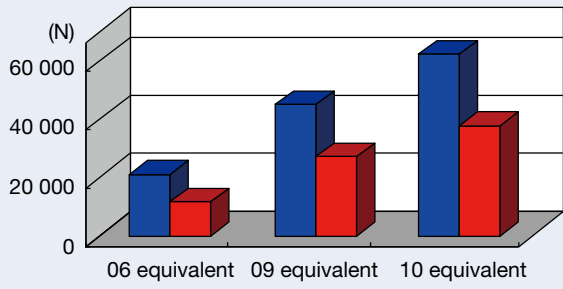
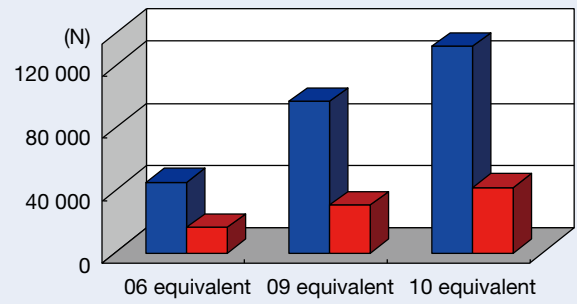Fig. 2 Basic dynamic load rating comparison

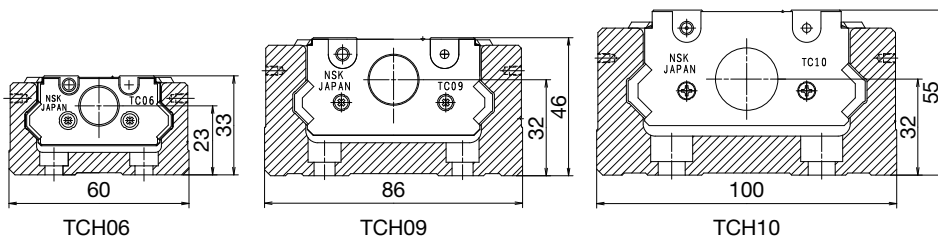Fig. 3 Basic static load rating comparison

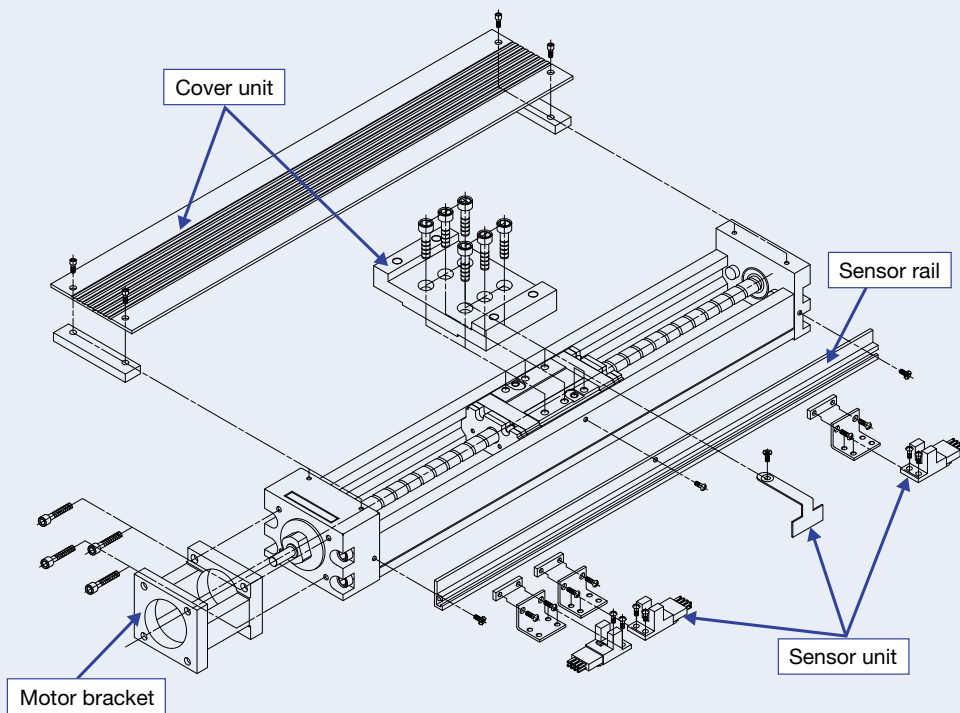Fig. 4 TCH Series cross sections

Fig. 5 TOUGHCARRIER accessories

NH Series and NS Series NSK Linear Guides: More than Twice the Life of Conventional NSK Linear Guides

Linear guides are used by production facilities for a wide range of applications for numerous industries, including semiconductors and automobiles, where these guides require a longer service life to meet demand for higher productivity and longer maintenance intervals.

NSK's LH and LS linear guide series have achieved widespread use since being introduced in 1989. With more than twice the service life, our new NH and NS series (Photo 1) also retain the remarkable features of the LH and LS series.

1. Specifications

The NH and NS series are pictured in Photo 1. While both series have the same basic structure, there are differences between them (Figure 1):
• NH Series: Larger ball diameter for extended life
• NS Series: Lower mounting height and compact

NH Series guides are available in sizes 15 to 65 and NS Series guides in sizes 15 to 35 (number indicates approximate rail width in millimeters).

The installation dimensions (mounting height/width, mounting hole diameter/pitch, etc.) of these guides are equal to those of the LH and LS series. Therefore, mechanical design does not require modification in order to use the NH and NS series.

2. Features

(1) More than twice the service life

The contact point between the balls and ball grooves supports load in linear guides, so a design and manufacturing technique for ball grooves has a significant impact on service life. Consequently, NSK has leveraged its technologies for analysis (simulation) and production to develop a ball groove with a new shape (Figure 2). Optimizing the distribution of surface contact pressure can allow for an exponential extension of service life.

As a result of this optimization, dynamic load rating is increased by 1.3 times and the service life is more than twice that of products in the LH and LS series (Figure 3). These characteristics are advantageous in that they extend equipment service life and support downsizing without affecting service life.

Photo 1 NH Series and NS Series

NH Series
Larger ball diameter to maximize service life

NS Series
Lower mounting height and compact

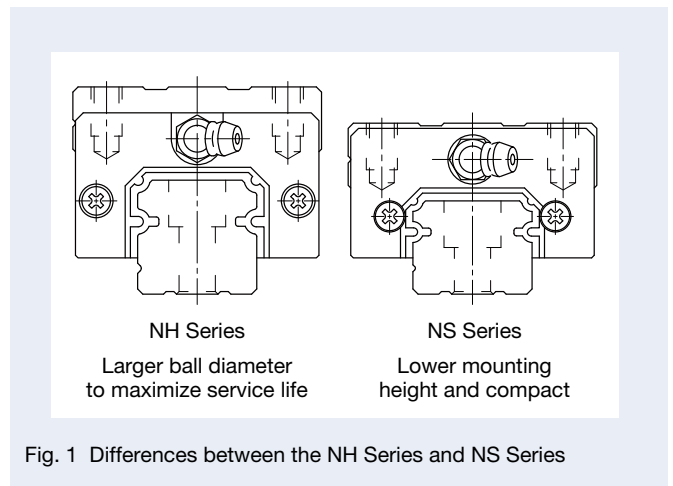Fig. 1 Differences between the NH Series and NS Series

(2) Increased maximum allowable speed

Maximum allowable speed was increased by improving the design of the recirculation parts. Table 1 shows the maximum allowable speeds. The maximum allowable speed of 15 to 35 of the NH and NS series is 5 m/s, which is nearly equivalent to three times 1.7 m/s, the maximum allowable speed of the LH and LS series.

Fig. 2 NH and NS series design concept

Fig. 3 Life of NH and NS series compared with life of LH and LS series
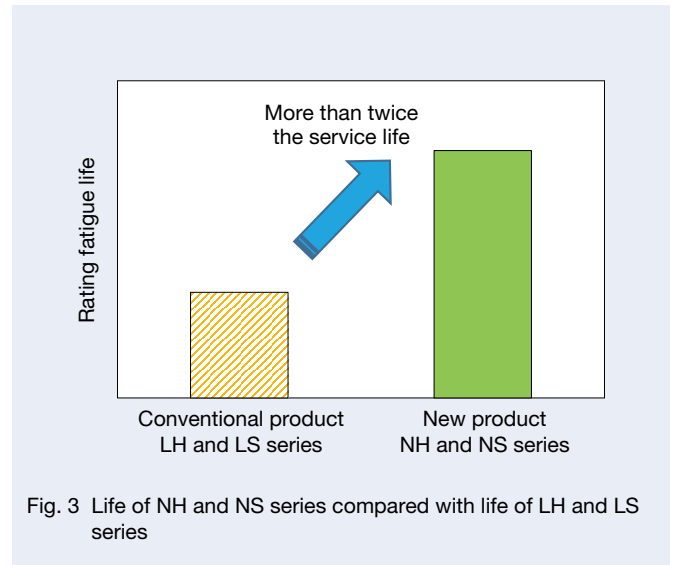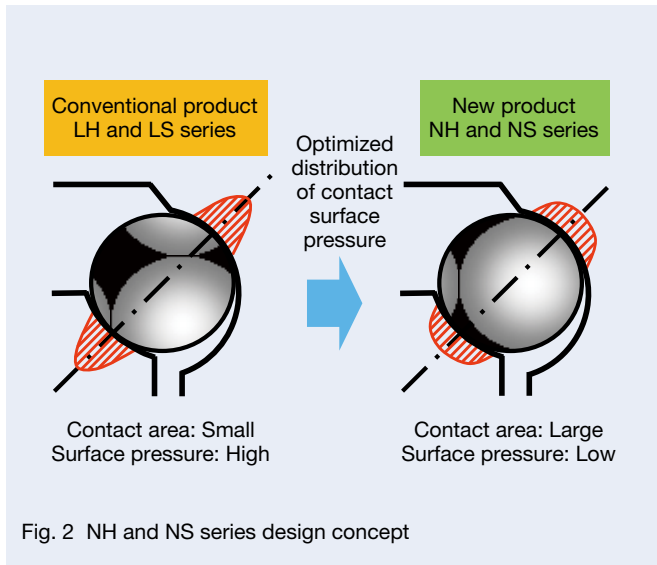
Table 1 Maximum allowable speeds of the NH and NS series

Unit: m/s

Model	NH15 NS15	NH20 NS20	NH25 NS25	NH30 NS30	NH35 NS35	NH45	NH55	NH65
Maximum allowable speed	5					3.3		2.5

(3) Easy-to-use standard linear guide

For wider usability, various options for the new series are available:

• Random-matching guides allow the user to freely combine rails and ball slides regardless of ball slide shape, accuracy grade, or preload, and also allow for quick delivery.

• A robust line-up of options includes the NSK K1™ lubrication unit for long-term maintenance-free operation, a double seal, protector, and surface treatment.

3. Applications

The NH and NS series can be used for a wide range of applications, including:

• LCD/semiconductor manufacturing equipment
• Automobile production equipment
• Material handling equipment
• Machine tools
• Platform gates
• Medical equipment

4. Summary

While it had seemed as though linear guides, having few components or mechanical elements, could not be improved much further, our new NH and NS series are significantly enhanced guides for more robust functionality, achieved by incorporating new technology and NSK's extensive experience as a leader in bearing manufacturing. We are committed to introducing attractive products into the market now and in the future.

MEGATORQUE MOTOR PB Series

In the wake of increased demand for smartphones and tablet devices, production of electronic components has rapidly expanded in East Asia, such as in China, Taiwan, and South Korea. At the same time, emerging countries are seeing more investment going into facilities so that production can be expanded. However, staff at these places are not accustomed to operating this equipment, and so it must be easy to use and require less maintenance. It must also be compact so that it can be installed where there is limited space. To address these new market needs, NSK created the MEGATORQUE MOTOR PB Series (Photo 1), targeting a market that is different from those using our conventional high-accuracy PS and PN series (Figure 1).

1. Construction, Structure, and Specifications

The MEGATORQUE MOTOR PB Series consists of a MEGATORQUE motor, an EGA model driver, and an ECC model converter (Figure 2).

Four types of motors are available, each with different maximum torque and for use in various applications. In addition, two types of drivers with a different maximum current are provided. A converter is used to convert analog signals related to the motor's rotary position into digital signals. The converter for the new product is provided as an external unit, which is different from the combination of converter and driver in conventional products. This allows for placement of the converter near the motor, which shortens the distance that the analog signal travels and thereby improves signal transfer reliability.

Table 1 summarizes the specifications of the MEGATORQUE MOTOR PB Series.

2. Features

(1) Simple and compact
- Motor control uses only pulse command input.
- Only an incremental resolver is used for sensing position in order to meet the need for replacing the AC servo motor and gear reducer with this equipment.

Implementing these two functions reduces motor height by 10 mm and motor volume by half, compared to the conventional PS Series and EDC model drive unit.

At the same time, for simplicity and compactness, the motor hollows of the PB Series are the same size as those of the PS Series (ϕ35 mm for the PB1 model and ϕ56 mm for the PB3 model) to maintain the same piping for the absorption nozzle and signal wiring.

Photo 1 MEGATORQUE MOTOR PB Series

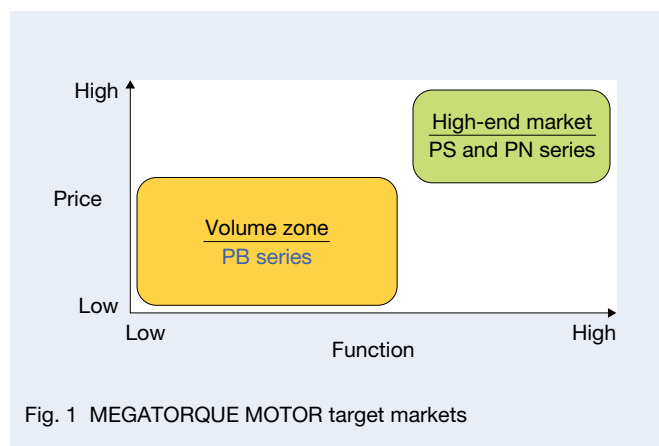Fig. 1 MEGATORQUE MOTOR target markets

(2) Functional improvement of auto-tuning

Initial setup has been simplified for faster launch of equipment operation.

(3) Setup software with multiple functions

The product comes with software for setting motor operation parameters, confirming motor operation using an oscilloscope, and calculating resonance point, which is effective for the setting of the notch filter.
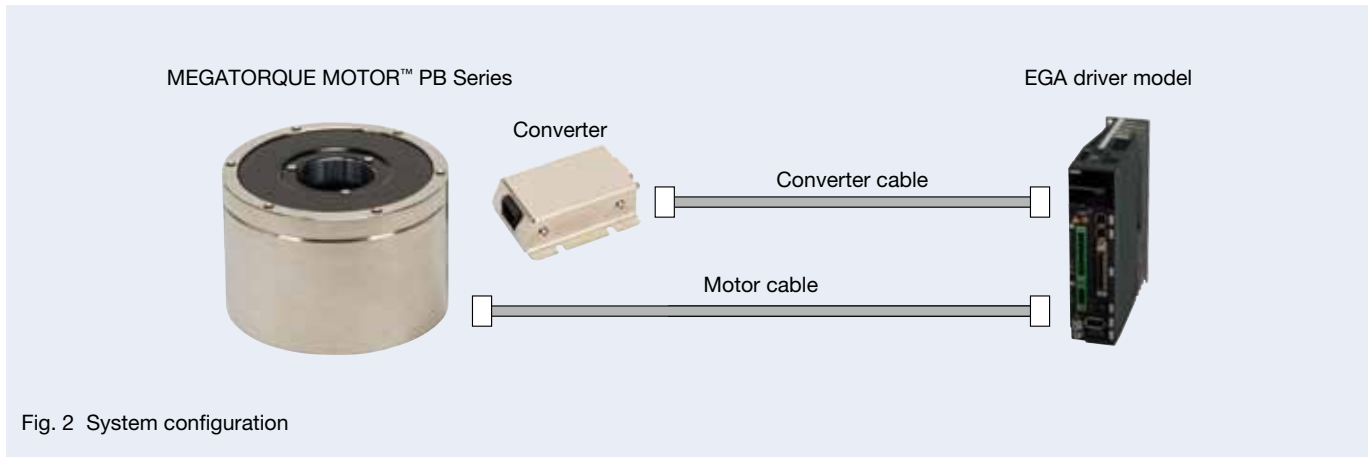
Fig. 2 System configuration

Table 1 Specifications

Item \ Motor size code	PB1006	PB3015	PB3030	PB3060
Outer diameter, mm	ϕ102	ϕ152		
Height, mm	75		92	126
Hollow diameter, mm	ϕ35	ϕ56		
Maximum torque, N·m	6	15	30	60
Rated torque, N·m	2	5	10	20
Maximum speed, s^{-1}	10			8
Rated speed, s^{-1}	5			1
Sensor resolution, counts/rev	524 288			
Absolute positioning accuracy, s	112			
Positioning repeatability, s	±5			
Maximum load inertia, kg·m^2	0–0.26	0–1.1	0–1.4	0–3.1
Weight, kg	2.6	5.8	7.2	10.2

3. Applications

- Supplying, testing, and selecting equipment for manufacturing electronic components
- Assembly equipment for smartphones and tablet devices
- Medical equipment for analysis of reagents and liquids

4. Summary

The MEGATORQUE MOTOR PB Series has attracted attention in East Asia for being a vital element in the construction of equipment for manufacturing electronic devices, conducting automotive tests, and assembling smartphones.

The structure of major industries has been changing, impacting the markets for smartphones and tablet devices as well as car-mounted electronic devices and medical and healthcare equipment. NSK is committed to widening the scope of application for the MEGATORQUE MOTOR PB Series while at the same time supporting industrial growth by closely monitoring diversifying needs.

Worldwide Sales Offices

NSK LTD.-HEADQUARTERS, TOKYO, JAPAN

Nissei Bldg., 1-6-3 Ohsaki, Shinagawa-ku, Tokyo 141-8560, Japan
INDUSTRIAL MACHINERY BUSINESS DIVISION-HEADQUARTERS
P: +81-3-3779-7227   F: +81-3-3779-7644
AUTOMOTIVE BUSINESS DIVISION-HEADQUARTERS
P: +81-3-3779-7189   F: +81-3-3779-7917

●Africa
South Africa:
NSK SOUTH AFRICA (PTY) LTD.
SANDTON   25 Galaxy Avenue, Linbro Business Park, Sandton 2146, South Africa
P: +27-11-458-3600   F: +27-11-458-3608

●Asia and Oceania
Australia:
NSK AUSTRALIA PTY. LTD.
MELBOURNE ☆   100 Logis Boulevard, Dandenong South, Victoria, 3175, Australia
P: +61-3-9765-4400   F: +61-3-9765-4466
SYDNEY   Suite A315, 20 Lexington Drive, Bella Vista, New South Wales, 2153, Australia
P: +61-2-9839-2300   F: +61-2-8824-5794
BRISBANE   1/69 Selhurst Street, Coopers Plains, Queensland 4108, Australia
P: +61-7-3347-2600   F: +61-7-3345-5376
PERTH   Unit 1, 71 Tacoma Circuit, Canning Vale, Western Australia 6155, Australia
P: +61-8-9256-5000   F: +61-8-9256-1044

New Zealand:
NSK NEW ZEALAND LTD.
AUCKLAND   3 Te Apunga Place, Mt. Wellington, Auckland 1060, New Zealand
P: +64-9-276-4992   F: +64-9-276-4082

China:
NSK (SHANGHAI) TRADING CO., LTD.
JIANGSU   No.8 NSK Rd., Huaqiao Economic Development Zone, Kunshan, Jiangsu, China (215332)
P: +86-512-5796-3000   F: +86-512-5796-3300

NSK (CHINA) INVESTMENT CO., LTD.
JIANGSU ☆   No.8 NSK Rd., Huaqiao Economic Development Zone, Kunshan, Jiangsu, China (215332)
P: +86-512-5796-3000   F: +86-512-5796-3300
BEIJING   Room 1906, Beijing Fortune Bldg., No.5 Dong San Huan Bei Lu, Chao Yang District,
Beijing, China (100004)
P: +86-10-6590-8161   F: +86-10-6590-8166
TIAN JIN   Room 06, 09F The Exchange Tower 2, No. 189 NanJing Road, Heping District,
Tianjin, China (300050)
P: +86-22-8319-5030   F: +86-22-8319-5033
CHANGCHUN   Room 902-03, Changchun Hongwell International Plaza, No.3299 Renmin Street,
Changchun, Jilin, China (130061)
P: +86-431-8898-8682   F: +86-431-8898-8670
SHENYANG   Room 1101, China Resources Building, No. 286 Qingnian Street,
Heping District, Shenyang Liaoning, China (110004)
P: +86-24-2334-2868   F: +86-24-2334-2058
DALIAN   Room 1805 Xiwang Tower, No.136 Zhongshan Road,
Zhongshan District, Dalian, Liaoning, China (116001)
P: +86-411-8800-8168   F: +86-411-8800-8160
NANJING   Room A1 22F, Golden Eagle International Plaza, No.89 Hanzhong Road, Nanjing,
Jiangsu, China (210029)
P: +86-25-8472-6671   F: +86-25-8472-6687
FUZHOU   Room 1801-1811, B1#1A Class Office Building, Wanda Plaza, No.8 Aojiang Road,
Fuzhou, China (350009)
P: +86-591-8380-1030   F: +86-591-8380-1225
WUHAN   Room 1110, New World International Trade Tower I, No.568 Jianshe Road, Wuhan,
Hubei, China (430000)
P: +86-27-8556-9630   F: +86-27-8556-9615
QINGDAO   Room 802, Farglory International Plaza, No.26 Xianggang Zhong Road, Shinan District,
Qingdao, Shandong, China (266071)
P: +86-532-5568-3877   F: +86-532-5568-3876
GUANGZHOU   Room 1011-16, Yuexiu Financial Tower, No.28 Zhujiang Road East, Zhujiang
New Town, Guangzhou, Guangdong, China (510627)
P: +86-20-3817-7800   F: +86-20-3786-4501
CHANGSHA   Room 1048, 10/F, Zhongtian Plaza, No.766 WuyiRoad, Changsha, Hunan, China (410005)
P: +86-731-8571-3100   F: +86-731-8571-3255
LUOYANG   Room 1108, Fangda Hotel, 6 XiYuan Road, LuoYang HeNan, China (471003)
P: +86-379-6069-6188   F: +86-379-6069-6180
XI'AN   Room 1007, B Changan Metropolis Center88 Nanguanzheng Steet, Xi'an, Shanxi,
China (710068)
P: +86-29-8765-1896   F: +86-29-8765-1895
CHONGQING   Room 2306, Unit B, No.137, Keyuan 2nd Road, Jiulongpo District, Chonqing,
China (400039)
P: +86-23-6806-5310   F: +86-23-6806-5292
CHENGDU   Room1117, Lippo Tower, No.62 North Kehua Road, Chengdu, Sichuan, China (610041)
P: +86-28-8528-3680   F: +86-28-8528-3690
NSK CHINA SALES CO., LTD.
JIANGSU   No.8 NSK Rd., Huaqiao Economic Development Zone, Kunshan, Jiangsu, China (215332)
P: +86-512-5796-3000   F: +86-512-5796-3300

NSK HONG KONG LTD.
HONG KONG ☆   Suite 705, 7th Floor, South Tower, World Finance Centre, Harbour City, T.S.T,
Kowloon, Hong Kong, China
P: +852-2739-9933   F: +852-2739-9323
SHENZHEN   Room 624-626, 6/F, Kerry Center, Renminnan Road, Shenzhen, Guangdong, China
P: +86-755-25904886   F: +86-755-25904883

Taiwan:
TAIWAN NSK PRECISION CO., LTD.
TAIPEI ☆   11F., No.87, Song Jiang Rd., Jhongshan District, Taipei City 104, Taiwan
P: +886-2-2509-3305   F: +886-2-2509-1393
TAICHUNG   3F. -2, No. 540, Sec. 3, Taiwan Blvd., Xitun Dist., Taichung City 407, Taiwan
P: +886-4-2708-3393   F: +886-4-2708-3395
TAINAN   5F. No.8, Daye 1st Rd., Southern Taiwan Science Park, Tainan City 741,
Taiwan
P: +886-6-505-5861   F: +886-6-505-5061

TAIWAN NSK TECHNOLOGY CO., LTD.
TAIPEI ☆   11F., No.87, Song Jiang Rd., Jhongshan District, Taipei City 104, Taiwan
P: +886-2-2509-3305   F: +886-2-2509-1393
TAICHUNG   10F-3, No.925, Sec.4, Taiwan Blvd., Xitun Dist., Taichung City 407,
Taiwan
P: +886-4-2358-2945   F: +886-4-2358-7682
TAINAN   5F. No.8, Daye 1st Rd., Southern Taiwan Science Park, Tainan City 741,
Taiwan
P: +886-6-505-5861   F: +886-6-505-5061

India:
NSK INDIA SALES CO.PVT.LTD.
CHENNAI ☆   6th Floor, Bannari Amman Towers, No.29 Dr. Radhakrishnan Salai, Mylapore,
Chennai-600 004 Tamil Nadu, India
P: +91-44-2847-9600   F: +91-44-2847-9601
GURGAON   Unit No-202, 2nd Floor, Block-A, Iris Tech Park, Sector-48, Sohna Road,
Gurgaon-122018, Haryana, India
P: +91-124-4104-530   F: +91-124-4104-532
MUMBAI   321, 'A' Wing, Ahura Centre, 82, Mahakali Caves Road, Andheri (East), Mumbai
-400 093, India
P: +91-22-2838-7787   F: +91-22-2838-5191

Indonesia:
PT. NSK INDONESIA
JAKARTA   Summitmas II, 6th Floor, Jl. Jend Sudirman Kav. 61-62, Jakarta 12190, Indonesia
P: +62-21-252-3458   F: +62-21-252-3223

Korea:
NSK KOREA CO., LTD.
SEOUL   Posco Center (West Wing) 9F, Western-wing, 440, Teheran-ro, Gangnam-gu,
Seoul, 135-777, Korea
P: +82-2-3287-0300   F: +82-2-3287-0345

Malaysia:
NSK BEARINGS (MALAYSIA) SDN. BHD.
SHAH ALAM ☆   No. 2, Jalan Pemaju, U1/15, Seksyen U1, Hicom Glenmarie Industrial Park,
40150 Shah Alam, Selangor, Malaysia
P: +60-3-7803-8859   F: +60-3-7806-5982
PRAI   No.24, Jalan kikik, Taman Inderawasih, 13600 Prai, Penang, Malaysia
P: +60-4-3902275   F: +60-4-3991830
JOHOR BAHRU 88 Jalan Ros Merah 2/17, Taman Johor Jaya, 81100 Johor Bahru, Johor, Malaysia
P: +60-7-3546290   F: +60-7-3546291
IPOH   Gr. Floor, 89 Jalan Bendahara, 31650 Ipoh, Perak, Malaysia
P: +60-5-2555000   F: +60-5-2553373

Philippines:
NSK REPRESENTATIVE OFFICE
MANILA   8th Floor The Salcedo Towers 169 H.V. dela Costa St.,
Salcedo Village Makati City, Philippines 1227
P: +63-2-893-9543   F: +63-2-893-9173

Singapore:
NSK INTERNATIONAL (SINGAPORE) PTE LTD.
SINGAPORE   238A, Thomson Road, #24-01/05, Novena Square Tower A, Singapore 307684
P: +65-6496-8000   F: +65-6250-5845
NSK SINGAPORE (PRIVATE) LTD.
SINGAPORE   238A, Thomson Road, #24-01/05, Novena Square Tower A, Singapore 307684
P: +65-6496-8000   F: +65-6250-5845

Thailand:
NSK BEARINGS (THAILAND) CO.,LTD.
BANGKOK   26 Soi Onnuch 55/1 Pravet Subdistrict, Pravet District, Bangkok 10250, Thailand
P: +66-2320-2555   F: +66-2320-2826

Vietnam:
NSK VIETNAM CO., LTD.
HANOI   Techno Center, Room 204-205, Thang Long Industrial Park, Dong Anh District,
Hanoi, Vietnam
P: +84-4-3955-0159   F: +84-4-3955-0158
NSK REPRESENTATIVE OFFICE
HO CHI MINH CITY Suite 307, Metropolitan Building, 235 Dong Khoi Street, District 1,HCMC, Vietnam
P: +84-8-3822-7907   F: +84-8-3822-7910

Worldwide Sales Offices

P: Phone   F: Fax   ☆: Head Office

●Europe

United Kingdom:
NSK EUROPE LTD. (EUROPEAN HEADQUARTERS)
MAIDENHEAD   Belmont Place, Belmont Road, Maidenhead, Berkshire SL6 6TB, U.K.
          P: +44-1628-509-800   F: +44-1628-509-808

NSK UK LTD.
NEWARK   Northern Road, Newark, Nottinghamshire NG24 2JF, U.K.
          P: +44-1636-605-123   F: +44-1636-605-000

France:
NSK FRANCE S.A.S.
PARIS   Quartier de l'Europe, 2 Rue Georges Guynemer, 78283 Guyancourt, France
          P: +33-1-30-57-39-39   F: +33-1-30-57-00-01

Germany:
NSK DEUTSCHLAND GMBH
DUSSELDORF ☆ Harkortstrasse 15, D-40880 Ratingen, Germany
          P: +49-2102-4810   F: +49-2102-4812-290
STUTTGART   Liebknechtstrasse 33, D-70565 Stuttgart-Vaihingen, Germany
          P: +49-711-79082-0   F: +49-711-79082-289
WOLFSBURG Tischlerstrasse 3, D-38440 Wolfsburg, Germany
          P: +49-5361-27647-10   F: +49-5361-27647-70

Italy:
NSK ITALIA S.P.A.
MILANO   Via Garibaldi 215, Garbagnate Milanese (Milano) 20024, Italy
          P: +39-299-5191   F: +39-299-025778

Netherlands:
NSK EUROPEAN DISTRIBUTION CENTRE B.V.
TILBURG   De Kroonstraat 38, 5048 AP Tilburg, Netherlands
          P: +31-13-4647647   F: +31-13-4647648

Poland:
NSK REPRESENTATIVE OFFICE
WARSAW   Ul. Migdalowa 4/73, 02-796, Warsaw, Poland
          P: +48-22-645-1525   F: +48-22-645-1529

Russia:
NSK POLSKA SP. Z O.O.
SAINT-PETERSBURG Office I 703, Bldg 29, 18th Line of Vasilievskiy Ostrov, Saint-Petersburg, Russia, 199178
          P: +7-812-332-5071   F: +7-812-332-5072

Spain:
NSK SPAIN S.A.
BARCELONA   C/Tarragona, 161 Cuerpo Bajo, 2a Planta, 08014, Barcelona, Spain
          P: +34-93-289-2763   F: +34-93-433-5776

Turkey:
NSK RULMANLARI ORTA DOGU TIC. LTD. STI.
ISTANBUL   19 Mayis Mah. Ataturk Cad., Ulya Engin Is Merkezi No: 68 Kat. 6, P.K. : 34736,
          Kozyatagi-Istanbul, Turkey
          P: +90-216-477-7111   F: +90-216-477-7174

United Arab Emirates:
NSK BEARINGS GULF TRADING CO.
DUBAI   JAFZA View 19, Floor 24 Office LB192402/3, PO Box 262163, DownTown Jebel Ali,
          Dubai, UAE
          P: +971-4-804-8207   F: +971-4-884-7227

●North and South America

United States of America:
NSK AMERICAS, INC. (AMERICAN HEADQUARTERS)
ANN ARBOR   4200 Goss Road, Ann Arbor, Michigan 48105, U.S.A.
          P: +1-734-913-7500   F: +1-734-913-7511

NSK CORPORATION
ANN ARBOR   4200 Goss Road, Ann Arbor, Michigan 48105, U.S.A.
          P: +1-734-913-7500   F: +1-734-913-7511

NSK PRECISION AMERICA, INC.
FRANKLIN ☆   3450 Bearing Drive, Franklin, Indiana 46131, U.S.A.
          P: +1-317-738-5000   F: +1-317-738-5050
SAN JOSE   780 Montague Expressway, Suite 505, San Jose, California, 95131, U.S.A.
          P: +1-408-944-9400   F: +1-408-944-9405

NSK LATIN AMERICA, INC.
MIAMI   3470 NW 82nd Avenue Suite 625, Miami FL 33122, U.S.A.
          P: +1-305-477-0605   F: +1-305-477-0377

Canada:
NSK CANADA INC.
TORONTO ☆   5585 McAdam Road, Mississauga, Ontario, Canada L4Z 1N4
          P: +1-905-890-0740   F: +1-800-800-2788
MONTREAL   2150-32E Avenue Lachine, Quebec, Canada H8T 3H7
          P: +1-514-633-1220   F: +1-800-800-2788
VANCOUVER 3353 Wayburne Drive, Burnaby, British Columbia, Canada V5G 4L4
          P: +1-877-994-6675   F: +1-800-800-2788

Argentina:
NSK ARGENTINA SRL
BUENOS AIRES   Garcia del Rio 2477 Piso 7 Oficina "A" (1429) Buenos Aires-Argentina
          P: +54-11-4704-5100   F: +54-11-4704-0033

Brazil:
NSK BRASIL LTDA.
SAO PAULO ☆   Rua 13 de Maio, 1633-14th Andar-Bela Vista-CEP 01327-905 São Paulo, SP, Brazil
          P: +55-11-3269-4700   F: +55-11-3269-4720
BELO HORIZONTE Rua Ceara 1431-4th andar-sala 405-Funcionarios Belo Horizonte-MG, Brazil
          30150-311
          P: +55-31-3274-2591   F: +55-31-3273-4408
JOINVILLE   Rua Blumenau, 178-sala 910-Centro Joinville-SC, Brazil 89204-250
          P: +55-47-3422-2239   F: +55-47-3422-2817
PORTO ALEGRE Av. Cristovão Colombo, 1694-sala 202-Floresta Porto Alegre-RS, Brazil 90560 001
          P: +55-51-3346-7851   F: +55-51-3222-2599
RECIFE   Av. Conselheiro Aguiar, 2738-6th andar-conj. 604-Boa Viagem Recife-PE, Brazil 51020-020
          P: +55-81-3326-3781   F: +55-81-3326-5047

Peru:
NSK PERU S.A.C.
LIMA   Av. Enrique Palacios, N 360 Oficina 311, Miraflores, Lima, Perú
          P: +51-1-652-3372   F: +51-1-638-0555

Mexico:
NSK RODAMIENTOS MEXICANA, S.A. DE C.V.
MEXICO CITY ☆ Av. Presidente Juarez No.2007 Lote 5, Col. San Jeronimo Tepetlacalco,
          Tlalnepantla, Estado de Mexico, Mexico, C.P.54090
          P: +52-55-3682-2900   F: +52-55-3682-2937
MONTERREY   Av. Ricardo Margain 575, IOS Torre C, Suite 516, Parque Corporativo Santa
          Engracia, San Pedro Garza Garcia, N.L. Mexico, C.P.66267
          P: +52-81-8000-7300   F: +52-81-8000-7095

<As of November 2016>
For the latest information, please refer to the NSK website.
www.nsk.com

Motion & Control
No. 27 November 2016

Published by NSK Ltd.